Novel carbenes, and ruthenium-carbene complexes in ruthenium-based olefin metathesis

Petter Aarbø Thorsen

Master Thesis in Chemistry

Faculty of Mathemathics and Natural Sciences

UNIVERSITY OF BERGEN

2021

Acknowledgements

My sincerest thanks to my supervisors, prof. Vidar Jensen, and Dr. Giovanni Occhipinti, for letting me work in this challenging and interesting field and giving insight and guidance in the chemistry regarding ruthenium-based olefin metathesis. Giovanni has been facilitating and guiding the reactions done and have taught me a great deal in air sensitive organometallic chemistry. It has been an honor to work alongside this group as their work is respectable and their knowledge is vast, as I'm learning new things each meeting, and learning that there are many things yet to learn. My sincere thanks to the whole group, for good company. Additionally, thanks to prof. Erwan Le Roux and his group in collaboration with ours, for interesting seminars, and enjoyable gatherings. Thanks to people that come and go in the lab, for swift and interesting previews in their work, and thanks to Immanuel for providing insight in several organic reactions, and for helpful discussions regarding mechanisms.

Thanks to prof Karl. W. Tørnroos for being willing to fly down all the way to France for running X-ray crystal experiments, which is highly appreciated. Also, a big thanks to Bjarte Holmelid for running and interpreting the MS-experiments.

I would like to thank my friends for their support and motivation.

Thanks to Helene for her support and helping me getting through the finish line.

Ultimately, I wish to thank my family. Thanks to my parents for their monumental support throughout my studies.

Abstract

Ruthenium catalyzed olefin metathesis is a valuable and powerful tool to convert olefins into longer chains or other valuable products. The field of olefin metathesis is a rich field, and a vast number of studies have been characterizing the different properties of different catalysts, in the task to find optimal catalyst, for both general and specific purposes. Throughout modern times, carbenes have made a name for themselves. As they are able to stabilize the intermediates in the catalytic cycle and are more resilient against certain types of decomposition. The most recent and successful carbene is Cyclic Alkyl Amino Carbenes (CAACs), as they can perform catalysis at very low loadings. However, CAACs are less stereoselective, as in some reactions the Z-stereoisomer is preferred, due to its chemistry as a precursor. However, there are no Z-selective CAAC-based catalysts, and since selectivity is of focus in this group, this was attractive as a goal. To do this, thiolates was installed to the Ru-carbenes, as the group had previous success with using thiolates with respect to Z-selectivity. As the thiolates are available to manipulate the central intermediate in the catalytic cycle. These novel carbenes, did indeed increase Z-selectivity, however in a slight manner, due to the CAAC- being less synergic with the thiolates, in respect to the previous work done in the group.

The group had done some calculations, regarding a novel carbene.; A CAAC-like carbene, with beneficial symmetries. This carbene ligand was successfully synthesized, and metalated to a carbene, forming a novel catalyst, although this catalyst was not possible to isolate, this could potentially lead to new carbene class in Ruthenium olefin metathesis.

Table of contents

1. Introduction

1.1 Catalysis

A catalyst is a compound in which alters the course of a reaction, without appearing in the final product. The catalyst does so by affecting the reactions kinetics, while not affecting the thermodynamics.[1] Thermodynamics involves the energetics of the reactants and products, constituting state functions such as enthalpy and entropy. Enthalpy is the sum of the systems internal energy, such as pressure, volume, and composition. Entropy is the amount of disorder in a system, such as the components state of aggregation and the number of molecules in each state. Kinetics describes the reactions pathway, i.e how the reaction happens intermolecularly. [2]

Consider a chemical reaction in equilibrium with two substrates and a product, one reaction is catalyzed and the other is not.

$$S_1 + S_2 \rightleftharpoons P$$

$$S_1 + S_2 \overset{[M]_{cat}}{\rightleftharpoons} P$$

Scheme 1.1. Uncatalyzed (top) and catalyzed (bottom) reactions

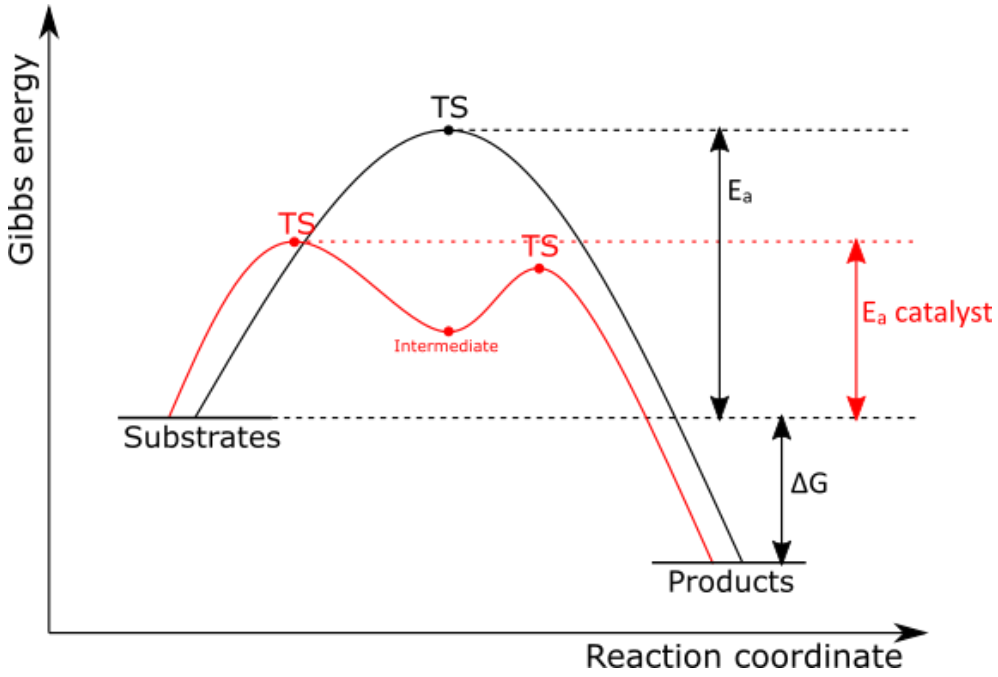

Fig 1.1 Energy diagram of **scheme 1.1**, Uncatalyzed reaction in black and catalyzed in red

The energy diagram (**fig 1.1**) describes the course of the reaction; The terminals, transition states (maxima) and intermediates (minima). The black curve describes the uncatalyzed reaction, in this case the reaction involves one transition state, a state where bonds are broken and formed simultaneously, causing strain on the molecule, and subsequently a peak in energy. The global maximum is also called the energy barrier; the energy needed to activate the reaction. The red curve describes the catalyzed reaction, here the global maximum is lower than the uncatalyzed reaction meaning less energy is needed to initialize the reaction. The catalyzed reaction also proceeds through an intermediate, a molecular state distinguishable from the substrate and product, which proceeds through a new transition state to form the product. Even though the path of the reaction (kinetics) is altered, the end point and start point is the same, which depend on thermodynamics. As stated earlier, enthalpy and entropy are state functions, meaning that they depend solely on the systems state, and not its pathway. The catalyst does not affect equilibrium, it rather helps the reaction reach equilibrium faster, as the equilibrium is determined by thermodynamics and not kinetics. [1–3] There are different types of catalysis; heterogenous and homogenous. Heterogenous involves the substrate and catalyst being in different phases, e.g gaseous substrate and solid catalyst. Homogenous involves the substrate and catalyst being in the same phase, e.g both are solvated. In this thesis, homogenous catalysis is in focus.

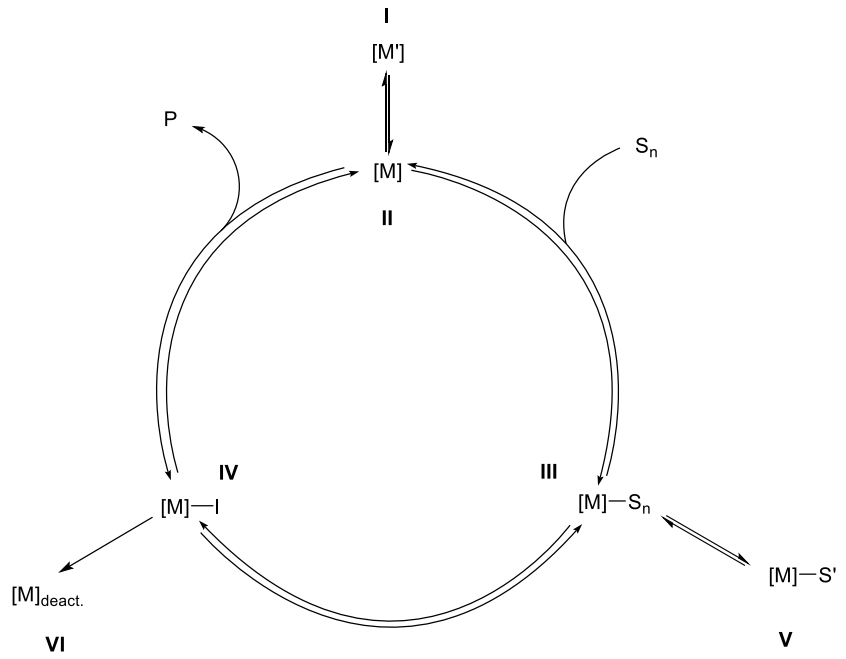

Scheme 1.2 General homogenous catalytic scheme[1]

As the catalyst is not a part of the final product, rather its regenerated, this regeneration allows the catalysis to follow a cyclic pathway. The cycle starts off as the pre-catalyst activates, this nature of this activation depends on the type of catalyst used, e.g the catalyst could dissociate a moiety, exposing its active site for coordination to substrate. The activated catalyst species (**II**) binds to the substrates forming a catalyst-substrate complex (**III)**. The complex further reacts into an intermediate complex (**IV**), the intermediate undergoes cleavage, resulting in the product and the regenerated catalyst. In the cycle (fig) there is included typical factors for decrease in activity: Inactive complex and decomposition. The catalyst-substrate complex (**III**) can form an equilibrium with an inactive intermediate (**V**), although reversible, the formation reduces the concentration of catalyst (**II**), subsequently reducing catalytic activity. The intermediate complex can irreversibly decompose to side-products and/or an inactive catalytic species (**VI**). Decomposition is particularly a hindrance in catalysis. [1]

1.2 Catalytic Activity and Productivity

One highly important and sought-after aspect with catalysts are their activity and productivity; Activity displays the reaction rate related to the concentration of the catalyst, meaning how many catalytic cycles each catalytic unit can perform pr unit of time. A common measure is Turn Over Frequency (TON).[1]

$$TOF = \frac{r_p}{C_{cat}} \qquad 1.1$$

Formula 1.1 Turn-over frequency expressed as rate of product formed (r_p), divided by catalyst concentrations (C_{cat})

The productivity of a catalyst reflects the amount of product that can be produced with a certain quantity of catalyst, meaning how many product forming catalytic cycles each unit of catalyst can complete at the given reaction conditions. Productivity is often reported in Turn Over Number (TON). [1]

$$TON = \frac{n_p}{n_{cat}} \qquad 1.2$$

Formula 1.1 Turn-over number expressed as number of molecules of product formed (n_p), divided by number of molecules of catalyst (n_{cat})

TOF and TON are related analogously as speed and distance covered are related. TOF are sometimes calculated by dividing TON by elapsed time, and TON by multiplying TOF by elapsed time. However, this only give an approximate and average value, as TON is a time integral of TOF.[4]

$$\overline{TOF} = \frac{TON}{t}\ , TOF = \frac{dTON}{dt} \rightarrow TON \int_0^{\infty} TOF(t)dt \qquad 1.3$$

Formula 1.3 expression of average TOF, and TOF and TON expressed at time intervals

1.3 Commercial importance of catalysts

As of 2021, catalysts are a vital part of a vast range of industries, from pharmaceutical, petroleum, cosmetic, plastic, food Industry and agriculture, to name a few. The importance of catalysts is reinforced by the fact that around 80% of all manufactured products have had a catalyst involved in their line of production. Additionally, catalysts are associated with approximately 30 % of the combined GDP in European economies alone.[5]

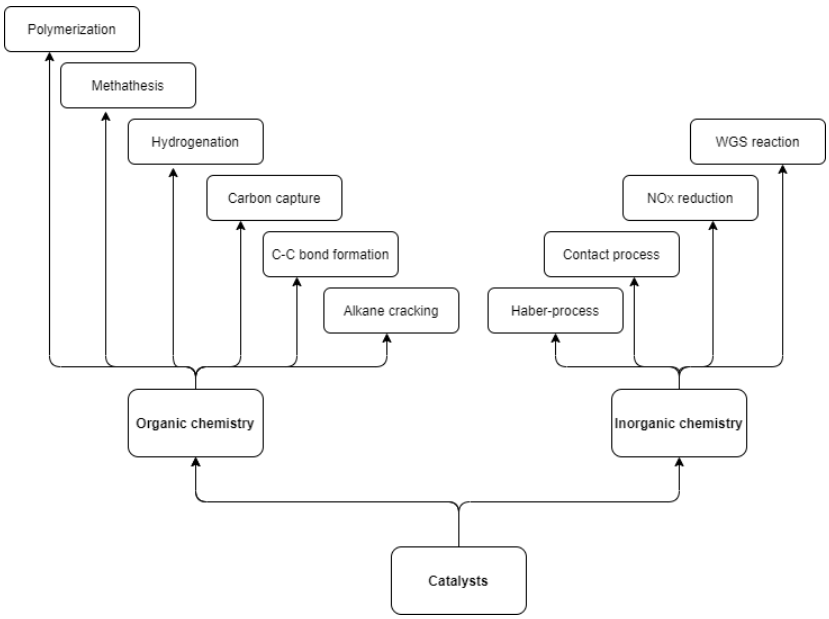

Fig 1.3 Selected industrial catalytic processes [3,6]

For instance, C-C cross coupling is a vital process in the pharmaceutical industry, the ability to link carbon atoms with different moieties is widely useful to produce complex drugs[7]. Also, the catalysis to produce polymers are useful to produce plastics in consumer goods, and the production of synthetic fabrics for both the textile and fiber industry.[8]

1.4 Metathesis

Olefin-metathesis is in essence a carbon-carbon double bond rearrangement (scheme x.x). It is a powerful tool in chemical synthesis and have a wide array of uses in industry. [9,10] The term metathesis bears Greek origin, meaning “change in position”.[11]

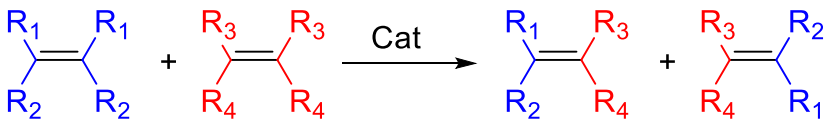

Scheme 1.3 General metathesis reaction

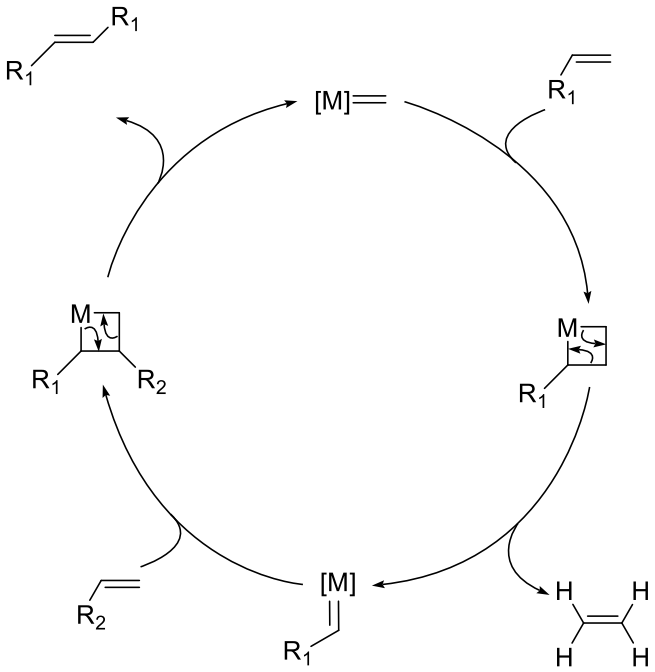

Scheme 1.4 Chauvin mechanism

Olefin Metathesis proceeds through the Chauvin mechanism[12]; which in essence involves an interconversions of double bonds between olefins and a metal-alkylidene proceeding via metallacyclobutane-intermediates. The catalytic pathway emphasized the presence of an alkylidene, a metal-carbon double bond, which is crucial for the cycle. This discovery by Chauvin skyrocketed the development of metathesis catalysts, as previous metathesis catalysts were metal salts with cocatalysts lacking alkylidenes. These early salts gave minuscule yields compared to the present-day catalysts.[13]

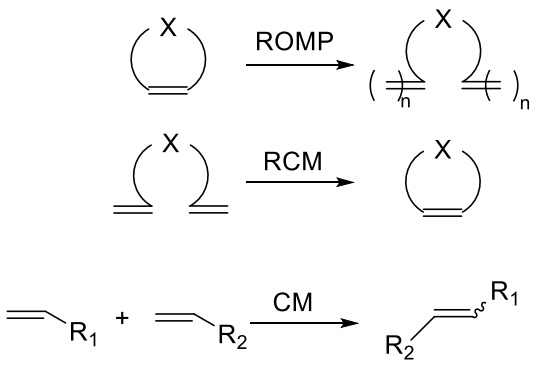

Scheme 1.5 Different types of metathesis

There are a several types of olefin metathesis; some of the most common are ROMP (Ring Opening Metathesis Polymerization), RCM (Ring Closing Metathesis) and CM (Cross Metathesis). ROMP was one of the earliest types of metathesis commercially performed. [14] ROMP is driven by ring strain release, hence the catalyst needed is not required to affect the kinetics that dramatically compared to other metathesis reactions. Additionally, the ROMP mechanism is irreversible, as the product is required to overcome a large energy-barrier to reform the substrates. RCM is driven by entropy, as one substrate molecule produces two molecules, the product other than the ring produced is often a gas (i.e ethylene), which further reinforces the reactions entropic incentive. CM however is a bit more challenging, as two substrate molecules form two molecules, although CM still produces volatile ethylene, which is an entropic driving force, but not in the same accord as RCM. The challenges around CM have led to it being less expressed in the field of metathesis, although new discoveries in the field have led to catalysts being able to effectively perform CM. The two predominant catalyst families in metathesis are Schrock- and Grubb's type. Schrock is the earlier type, Molybdenum-alkylidene complexes bearing alkoxy-ligands. Schrock catalysts are highly active, although highly sensitive and unbiased against functional groups. [13] Grubb's catalysts are ruthenium-alkylidene complexes, with various ligands impacting the catalysts properties.

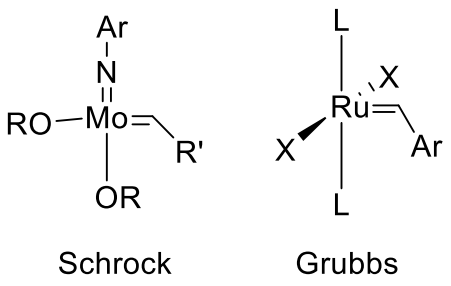

Fig 1.5 General structure of Schrock and Grubbs complexes

1.5 Ruthenium catalyzed olefin metathesis

Ruthenium-based catalysts are currently one of the best candidates for olefin metathesis. This is due to ruthenium being a noble metal, with electronic properties enabling stable 14- and 16 electron complexes. Additionally, ruthenium has a higher reactivity towards olefins, rather than other functional groups such as alcohols, carboxylic acids, aldehydes etc.[13] This fact of selectivity have led to the focus and further development of ruthenium based catalysts.

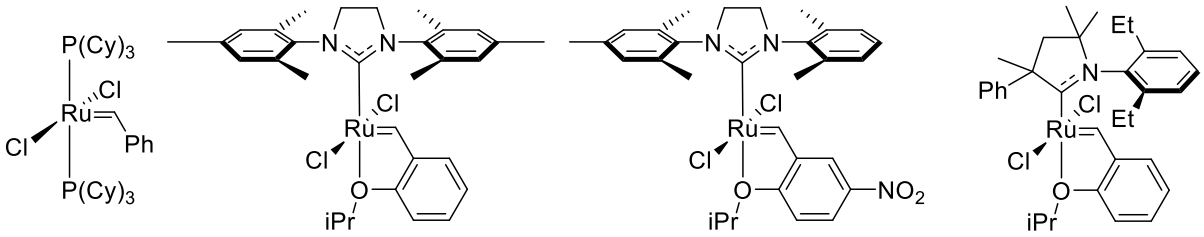

Grubbs 1.gen | Hovyeda-Grubbs 2.gen | Nitro-Grela | HG-CAAC

Fig 1.4 Some commercial Grubbs based catalysts

The 1.gen Grubb's catalysts bear two tricyclohexylphosphine (PCy_3) ligands, which are sigma-donating. This sigma donation facilitates the ligand cleavage of a PCy_3, forming the active catalyst. In addition to facilitating cleavage, the sigma donation stabilizes the 14 electron metallacyclobutane-intermediate. [15,16] Grubbs 2.gen catalysts bears a imidazoline-based N-heterocyclic carbene (NHC), which are stronger sigma donators, and slightly more pi-accepting compared to phosphines.[17] These properties made them attractive ligands for metathesis, as the activity were highly sufficient (TONS here) due to them being able stabilize the electron poor intermediates in the Chauvin cycle.[18] The second generation NHC's bears mesityl-substituted nitrogen atoms, which were proven to have best overall performance compared to phosphines. The Hoveyda catalyst (HG) is a phosphine free catalyst, where the monodentate benzylidene moiety is modified to a bidentate isopropoxy-benzylidene ligand. This bidentate alkylidene gives unprecedented stability and latency, although slower initiation rate.[19] The Nitro-Grela catalyst introduced a subtle yet influential change to the Hoveyda alkylidene; by substituting a nitro group on the meta-position on the benzylidene, the activity and rate of initiation was greatly increased for disubstituted olefins.[20] The newest carbene class are Cyclic Alkyl Amino Carbenes (CAAC), which are more sigma donating[21], and more pi acidic (susceptible to back-bonding)[22] than NHC's. These properties of CAAC's leads to strong metal-carbene bonds, and promotes stability and activity.

1.6Metathesis mechanism; a closer look

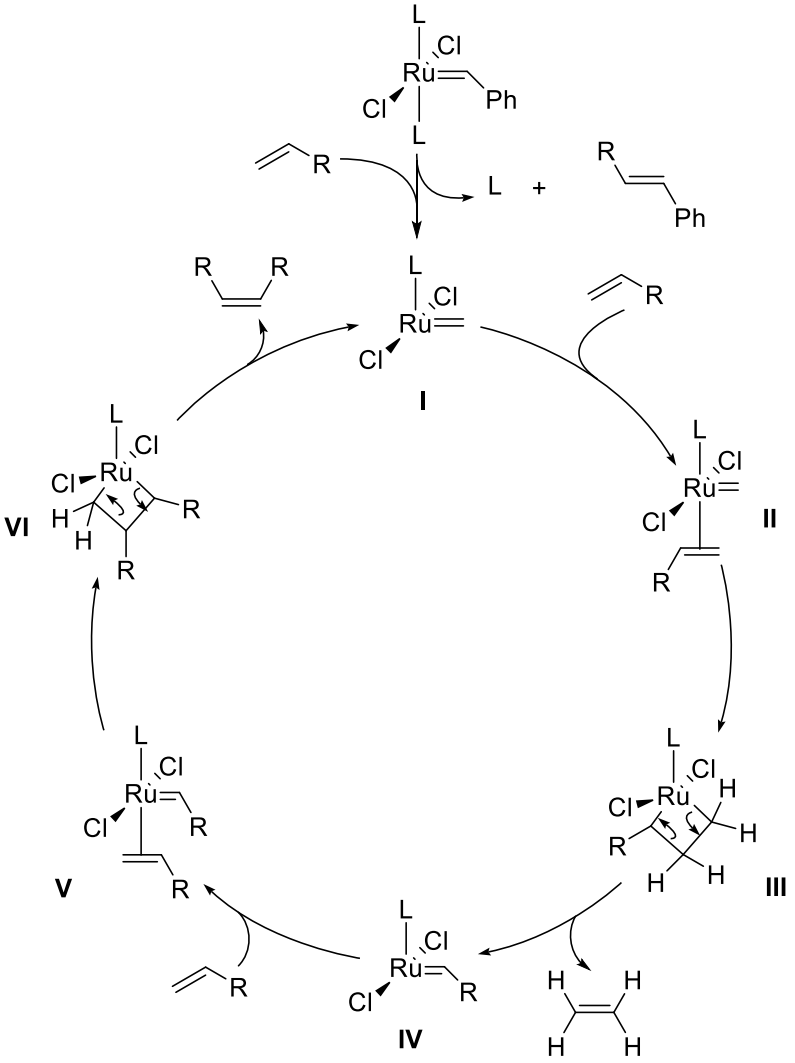

Scheme 1.6 Catalytic metathesis cycle of ruthenium

The cycle starts with the most labile ligand cleaving off, and the extrusion of the initial alkylidene moiety by metathesis, forming a 14-electron active methylene ruthenium species **I**. The active species coordinates to an olefin via the olefins pi-system, forming intermediate **II**. The metal undergoes 2+2 cycloaddition with the coordinated olefin to form a metallacyclobutane (**III**), which subsequently undergoes cycloreversion, forming ethylene and a 14 electron ruthenium species primed with the substrate (**IV**). The primed active species coordinates to a new olefin, undergoing 2+2 cycloaddition and cycloreversion anew (**IV**-**V**-**VI**), forming the product and the initial methylene ruthenium species (**I**).

1.7 Factors affecting initiation

As seen in scheme x.x, the initiation takes place when the most labile ligand is cleaved, and the alkylidene is exchanged via metathesis. The rate regarding initiation varies widely with the nature of each catalyst. As mentioned, the PCy_3-ligand in the 1.gen Grubbs facilitated cleavage of the other PCy_3 by the means of sigma donation. This effect is called "trans-influence"; stronger sigma donation by a ligand L_1, weaken and elongates the bond between a ligand L_2 and the metal, where L_2 is trans(opposite) to L_1.[23] This is also true for pi acceptors; stronger metal back-bonding increases the trans influence, which is why CAAC exhibits improved trans influence compared to NHC and Phosphines.[22] The lability of the ligand is also dependent on the type of ligand, for instance pyridines are a notable example, as these are highly labile, and the foundation for the 3.generation of Grubbs Catalysts. For catalysts, and organometallic complexes in general, the cleaving of the most labile ligand to form the active species can proceed in different ways: Associative, dissociative and interchange.

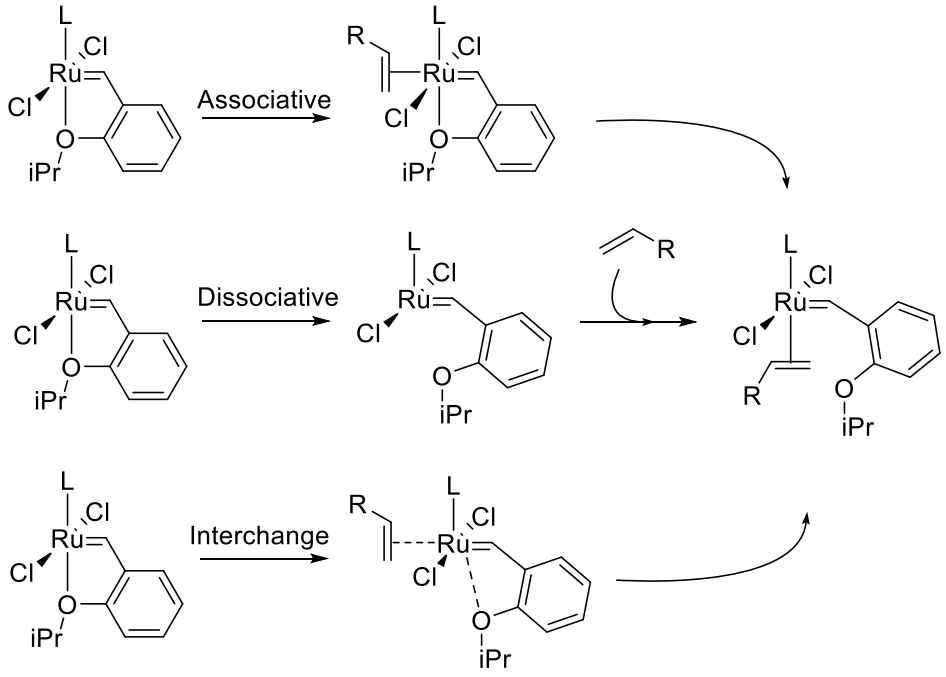

Scheme 1.7 Different mechanisms of activation for bidentate ligands, with Hoveyda alkylidene as example[24]

In respect to 16 electron pre-catalysts, the associative mechanism involves the coordination of the substrate, forming an intermediate 18 electron complex before the ligand is cleaved off. In the dissociative mechanism, the ligand is cleaved off before coordination. In the interchange mechanism, the coordination and cleavage occur simultaneously.[1,24] For

phosphines, the most common pathway is dissociative. For Hoveyda alkylidenes, the most occurring pathway of initiation is proposed as the interchange mechanism.[24]

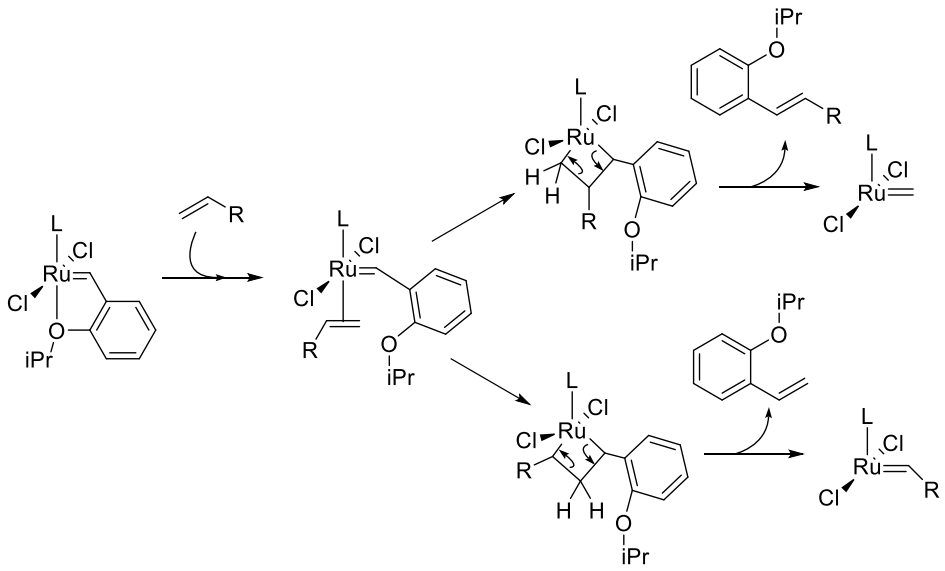

Scheme 1.8 Mechanism of Hoveyda-alkylidene [25]

The oxy-ligand is first cleaved off, resulting in a 14-electron species which opens a site up for the olefin to coordinate. The metal and the olefin undergo 2+2 cycloaddition, which depending on the orientation of the initial olefin coordination yield isopropoxy-2-vinylbenzene and an active substrate primed ruthenium species (bottom pathway), or a R-substituted isopropoxybenzene and an active ruthenium-methylidene species (top pathway). This dual pathway also applies for all pre-catalyst alkylidenes, the instance that the initially formed catalyst can be primed or not with the substrate.[9]However for the Hoveyda catalyst, the bottom pathway is the most favorable one.[25] The nitro-Grela catalyst presents higher initiation rates as the meta nitro-group exhibits an electron withdrawing effect, consequently weakening the Ru-Oxygen bond, which enhances cleavage. However, this nitro-group decreases stability. [20] Even though trans-influence is an important factor regarding initiation, the energy barrier of metathesis of the initial alkylidene is highly important. The energy-barrier depends on factors such as sterics, electronic properties and even the substrate. [19,25,26]

1.8**Paths of decomposition**

Decomposition is a hurdle in any type of catalysis, as it decreases the concentration of the active species. It can also produce unwanted side-products. Olefin metathesis is not an exception.[9] To gain an insight to metathesis decomposition, one must consider the cycle (scheme x.x) and non-productive metathesis:

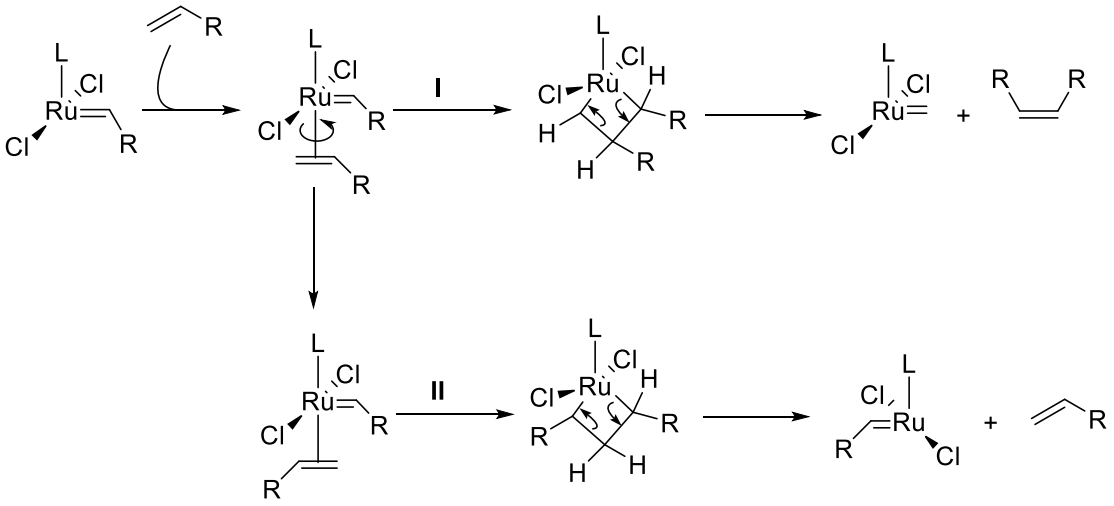

Scheme 1.9

As the olefin is coordinated, it is allowed to shift in coordination (180° rotation), subsequently affecting the geometry of the metallacyclobutane.[1] Scheme x.x exhibits two pathways, one where the metallacyclobutane bears the substituents of interest in a 2,3 position (**I**). After cycloreversion this pathway results in the product and the metal-alkylidene which will undergo the cycle anew. Pathway **II** shows the substituents of interest oriented in 2,4 positions, after cycloreversion this pathway yields the starting materials, as nothing has occurred in the first place. This pathway is called non-productive, or degenerate metathesis. Nonproductive metathesis does indeed happen, and the frequency depends on the catalyst's nature as well as the substrate. In RCM of diethyl diallylmalonate, NHC bearing Ru-catalysts exhibited a ratio between productive and non-productive metathesis of 1:10, while CAAC bearing Ru-Catalysts revealed a ratio of nearly 1:1.[27] The non-productive pathway does indeed affect the activity of the catalyst, moreover the TOF. If a catalyst does four catalytic cycles per second, but half om them are nonproductive, the TOF of interest are half of the actual cycles performed. Although non-productive metathesis ideally does not directly cause a net change

in the catalyst's concentrations, it does so in reality. Non-productive cycles allow for additional opportunities for the catalysts do decompose, as some of the intermediates in the cycle are more vulnerable to decomposing pathways .[28] The two most central pathways of decompositions are Bi-Molecular-Coupling (BMC) and beta-hydride elimination:

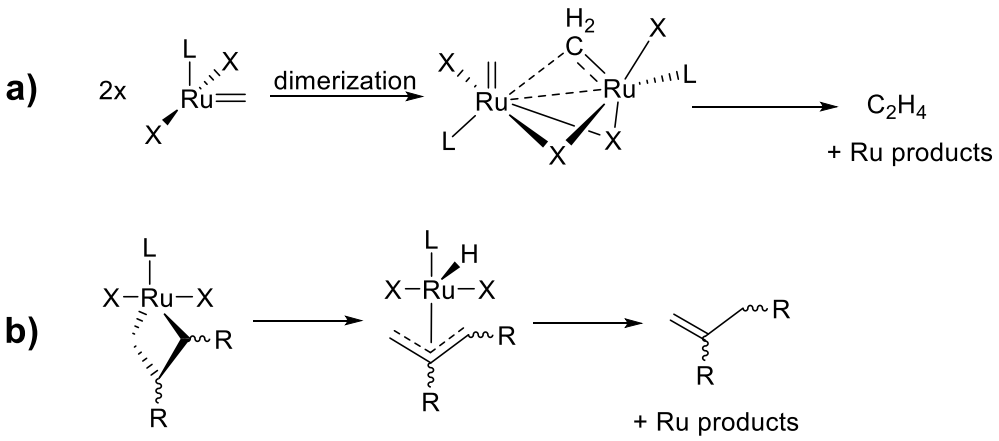

Scheme 1.10 Pathways of decomposition a) BMC, b) beta-hydride elimination[29]

BMC is essentially the catalyst doing self-metathesis on its own alkylidenes; Two ruthenium-methylene species dimerizes, one of the methylene are sufficiently sterically hindered to interact with one of the ruthenium centers, while the other does not. Subsequently, the uncoordinated methylene coordinates with the other one, forming a dimetallacycle, which cycloreverses to produce the decomposition-products.[30] One dimerization incapacitates two catalyst molecules, impeding activity drastically when happening frequently. BMC is heavily reliant on catalyst concentrations, as higher concentrations increase the probability of the species to connect and dimerize. This can also happen with the pre-catalyst when heated, resulting in the elimination of stilbene for the phenyl-alkylidenes, and bis(2-isopropoxybenzene)ethene for the Hoveyda catalysts, in addition to ruthenium products. This pre-catalyst decomposition is not directly a part of the catalytic cycle, although it exhibits that ruthenium-alkylidene complexes are sensitive to storage-conditions when in solution. Beta-hydride elimination is essentially a hydrogen transfer occurring at the metallacyclobutane-intermediate. The transfer forms a metal hydride, which disrupts the metallacyclobutane and extrudes an unfinished olefin.[31] Unsubstituted metallacyclobutanes are particularly more prone to beta-hydride elimination,[32] and beta hydride elimination is reliant on the concentration of ethylene in the catalytic system, as coordination of ethylene in the catalyst

precedes the formation of unsubstituted MCBs[31,32]. Ethylene concentration is not the sole factor in beta-hydride elimination, as the barrier for hydride transfer is also a major factor. Pathways of decomposition can lead to isomerization; the formation of undesired side products, due to C=C migration. [33] As the side-products of decomposition often bears double bonds, the catalyst can perform metathesis on these together with substrate, forming different carbon chains than the expected product.

NHC's are particularly resilient to BMC, as their symmetrical structure resembles that of an umbrella, which prevents the alkylidenes to interact with the nearby metal centers in the same magnitude as other catalysts such as phosphines and CAACs. CAACs are especially susceptible for BMC, since the amount of back-bonding the CAAC introduces creates a more electrophilic metal center, which will increase the likelihood of dimerization.[29] However, CAACs are much more resilient against beta-hydride elimination than NHCs, and phosphines. This is due to CAACs being able to stabilize the metallacyclobutane in such a matter that hydride-transfers are unfavorable.[29] The resilience against beta-hydride elimination enables CAAC-based catalysts to perform ethenolysis, the opposite of terminal olefin metathesis. Ethenolysis is the process involving the cleavage of larger internal olefins, to form smaller terminal olefins, usually under an atmosphere of ethylene. **HG-C1** managed to perform ethenolysis of internal olefins under ethylene, reaching TONs up to 340K.[34] This atmosphere of ethylene would be devastating to phosphines and NHC's.[31,32] An additional path of decomposition is the nucleophilic attack of the alkylidene, called methylene abstraction.[35]This is particularly the case for cleaved phosphines; the phosphine attacks the methylidene, forming a zwitterionic intermediate, resulting in cleavage and abstraction of methyl-phosphonium chloride. This is one of the reasons why the Hoveyda class is more active than their 1.gen phosphine counterparts. [36]

1.9Factors affecting selectivity

As metathesis revolves around the breakage and forming of a double bond, stereochemistry must be considered for the products. There are two possible diastereomers: *Z*-(together-*Zusammen*) and *E* (opposite- *Entgegen*).[37]

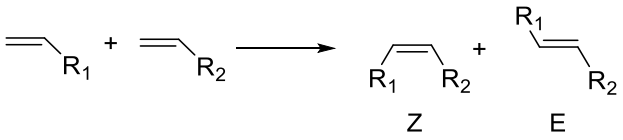

Scheme 1.11 CM-resulting in different isomers

One or the other is preferred depending on the products nature, as they incorporate different chemical properties as reactants. *E* diastereomer is the most thermodynamically stable one. This discrepancy in stability is due to the *Z* isomer being less stable considering the non-bonding interactions between the two groups on the same side of the double bond, which are causing steric strain. The fact that the *E* diastereomer is more favorable is unfortunate in olefin metathesis when the *Z*-diastereomer is preferred. However, it is possible to strengthen the formation of *Z* olefins, due to manipulations of the intermediates: The metallacyclobutane in the Chauvin mechanism can be oriented in two ways, bottom pathway, and side pathway.

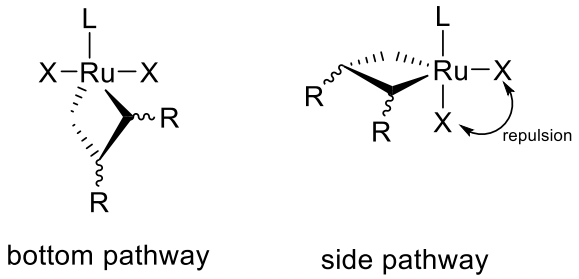

Fig 1.6

The bottom pathway is the pathway most encountered in commercial olefin catalysts, due to them bearing ionic monodentate X-ligands with a partial charge. If the metallacyclobutane were to exhibit a side pathway, the X-ligands would repel each other, causing strain. Nonetheless, it is possible to promote the side pathway, if the two X-ligands are substituted for a bidentate ligand, the effect of repulsion is negated.[38] The different pathways are not affecting selectivity intrinsically, but they introduce different ways to do so. Focusing on the bottom pathway; if a ligand is able to act as a lid on one side of the MCB, the syn isomer would be favorable, favoring the production of the Z-isomer. This is done various ways[39,40], but for

the sake of simplicity, let's focus on thiolates. Bulky aryl thiolates in addition to other thiolates have the special properties of high bond angles, as the sulfur has two lone pairs which repel each other. The lone pairs will occupy a greater radial space since the lone pairs exhibits greater repulsion between themselves compared to lone pairs and bonded electrons. This bonding angle orients the aryl groups of the thiolate in a manner such that the anti-MCB, i.e the pathway to E-stereoisomers, less favorable. [40]

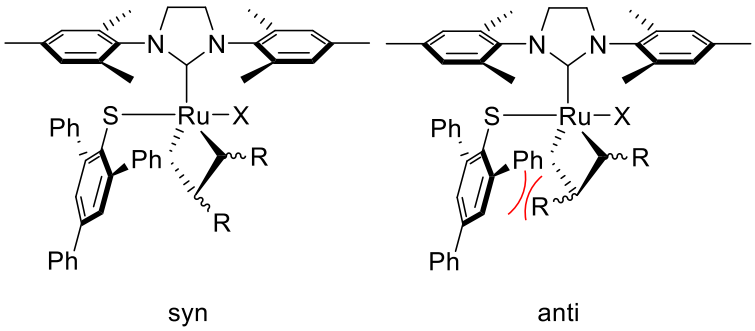

Fig 1.7

The catalysts following the bottom pathways are generally less active than their side-pathway counterparts, as well as their thiolate-free precursors. Additionally, Hoveyda alkylidenes with thiolates tends to initiate slower, as the thiolate increases the barrier of initiation. However, Occhipinti, Jensen, and colleagues made a notable progress when they synthesized thiolate bearing NHCs, with pyridine as the labile ligand. This catalyst gave a Z-selectivity of 81-86%, with yields ranging from 41-33 % respectively in the metathesis of allylbenzene with loadings of 1mol%. [41] These results are better than the Hoveyda-counterparts, both for NHC[41] and phosphines[42] (81-87% Z, 2-3% yield, 81% Z, 13% yield respectively). This is partially due to the acute angle of the thiolate in the NHC catalyst with pyridine, as the NHC is able to press the thiolate downwards, resulting in a Ru-S-Ar angle of 107°. The addition of pyridines also increases the initiation, compared to Hoveyda alkylidenes with respect to thiolates.[40,41]

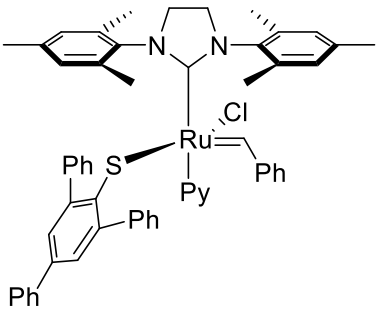

Fig 1.8 Fast initiating and Z-selective monothiolate Ru-catalyst

1.10 Summary of factors

To emphasize the factors which are the motivators behind the development of new catalysts, a summary is in order:

- **Initiation:** Particularly in catalysts bearing phosphines as labile ligand, a stronger sigma donation, and pi-backdonation strengthens the trans-influence, facilitating the cleavage and initiation to form the active catalytic species. However, for several phosphine free catalyst the initiation also depends on the barrier of metathesis for the alkylidene.

- **Decomposition:** The stability of the intermediates; ensuring the pathways involving decomposition are unfavored, are important for ensuring a steady concentration of catalyst in the system. This is done by the means of introducing steric bulk, and electronic effects on the metal center.

- **Activity:** Factors such as initiation, affinity to the substrate, barrier of metathesis of substrate, decomposition, and the ability to stabilize the intermediates, plays a vital role in ensuring high and quick productive turnovers.

- **Selectivity:** Steric bulk and is the main factors regarding selectivity, the ability to force the orientation of the substituents on the metallacyclobutane favors one isomer over the other.

1.11 Motivations and aim of this study

The aim of this study is to use the superior stability of CAAC-based carbenes to synthesize thiolate bearing analogues which may be more Z-selective than their precursors. As Z-selectivity is of interest in the group (Jensen Group). This group had previously been using thiolates to modify the steric bulk, moreover the orientations of the substituents on the MCB. These attempts were successful for NHCs and phosphines but had not yet been attempted with CAACs. Z-selective CAAC-derived catalysts has also not yet been described. This galvanized the interest to modify existing CAAC-catalyst to investigate any changes in selectivity, a. Thus, the first part in this thesis is to synthesize novel thiolate and NCO bearing CAAC based catalysts using known procedures, and to evaluate their catalytic properties.

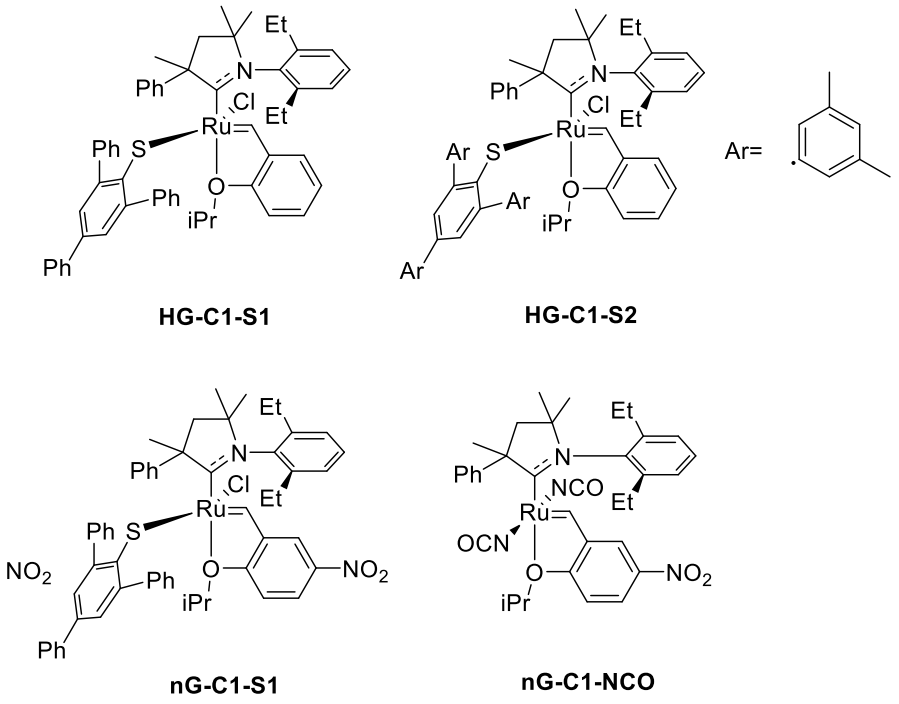

Fig 1.9 overview of the novel catalysts synthesized

Diana Heberle, a previous member of Jensen Group, performed some calculations regarding bonding energies in various carbenes. In particular, she found that a trimesitylsubstituted pyridinium-carbene had viable HOMO and LUMO energies for strong sigma donation and strong pi back-donation. The molecule is also reasonable symmetrical when regarding steric bulk, which would stand as a reasonable fundament for further catalyst development with respect to selectivity in addition to resilience against BMC, if successful. This sparked an

interest to try to synthesize and metalate it to a ruthenium pre-catalyst to investigate that the theoretical properties are in accord with reality.

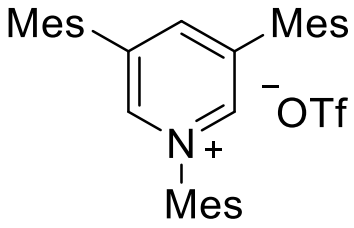

Fig 1.10 Ligand precursor for the novel Ru-carbene class

2. Methods and Theory

2.1 Analysis

2.1.1 NMR

*excerpt from Friebolin, H.; Becconsall, J. K. *Basic One- and Two-Dimensional NMR Spectroscopy*; Wiley, 1998.[43]

NMR utilizes the spin in certain types of nuclei to characterize and examine compounds. Most nuclei hold a nuclear angular momentum, i.e they spin around their own axis. Quantum mechanics show that together with other atomic properties, nuclear angular momentum is quantized:

$$P = \sqrt{I(I+I)}\hbar \qquad 2.1$$

Formula 2.1 P is nuclear angular momentum. I is angular momentum quantum number, $\hbar$ (h-bar) is simply $\frac{h}{2\pi}$ where h is Planck's constant.

I is also called nuclear spin, which can have values ranging from 0 to 6 with intervals of ½, i.e $0, \frac{1}{2}, 1, \frac{3}{2}, 2..$ Intrinsically the nuclear angular momentum **P** is associated with a magnetic moment μ, they are proportional to each other:

$$\mu = \gamma P \qquad 2.2$$

Formula 2.2 μ is magnetic moment, P is nuclear angular momentum, γ is a constant called the gyromagnetic ratio.

The gyromagnetic ratio γ is different for each nuclide i.e both for element and its associated isotopes. The magnitude of γ largely influences the sensitivity of the NMR-experiment, meaning that nuclei with larger γ are easier to observe and requires relatively small concentrations to adequately analyze.

By combining all the terms from the formulas, we end up with:

$$\mu = \gamma\sqrt{I(I+1)}\hbar \qquad 2.3$$

Formula 2.3 Expression of the magnetic moment

When considering formula xx it is evident that nuclides with spin I=0 have no magnetic moment, which means they cannot be observed in NMR spectroscopy. ^{12}C and ^{16}O, the main

building blocks in organic chemistry have no magnetic moment. To address this gap the other isotope of the elements (^{13}C and ^{17}O) is utilized, but to the inconvenience that these isotopes is less abundant than their lighter isotopes, which decreases sensitivity.

When a nucleus with spin is placed in a static magnetic field (B_0), the angular momentum is influenced such that it commences an angled orientation along the magnetic field, i.e the nucleus' axis of rotation precess along the magnetic field vector.

$$P_z = mh \tag{2.4}$$

Formula 2.4 Expression for the direction along the z-axis ***Pz***, *m* is directional quantum number

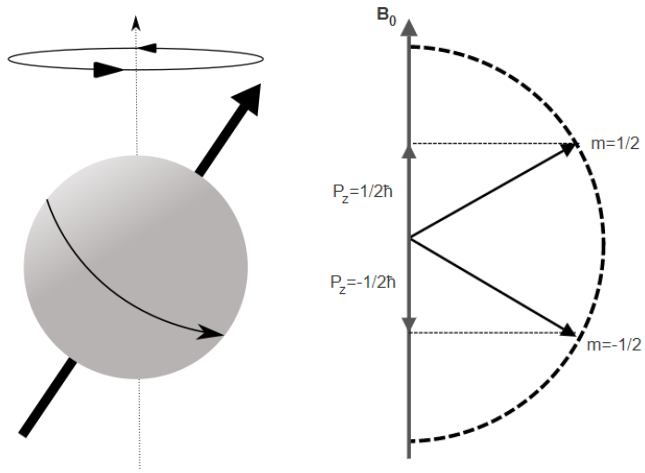

Fig 2.1/2.2. Visualization of the alignment the nucleus can exhibit, together with $\mathbf{P_z}$-values of the H^1 nucleus.[43]

The rate (period) at which this precession takes place is called the Larmor frequency

$$v_l = \left|\frac{\gamma}{2\pi}\right| B_0 \tag{2.5}$$

Formula 2.5 Expression of the Larmor frequency $\mathbf{v_l}$

The axis of rotation can be parallel to the magnetic field, or anti-parallel (as seen in fig x.x), where the former is the most energetically preferred.

$$E = -m\gamma\hbar B_0 \tag{2.6}$$

Formula 2.6 Expression of the energy values for the possible precession alignments

$$\Delta E = \gamma \hbar B_0 \qquad 2.7$$

Formula 2.7 The energy difference between the values

From the formula above it is palpable that the difference in energies corresponds to the strength of the magnetic field.

When observing nuclei on a macroscopic scale in thermal equilibrium, the nuclei populate all states, even though one state is more favorable. The difference in population can be provided by Boltzman statistics:

$$\frac{N_\beta}{N_\alpha} = e^{\frac{\Delta E}{k_B T}} \approx 1 - \frac{\Delta E}{k_B T} = 1 - \frac{\gamma \hbar B_0}{k_B T} \qquad 2.8$$

The energy difference ΔE for all nuclei are very small compared to $k_B T$, therefore the difference in populations is minuscule. The population with lower energy occupies only an excess of a few parts per million (ppm). Although a very small difference in population, the excess population is the key part of NMR; The opposite the magnetic moments of the populations cancel one another, and the system is left with a net magnetic vector (M_0) along the magnetic field. When a radio-pulse containing frequencies that match the Larmor frequencies, the angle of precession is affected; The angle gets deflected from its original equilibrium which will also deflect the net magnetic vector (M_0). When the pulse is terminated the precession returns to its equilibrium together with M_0, which will precess as well. The precession of M_0 along the transverse plane relative to B_0 (the initial alignment of M_0) induces a current in a detector.

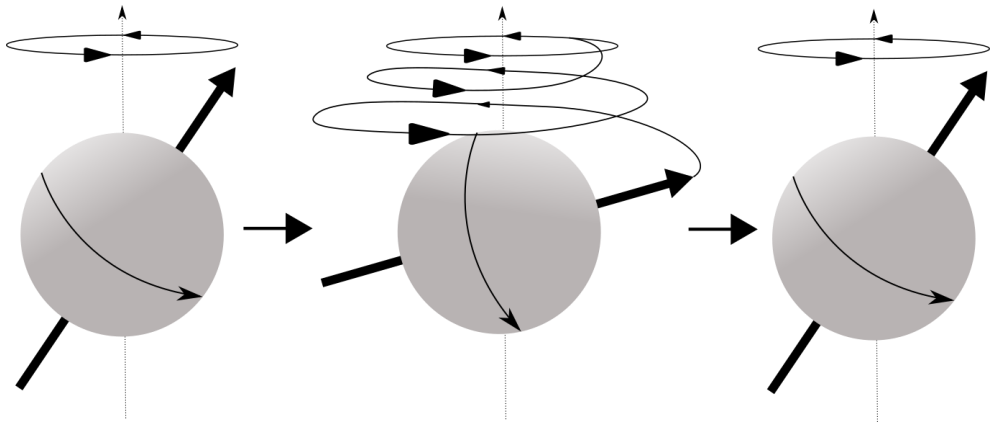

Fig 2.3 Visual representation of a precessing exited nucleus relaxing back to its ground state.

The signal the detector picks up is called Free Induction Decay (FID). This is an aggregate of all the different frequencies of the nuclei in the sample. To unravel this aggregate, Fourier Transform (FT) is utilized, which separate all the frequencies in the FID, outputting a spectrum. One would think that all the nuclei in a molecule would have the same frequencies, this is not the case; Each nucleus is surrounded by electrons, (and other nuclei that affect electron density). The electrons are in motion, subsequently inducing a magnetic field. This induced magnetic field opposes the magnetic field in the instrument, shielding the nuclei and reducing the magnetic force the nuclei experiences. As noted in formula x.x the precession frequency relies on the strength of the magnetic field *experienced* by the nuclei; the more shielding, the lower precession frequency. This effect is called chemical shift; the different frequencies that indicate the different environments of the nucleus. For instance, protons that are bonded to halogenated carbons experience de-shielding since the electronegative halogens are pulling on the carbon's electrons, moving them away from the hydrogen, hence the de-shielding. Aromatic and olefinic systems also influence shielding, the circular movement of the pi electrons parallel to the double bond induces an electromagnetic field parallel the to the double bond. This induced field reinforces the external magnetic field outside of the double bond, de-shielding the electrons.

Splitting

Neighboring, non-equivalent protons magnetically interact with each other. As the nuclei can have different spins, each alignment induces a field in the neighboring atoms, splitting the signal. For instance, if a proton has three neighboring protons, each proton can align itself with or against the magnetic field.

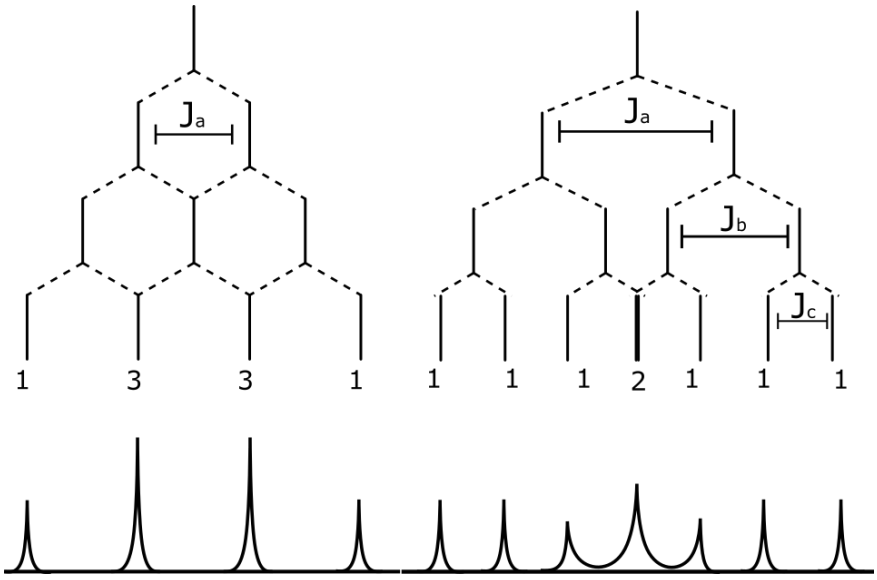

Fig 2.4. Splitting patterns

2.1.2 Mass Spectrometry

Mass spectrometry (MS) utilizes the mass of ions to determine the analytes molecular mass, and even its structure. MS works by ionizing the analyte by employing an ionization source. The analyte gets destroyed by ionization, the ionization source knocks off electrons in the sample's molecules, giving a positive ion counterparts of the analyte. The ions get accelerated via a strong current, such that each ion have the same kinetic energy. The ions get accelerated through a deflector; a bent pathway surrounded by an electromagnet, which repels the positive ions. Higher masses have greater inertia, so their angle of deflection is less than lighter ions, this causes the heavier molecules to travel slower, the time traveled from the distance (D) between the accelerator and detector is called time of flight (TOF). The TOF is then interpreted and related to the ions mass, giving the value in m/z (mass/charge).

$$zV = \frac{1}{2}mv^2 \qquad 2.8$$

Formula 2.8 Expression of the potential energy of the potential energy of the ion (zV) when it reaches the detector, with mass (m) and velocity (v)

$$zV = \frac{1}{2}m\left(\frac{D}{t}\right)^2 \rightarrow \frac{m}{z} = \frac{2Vr^2}{D^2} \qquad 2.9$$

Formula 2.9 exression of m/z, D is distance, t is time, r is the radius of the bent pathway

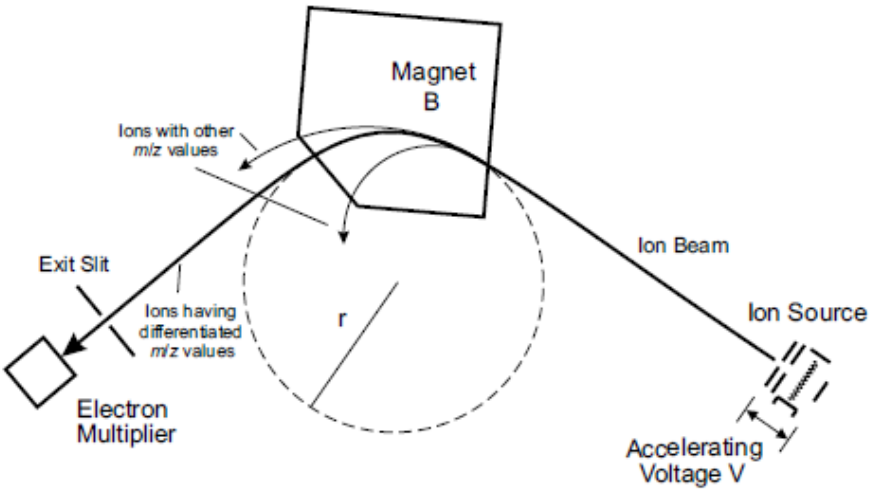

Fig 2.5. Schematic of a mass spectrometer *Smith, R. M.; Busch, K. L. Understanding Mass Spectra: A Basic Approach; Hoboken: John Wiley & Sons, Incorporated: Hoboken, 2004.*[44]

2.1.3 Single Crystal X-ray Diffraction

Single Crystal X-ray Diffraction (SCXD), uses X-rays to determine a crystals structure. Crystals are relatively stationary (compared to a solvated molecule) and have rigid bonds in a crystal lattice. This rigid nature allows for X-rays waves to pass through the atoms, since the wavelength of X-rays corresponds to the spacings between the atoms in the crystal. A usual setup is that the source of monochromatic X-rays is static, and the detector and sample containing crystals in different orientations rotates in front of it on the same plane as the source. When x-rays hit the crystals at certain angles, they bounce off the atoms, disturbing the x-rays path, either not reaching the detector at all, or undergoing destructive interference, canceling out each other. However, if the x-rays hit the atoms in just the right spots, the waves get collectively deflected and exhibits both the same phase and lateral distance, reaching the detector in with a larger amplitude, creating a peak. This is the condition of Bragg's Law:[45]

$$n\lambda = 2d(sin\theta) \qquad 2.10$$

Formula 2.10. Bragg's law, *n* is the diffraction order, *d* is the distance between the layers of atoms in the lattice, θ is the angle of incident light.

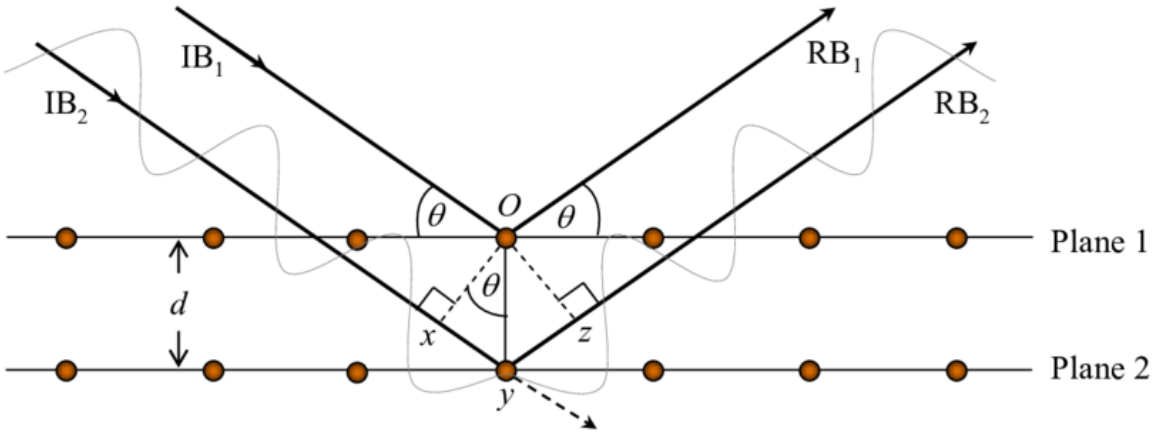

Fig 2.6 Conditions of Braggs law visualized. *Thomas, E. Crystal Growth and the Search for Highly Correlated Ternary Intermetallic Antimonides and Stannides.* ***2006****.*[46]

These peaks are interpreted to determine the crystal structure and composition of the crystal analyzed.

2.2 Organometallic theory

2.2.1 Transition metals

The transition metals are a part of the d-block elements, where the former is defined by IUPAC as elements which atom has an incomplete d-subshell or atoms that institute ions with an incomplete d-subshell.[47] This intrinsic property of the metals facilitates the formation of complexes, due to the metal's tendency to fill its orbitals to acquire the electron structure of noble gases. This fulfilling is can be attained by bonding to different ligands, which in turn alters the properties of the metal and the molecule *en bloc*. Transition metals are viable in catalysis because of their unfilled d orbitals; As an effect they can possess a variety of different stable oxidation states, which allows them to constitute various transition states and intermediates together with a substrate.[1,3,48] These transition states (TS) can have a lower energy than the TS (and intermediates) for the substrate's initial pathway. As described, the unfilled d-orbitals allows for bonding between ligands. These ligands may help stabilize the TS and intermediates, depending on the nature of the ligand. Ligands can also guide the reaction mechanism a desired way, e.g by the means of steric strain.[1,3]

2.2.2 Complexes

The total number of electrons a transition metal have in its outer shell (it's valence shell), are coined number of valence electrons (NVE)[48].

$$NVE = n_M + 2n_L + n_x - q \tag{2.11}$$

Formula 2.11. Number of valence electrons defined by the number of initial valence electrons in the metal(n_M), number of L ligands ($2n_L$), number of X-ligands(n_x) and charge of complex (q).

The oxidation state of the metal describes its theoretical charge:

$$OS = n_x + q \tag{2.12}$$

Formula 2.12. Expression of the Oxidation state

2.2.3 Ligands

There are currently existing two classes of ligands, with the premise that all ligands are considered neutral; Ligands giving one or more electron pairs to the metal are termed L or L_n where n is the number of electron pairs transferred to the metal. L- or L_n ligands (generally) do not accept valence electrons from the metal because the metal-part of the bond is an empty orbital (donor-acceptor species).

Ligands termed as X, are radical-type ligands, i.e they bring one electron to the metal whilst accepting electrons from the metal, resembling a covalent bond between the ligand and the metal. There are also several combinations with the two types of ligands (L and X), such as L_nX_m. With each LX combination donating an odd number of electrons to the metal and accepting one valence electron from the metal for each X-ligand, except for when n=m, where the number of donated electrons is even.

Common L-Ligands are H_2O, carbenes (nonbonded), NH_3, trisubstituted- amines and phosphines, carbon monoxide, alkoxy and isonitriles, with the characteristic feature of having one non-bonded electron-pair of a heteroatom. Additionally, bonded electron can also function as L-ligands[48]

Fig 2.7. Common L-ligands with a lone electron pair

Common X-ligands are halides, alkyl, methyl, hydroxy, PR_2, ligands that form a single electron-sharing bond with the metal.

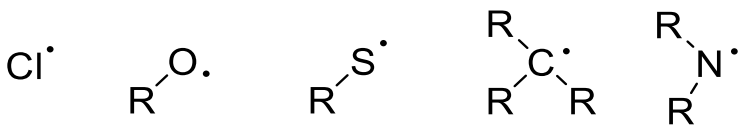

Fig 2.8 Examples of X-ligands

Common X_2 ligands are some carbenes, depending on the moiety and metal, forming a double bond.

2.2.4 Orbitals

Since electrons behave in such a peculiar manner compared to a relative stationary nucleus which the electron orbits, one needs a particular way of describing them. The current paradigm is called orbitals. The electron behaves both as a particle and a wave with an accompanied wavefunction. The wavefunction describes the electrons properties, such as energies and distribution of probability. Orbitals are a third-dimensional wavefunctions which each describes the properties of two electrons with opposite spin. There are four orbital subshells- s, p, d and f, accompanied principal quantum numbers. The principal quantum number *n* designates the shell, moreover the distance of the orbital from the nucleus, which increases with n.[3]

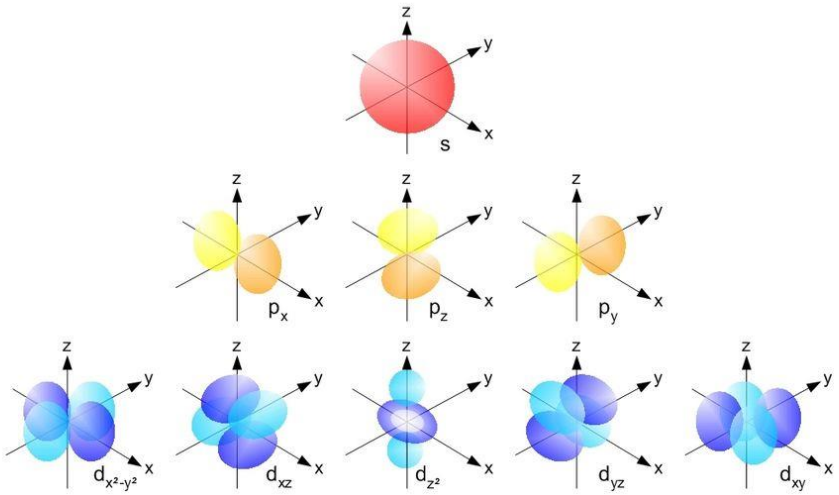

Fig 2.9 3-D wavefunctions for single electron orbitals *Atkins, P. W.; Shriver, D. F. Shriver & Atkins' Inorganic Chemistry, 5th ed.; Oxford University Press: Oxford, 2010.*[49]

Electrons are singlehandedly the most important part in the formation and breaking of bonds. Since orbitals systematically describe electrons, they also give an understanding of bond formations. Covalent bonds consist of two bonds, sigma- () and pi () bonds. Sigma bonds are the strongest covalent type, it is constituted by a direct overlap of two orbital lobes. An example is ethane, each carbon is sp_3-hybridized, meaning it mixes its four orbitals (1s, and three 1p orbitals, (scheme x.x)), forming four equivalent(degenerate) orbitals. The sp_3 orbitals each overlap with the lobes of its substituents, forming four covalent sigma bonds. In ethylene, the carbon is sp_2 hybridized, one 1s and two 1p are combined to form three degenerate orbitals, with one p lobe aligned perpendicular relative to them. The sp_2 orbitals

form sigma bonds with their substituents, however the two perpendicular p-orbitals interact to form two bonds parallel to the C-C carbon bond, this is called a pi bond. [3]

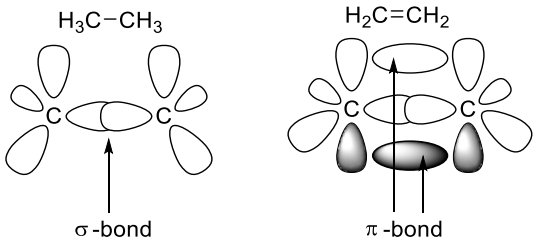

Fig 2.10 orbital scheme of sigma and pi bonding (hydrogens are omitted)

2.2.5 Bonding in Metals

The d-orbitals can be divided into two sets: t_{2g} and e_g. The t_{2g} (d_{xz}, d_{yz}, d_{xy}) set have their lobes aligned away from the axes on the coordinate (Fig x.x), while the e_g ($d_{x^2-y^2}$, d_{z^2}) set have their lobes aligned with the axes. The core of the theory is that a ligand can only approach along the axes and for bonds to interact there must be an overlap (sigma bonds), or sideways symmetry (pi interactions). By these criteria, the t_{2g} set is non-bonding, while the e_g set is bonding (with respect to sigma bonding). Even though the t_{2g} set is non-bonding, the alignment allows for pi-interactions.[3] There are different pi interactions, reliant on the ligand and the metal's needs; pi accepting and pi donation (with respect to the ligand). A pi-accepting ligand allows the metal do give some of its electron density from the t_{2g} set to the ligands anti-bonding orbitals, called back-bonding. Back bonding allows the metal to be stable in a state it otherwise would be too electron dense for, due to the delocalization of negative charge away from the metal center. Back-conation strengthens the metal-ligand bond, conversely the bond between the coordinating atom and its substituents become lengthened. A pi-donating ligand provides density to the t_{2g} metal through an occupied p-orbital. This is often the case with L-donors that have occupied p-orbitals, which can interact with the metal-orbitals, forming a stronger bond that resembles a double covalent bond. Sigma donation is the overlap of the metals e_g set and the ligands electrons, where the ligand donates the electrons to the metal, forming a coordination-bond. These overlapping electrons from the ligand can for instance reside in a lone pair or in a degenerate orbital. [48]The magnitude of sigma-donation depends on factors such as the highest occupied molecular orbital (HOMO), as higher HOMO values for the electrons in the ligand coordination site leads to stronger donations;[50–52] the HOMO is in

turn reliant on the ligands coordinating molecule, and its substituents. For instance, if a coordination site in a ligand is stabilized by an electron-donating system, it is more able to donate its electron pair to the metal. Stronger sigma donation leads to a stronger metal-ligand bond, and it can also weaken the other sigma bonding ligands, as the overlap between the stronger sigma donator and the metal becomes larger, the other overlap between the weaker sigma bonds and metal becomes smaller, subsequently weakening it. This is called the trans effect. Conversely to sigma donation, back-bonding is dependent on factors such as the lowest unoccupied molecular orbital (LUMO), as backdonation is the t_{2g} orbitals donating electrons to antibonding orbitals in the ligand.[48] The energies of the antibonding orbital in the ligand have to be sufficiently low enough to accept this donation, which corresponds to LUMO. The LUMO values are for instance increased with higher conjugation, as delocalized electrons are able to stabilize and distribute electron density. [37]

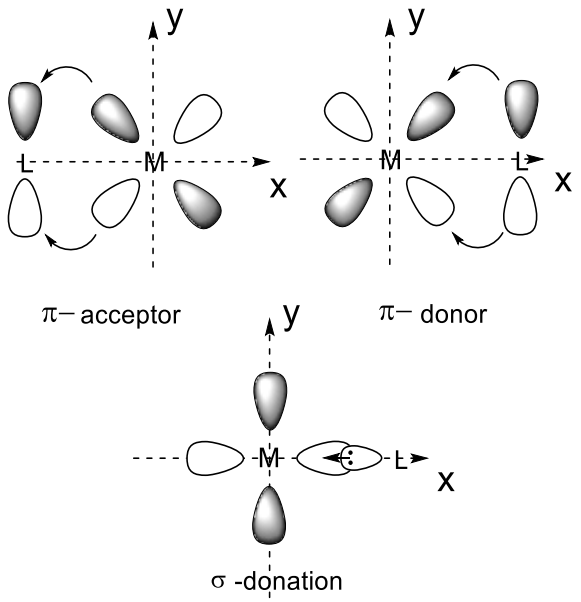

Fig 2.11. Orbital figures visualizing different metal-ligand bonding interactions

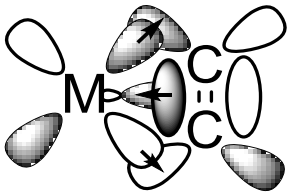

Fig 2.12 Ethylene as an L-ligand, with the pi-electrons as sigma donors, and antibonding p-orbitals as pi-acceptors.

2.2.6 Carbenes

Free carbenes are sp_2 hybridized divalent neutral molecules, with the carbon bearing only 6 electrons (4 from covalent bonds and 2 from itself in a lone pair). Carbons usually form four bonds to gain a full octet (8 outer electrons), forming stable and neutral molecules. It follows then that the carbenes are unstable and highly reactive by nature. Carbenes occur in two forms: singlet and triplet. [48]

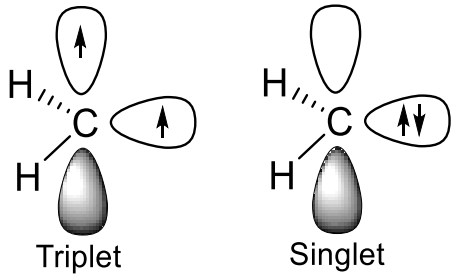

Fig 2.13 Triplet and singlet carbenes

Free carbenes are usually in triplet form; a lower energy-state, owing to Hund's rule; electrons would rather be alone than in pairs. For carbenes to be in the singlet state it needs to get stabilized by its substituents. As stated, carbenes can both be a L ligand and a X_2 ligand depending on its nature.

2.2.7 Metal-Carbene bonds

The bond between a carbene and a metal is polarizable; meaning the carbene can mimic a cationic, neutral, or anionic character, depending on the carbenes moiety and the electronic nature of the metal:

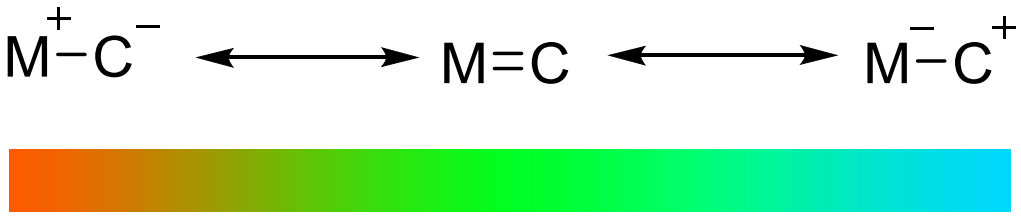

Fig 2.14. Polarization of a metal carbene bond, color gradient representing relative electron density on carbon.

Carbenes with electrophilic properties together with a metal fragment can be considered as being in singlet form, donating its electron-pair to the metal, acting as an L-ligand. Conversely, a carbene with nucleophilic characteristics with a metal fragment can be considered as being

in triplet form, forming a covalent bond between the carbene and the metal analogous to an organic C=C bond, acting as a X_2- ligand.[48]

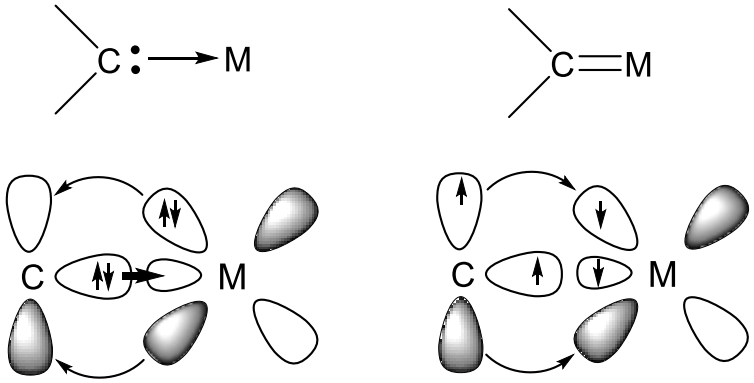

Fig 2.15. Metal carbene interaction with singlet carbenes and triplet carbenes.

The singlet carbene complex allows for pi-backdonation, where the metal gives some of its electron density back to empty orbitals in the carbene. Pi-backdonation introduces stability to the complex through the means of delocalizing negative charge from the metal center.

The triplet carbene however does not share this back-bonding effect to the same extent. Unlike singlet carbenes which have their p-orbital formally empty, making them susceptible to nucleophilic attack, triplet carbenes have their p-orbitals partially filled, enabling them to donate to the metal. This donation subsequently mimics the formation of a double bond. These carbenes are often termed Schrock carbenes or alkylidenes. However, the nature of the metal plays a major role in the type of bond formed.[53]

Oxidation state in Ru-complexes

One would think that Ru-center in the pre-catalyst would have a formal charge of +4, since the alkylidene would act a X_2 ligand and two chlorides act as X ligands. However, this is not the case with Ru-benzylidenes, as the phenyl group is conjugated, the pi-stabilization leads to a polarization towards the ruthenium center.[18] Although covalent, the metal-carbene bond is can be deemed “electrophilic-covalent”;[53] a likeness to singlet carbenes, although still in triplet form, but with higher bond order. This is one of the reasons why ruthenium pre-catalysts have formal oxidation number of 2+. However, the metallacyclobutane in the Chauvin mechanism bear a higher oxidation state; a study found this state to be in-between

+2 and +4, where the latter is related to better activity. [18] This is why NHCs and CAACs perform better than phosphines as mentioned in ***1.5***. NHCs and CAAC are less sigma *charge* donating, due to factors such as back-nonding (as they are singlet carbenes) the weaker charge donation allows the ruthenium metallacycle to constitute a higher oxidation state (+4), increasing activity.

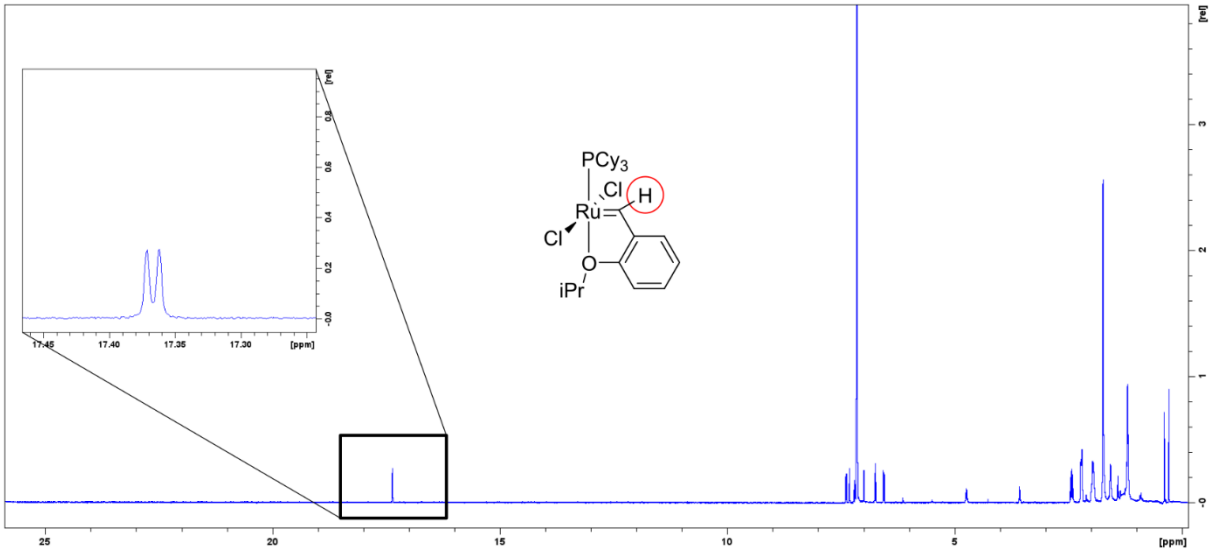

Fig. 2.16 Alkylidene peak for Hoveyda-Grubbs 1. Generation

Ru-alkylidenes containing a hydrogen as an R group, are quite unique when regarding chemical shift for the proton. Since the carbon is donating a lot of electron density to the metal, the hydrogen is heavily de-shielded due to the emigration of the local electron cloud, subsequently shifting the hydrogen down-field. The alkylidene peak varies widely with substituents to the metal center, nonetheless it is a good marker for different compounds as this peak is often the most distinct peak since complexes can contain wide range of different protons. [9]

2.2.8 Organometallic reactions

Transition metals can undergo a variety of different reactions. Each reaction may impact the properties of the metal in different ways.

Ligand cleavage and ligand coordination

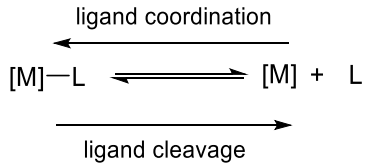

Scheme 2.1. Ligand cleavage/dissociation

Ligand cleavage is the loss of a ligand, which generates unsaturated complexes. The metal loses two electrons in its valence electron count and its coordination number lowers by one (if coordination of solvent is not considered). The reverse is named ligand coordination. When both cleavage and coordination are involved it's called a ligand substitution, which can progress in different pathways: The most important ones are dissociative and associative ligand substitution (LS). Dissociative LS involves the cleavage taking place before coordination. Associative LS involves coordination before cleavage,

Oxidative addition and reductive elimination

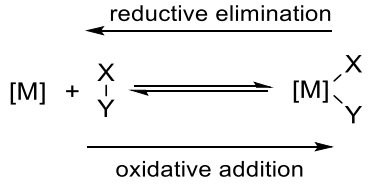

Scheme 2.2 Oxidative addition/reductive elimination

Oxidative addition occurs when the addition of a substrate (X-Y) to a complex, results in the cleavage of the substrate bond. The breakage between the bond prompt a formation of two new bonds, M-Y and M-X. The names stem from the trait that the metal is oxidized i.e., it's valence electron count is increased by two, and subsequently its oxidization number is also increased by two. The coordination number is also increased by two.

Transmetallation

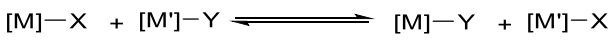

Scheme 2.3. Transmetalation

Transmetallation is the transfer of a ligand from a metal to another. The electron gain for the receiving metal depends on the nature of the ligand; if it's an X- or L-ligand. If all ligands in **scheme 2.3** are considered X-ligands the net electron gain is zero, because the donating metal receives an X-ligand themselves. Transmetallation is also possible where the receiving metal gains a ligand and the donating metal loses one, coined redox transmetallation, where the receiving metal is oxidized, and the donator is reduced.

Oxidative coupling and reductive cleavage

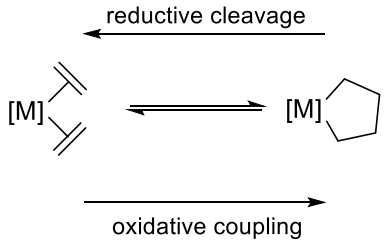

Scheme 2.4 oxidative coupling /reductive cleavage

Oxidative coupling involves the formation of a pi complex, either with alkenes or alkynes. The complexes are then converted into metallacycles via C-C bond linkage. As the name states, the oxidation number of the metal is increased by two as a result by the coupling. The valence electron count is decreased by two, since the two L-ligands (pi complexes) are converted to two X-ligands. The reverse is called reductive cleavage.

This step has a related reaction called 2+2 cycloaddition. Where a carbene-olefin complex converts into a metallacyclobutane (MCB) complex.

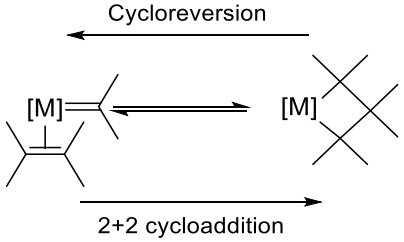

Scheme 2.5 2+2 cycloaddition/cycloreversion

If the carbene is counted as a L-ligand, the metals oxidation number is not increased due to the conversion to two X ligands. Although the valence electron count is decreased by two as the L ligand is transformed to an X ligand.

3. Results and discussion

3.1 CAAC-derived catalysts

3.1.1 Synthesis of HG-C1

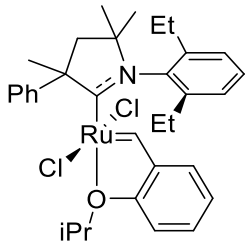

HG-C1

HG-C1 is prepared from Hoveyda Grubbs 1. Generation (**HG 1**), with the addition of the carbene precursor and a base. [54] The base deprotonates the N-double-bonded carbon to generate the carbene, which will substitute cyclohexylphosphine on the precursor (scheme x.x).

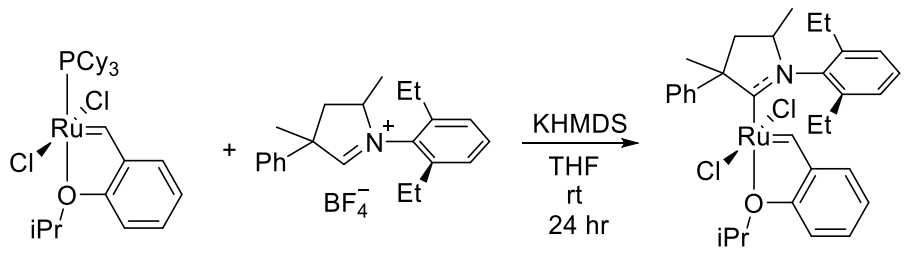

Scheme 3.1 formation of **HG-C1**

For the first run 10 mg (1 eq) **HG1** was reacted with 1-(2,6-diethylphenyl)-2,4-dimethyl-4-phenyl-3,4-dihydro-2H-pyrrol-1-ium tetrafluroborate (2,4 eq) together with KHMDS (2,8 eq) in 3mL THF. The solution was stirred for 24 hours in room temperature. There was a color change from brown to green. The reaction mixture was evaporated, and the residue was filtered through celite and eluted through DCM and concentrated. The alkylidene proton (17,37 ppm) of **HG1** is a doublet due to coupling with phosphine. This doublet was not present in the crude, however two new peaks (17.90-,16.50 ppm) had formed. These alkylidene peaks are associated with the CAAC ligand and are coined rotamers. Due to the CAAC-ligand being non-symmetric, the ligand can be orientated with the nitrogen being cis or trans to the alkylidene, shielding the alkylidene distinctively. The presence of rotamers indicated that the

reaction had gone to completion. A larger run was done with 100 mg starting material instead. This time the crude was purified using flash chromatography (Hexane/EtOAc 8:2), giving a green solid (32mg, 26% yield).

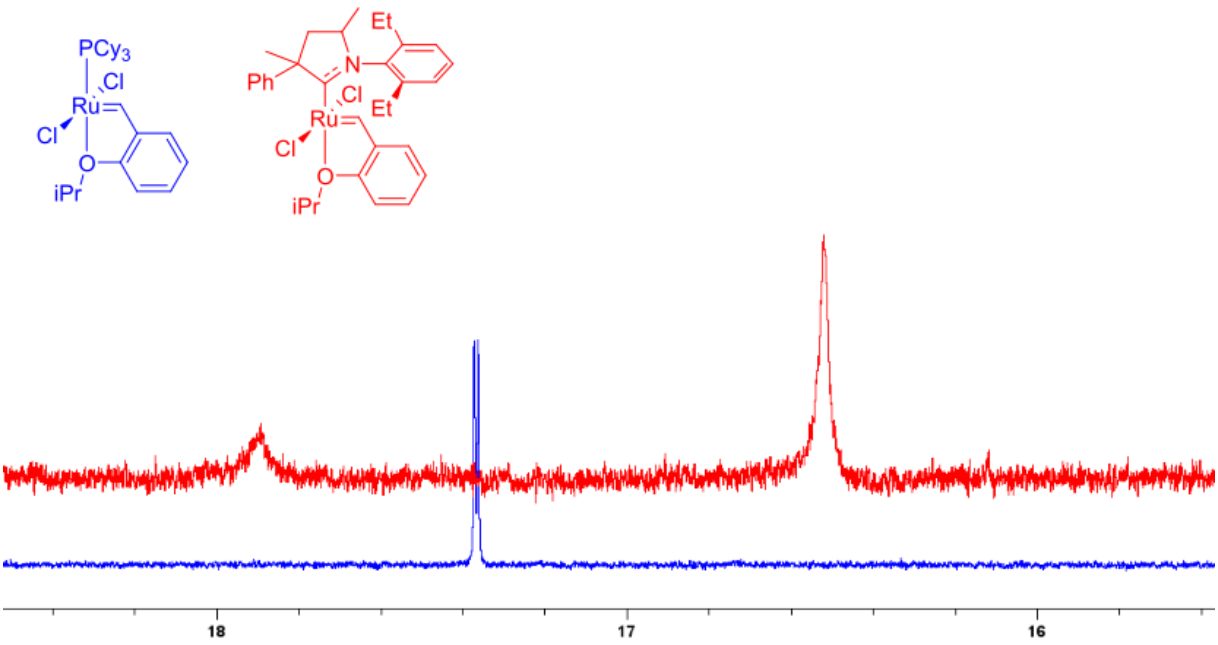

Fig. 3.1 Comparisons of alkylidene peaks

3.1.2 Synthesis of HG-C1-S1

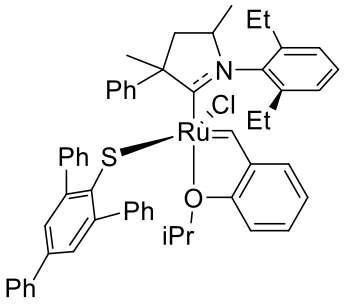

HG-C1-S1

HG-C1-C1 is prepared by reacting **HG-C1** with a thiolate salt.[55] Thiolates are a soft lewis base, whereas chlorine is a hard Lewis base. The thiolate will have a higher affinity for the ruthenium metal center which act as a soft Lewis acid in this case, subsequently replacing the chlorine. The substitution is also favored because of Ru-S bonds are stronger than Ru-Cl bonds.

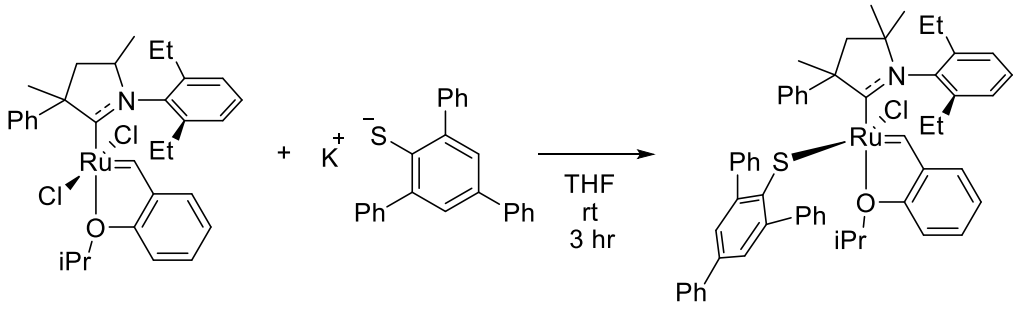

Scheme 3.2 formation of **HG-C1-S1**

The first run was done with 12 mg **HG-C1** and 1,3,5-triphenyl-phenylthiolate (1,1 eq) in 3mL THF. Color change from green to ochre-yellow was immediately apparent. An NMR was taken after 1 hour, indicating that the alkylidene peaks had shifted downfield. This shift is due to the thiolate being a softer Lewis base than chlorine, reducing the acidity of the metal center, subsequently giving some electron density back to the alkylidene carbene. This back-migration of electron density shields the electron, shifting it downfield compared to the dichloride counterpart. However, there was still some precursor left, so the reaction was resumed for two hours, resulting in full conversion, affording 4,2 mg of the thiolate (30% yield). For the second run 29 mg **HG-C1** was used with the same conditions, the crude was crystallized in pentane/toluene affording 14 mg **HG-C1-S1** as nodule-shaped clusters (37% yield).

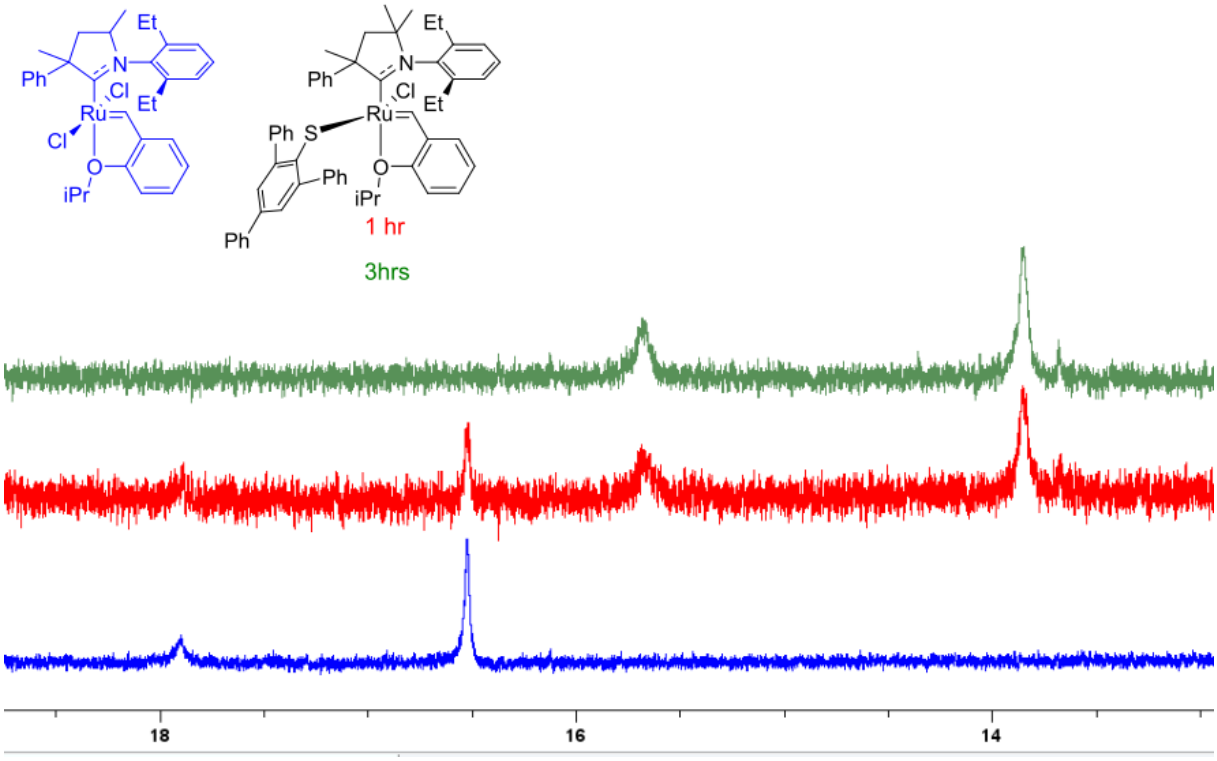

Fig.3.2. Comparisons between HG-C1 and HG-C1-S2 after 1-hour reaction

3.1.3 Synthesis of HG-C1-S2

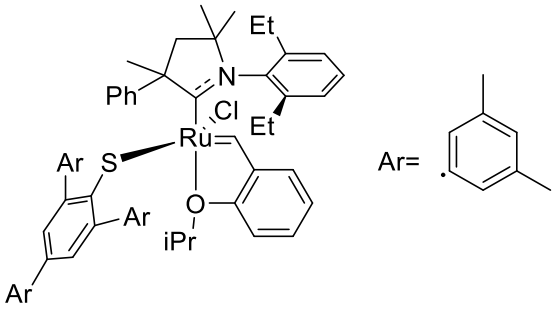

HG-C1-S2

This monothiolate-complex is relatively similar to **HG-C1-S1**, with the difference being each of the three phenyl groups on the thiolate moiety bearing 2,4-dimethyl groups. The complex was prepared using 23 mg **HG-C1** following the same procedure as **HG-C1-S1**, except purification with basic alumina was performed additionally. Crystallization afforded 10 mg **HG-C1-S2** as prism-like crystals (28% yield).

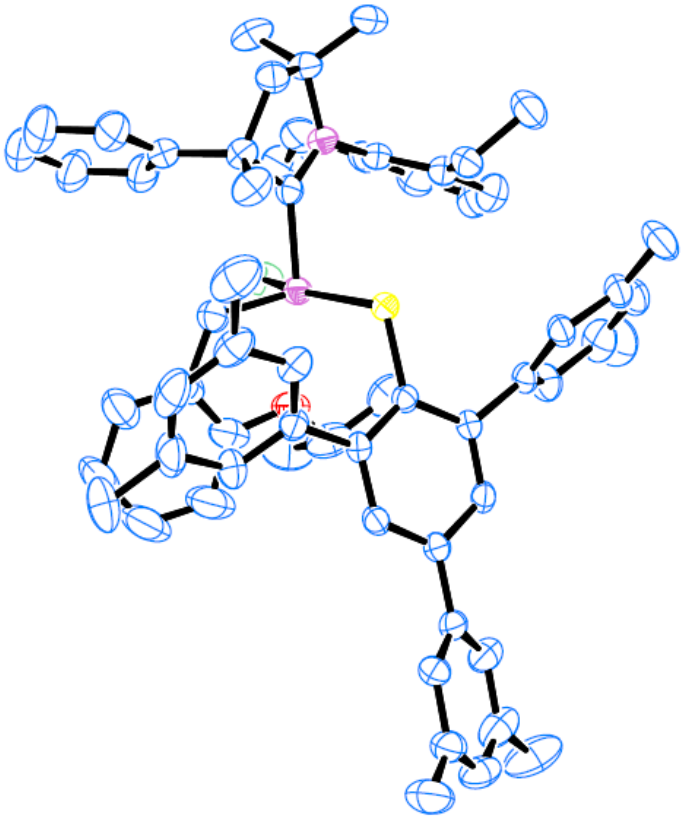

Fig 3.3. Crystal structure of **HG-C1-S2** with 50% probability, hydrogens omitted for clarity, Ru=purple, N=pink, S=yellow, O=red, Cl=green

Table 3.1 Selected bond lengths and angles for HG-C1-S2

	Bond lengths (Å)
Ru-C (CAAC)	1,979
Ru-S	2,311
Ru-C (alkylid.)	1,837
C(CAAC)1-N	1,344
Ru-O	2,325
	Bond angles (°)
Ru-S-C	111,9

As seen in Fig x.x it is visible that the complex constitutes a distorted square pyramidal geometry, as is common for most Ru-based catalysts.[9,20,34,42] A notable value is the bond angle Ru-S-C, (111,9°), which is typical for Ru-thiolates, although higher than the NHC-variants (107,6°)[41]. It is also evident that the Ru-alkylidene bond length (1,837 Å) is smaller than the Ru-C(CAAC) bond (1,979 Å), owing to the more covalent character of the alkylidene.

3.1.4 Attempt at metalating triphenylmethanelthiolate

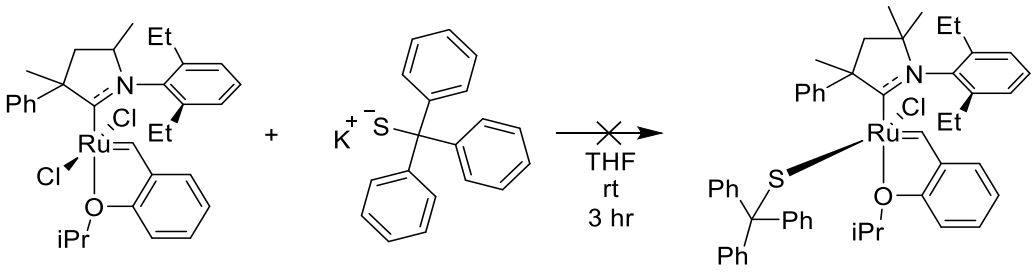

Scheme 3.3 Attempt at metalating the methanethiolate

A metalation of a steric thiolate with a tert-substituted sulfur bound carbon were attempted, following the same procedure as the other thiolates. After three hours the NMR indicated decomposition of the alkylidene. This might be accredited to the electron rich nature of the sulfur atom, which may destabilize the alkylidene. The stable nature of S1 and S2 are due to the delocalization of the sulfur electrons when the sulfur substituted directly to an aromatic system, compared to when the sulfur is substituted to a triphenylmethane. Steric factors may also play a part, if the thiolate is coordinated, the steric populations might be highly strained, extruding the alkylidene.

3.1.5 Synthesis of ng-C1-S1

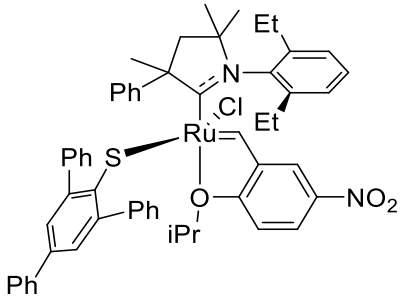

nG-C1-S1

The nitro-Grela (**nG-C1**) catalyst exhibits properties such as high activities and fast initiation times, although low stereoselectivity.[20] It was suspected that chlorine substitution with thiolate would affect selectivity. 30 mg **nG-C1** was used following the same procedure as the other thiolates, yielding a brown solid after crude purification and crystallization.

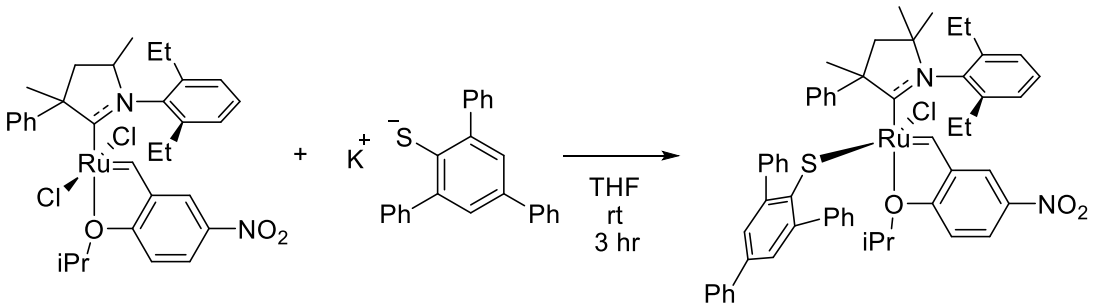

Scheme 3.4

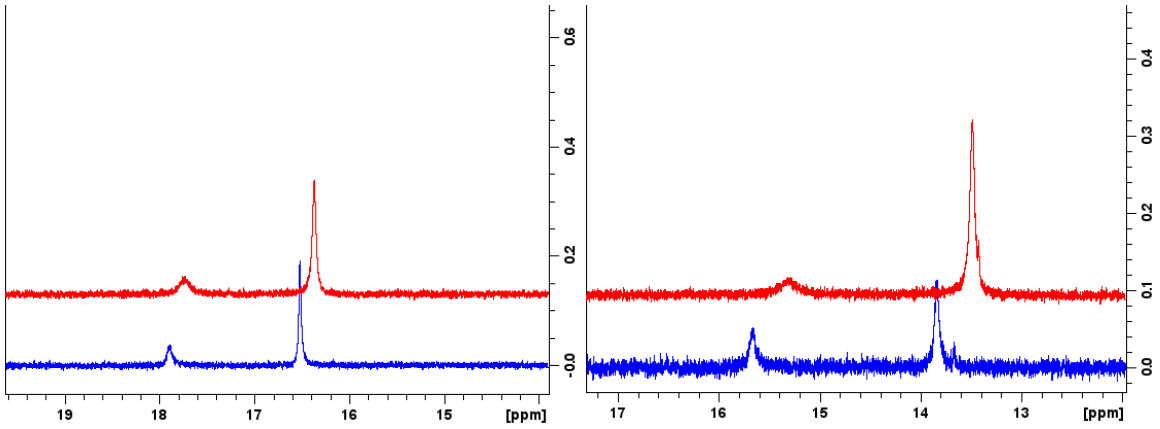

Fig 3.4 Alkylidene-peak comparisons between Hoveyda (blue) and nitro Grela(red) catalysts with different X-ligands; chloride and thiolates presented respectively.

It should be noted that the alkylidene peaks for nitro-Grela are shifted (**fig 3.4**) downfield compared to HG, due to the electron-withdrawing effect of the nitro-group. This is also evident when metalating the thiolate to the **nG** catalyst, indicating that the metalation was successful.

3.1.6 Synthesis of nG-C1-NCO

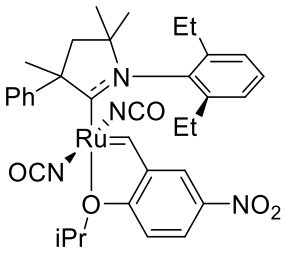

nG-C1-NCO

Isocyanate ligands are known as pseudo-halogens, as they exhibit similar properties, although the isocyanate is linear and is less sterically demanding, as the nitrogen is smaller than the chlorine it replaces. The isocyanates are prepared using **nG-C1** and silver cyanate, the cyanate undergoes tautomeric rearrangement such that the nitrogen bears negative charge, which will substitute the Ruthenium-bound chlorides.

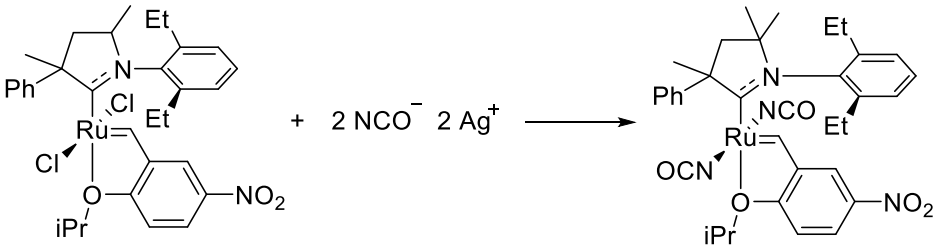

Scheme 3.4 Formation of **HG-C1-NCO**

The first run with 30 mg **nG-C1** was unsuccessful as the amount of silver(I)cyanate used was only 2,2 equivalents. The second run as corrected using 25 mg **nG-C1** and 3,2 eq cyanate resulting in 76% yield. The alkylidene peaks for **nG-C1** and its respective isocyanate are congruent, indicating that the electronic properties are similar, hence the name pseudo-halogens.

3.1.7 Catalytic tests

Determining stereoselectivity

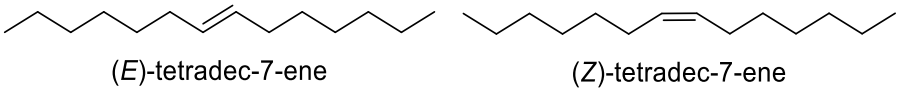

(*E*)-tetradec-7-ene (*Z*)-tetradec-7-ene

The product region 5,30-5,40 ppm contains both the Z and E stereoisomers, the E-isomer is more downfield due to the increased coupling constant between the protons on each side of the double bond, since coupling constant is dependent on factors such as the length between the coupled protons. Each multiplet for the products account for two protons. The substrate multiplet at 4,90-5,00 ppm is in fact two quartets (4,97 ppm) and two double triplets (4,91 ppm), which collectively accounts for two protons. This complex splitting pattern stems from the interaction at the same side and across the double bond since the substrate has vicinal and geminal protons. It is possible to determine the concentration of the substrate and the product by quantitative integration. This means that the substrates multiplets are integrated once while the product region is integrated twice, this discrepancy in integration is due to the fact that two substrate molecules are needed to yield one product molecule.

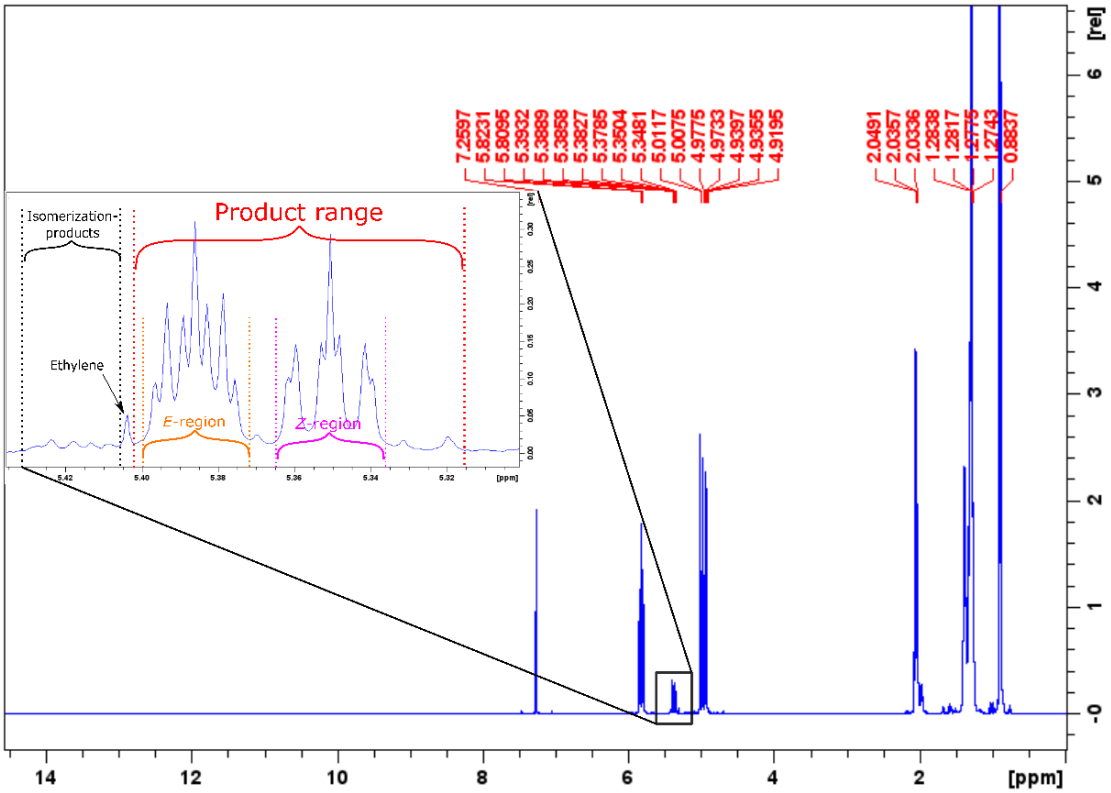

Fig 3.5 NMR spectra of a typical CM of 1-octene (ranges included)

The stereoisomer-region is in reality larger than shown in fig x.x, as the peaks are rather complex, and contain satellites. However, due to peak overlap it is reasonable to compare the two using the outlines as demonstrated. The turnover number (TON) is estimated by multiplying the yield-percentage by the respective loading divided by two. As two substrate molecule form one product molecule. As an example, for 1ppm loadings the yield is multiplied by 500K, so if the yield was 62%, the TON would be 310K. Cross metathesis of 1-octene is used as a benchmark in this thesis. The method of analysis was NMR, although GC should be used instead as it has better sensitivity in addition to separating the different compounds.[56]

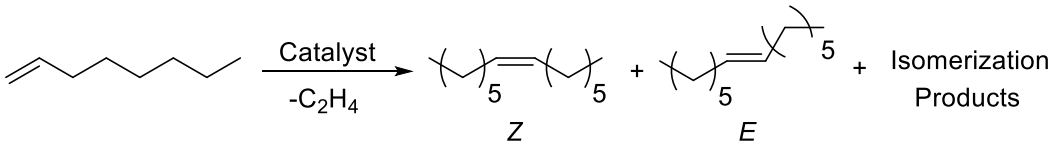

Scheme 3.5 Metathesis of 1-octene and its respective products

3.1.8 HG-C1-S1 and S2 vs HG-C1

Table 3.2: Catalytic properties of 1 ppm loading at 60°C for 24 hours

1 ppm,24 hr	Conversion (%)	Yield (%)	Iso (%)	%Z	TON (K)
HG-C1-S1	40,4	38,4	2,0	39	192,2
HG-C1-S2	38,1	35,5	2,6	41	177,3
HG-C1	78,5	76,6	1,9	26	383,0

Table 3.3: Catalytic properties of 10 ppm loading at 60°C for 24 hours

10 ppm,24 hr	Conversion (%)	Yield (%)	Iso (%)	%Z	TON (K)
HG-C1-S1	29,9	18,6	11,3	30	9,3
HG-C1-S2	54,3	42,7	11,5	34	21,4
HG-C1	61,8	57,9	3,8	34	29,0

Table 3.3: Catalytic properties of 10 ppm loading at 60°C for 24 hours

100 ppm, 72 hr	Conversion (%)	Yield (%)	%iso	%Z	TON (K)
HG-C1-S1	76,5	70,1	6,3	26	3,5
HG-C1	86,0	80,5	5,4	20	4,0

Overall **HG-C1** performed better than the thiolates, as it is both more active and less isomerizing as seen in the tables above. The S2 variant performed better than the S1 variant in terms of less overall isomerization regarding the 10 ppm loadings, as the S2 variant handled ethene choking well, compared to HG-S1. Ethene is detrimental to the cross metathesis-catalytic cycle, as the catalyst is able to coordinate to it, enabling ethylenolysis and beta hydrogen elimination. The S2 variant exhibited the lowest isomerization values under choking (**appendix1-4**), however the HG-C1 had the lowest isomerization numbers overall. All thiolates exhibited overall higher Z-selectivity than their dichloride counterparts, although the selectivity for the thiolate diminishes with higher loadings and longer reaction time, attributing that the E-isomer is more thermodynamically stable. The ratio in selectivity did not compare to the monothiolate-NHC catalysts used by Occhipinti and colleagues, this might be accredited to that thiolates might not be as compatible with CAAC's compared to NHC regarding both Z-selectivity and activity. As the Ru-S-C bond in the reported NHC complexes are 107,6°C, compared to 111,9° in HG-C1-S2, which are less acute.[41] This increase in the bond angle might weaken the steric effect of the thiolate, which were expected to favor the syn-pathway over the anti. The comparisons with respect to overall steric bulk are also significant; in the CAAC-thiolate the phenyl on the quaternary (CAAC)carbon is oriented away from the thiolate moiety, increasing the steric bulk anti to the thiolate, while also not forcing the thiolate downwards, as was the case with NHC's. These characteristics are unfavorable regarding selectivity. Still, the thiolate does increase the Z-selectivity, although not in a significant manner.

3.1.9 nG-C1-S1 vs nG-C1

Table 3.4:

0.1 ppm, 30 min	Conversion (%)	Yield (%)	%iso	%Z	TON (estim)
nG-C1-S1	3,0	2,5	0,9	36,6	125,4
nG-C1	12,3	12,0	0,6	40,0	599,4

nG-C1-S1 performed poorly with low loadings in the 0,1-ppm range. In some runs the product-region was so obscure that determining yield and selectivity were challenging. There is however an outlier in entry 3, where the conversion is about 12%, this should be disregarded. Regardless, the runs for the thiolate exhibited low activity at low loadings overall, hinting to that beta-hydride elimination might be the culprit regarding these low activities. The Z-selectivities were low, which were around or under 40%. nG-C1 however, vastly outperformed the monothiolate, the different runs resulted in a median of 12,4 % yield, relating to a TON of 620K. The initiation of the nG-C1 were remarkable, as all reactions had reach completion after 1 hour, and exhibited little to no change after this mark. The results of the nG-C1 cat were not unexpected, as the CAAC catalysts are resilient to beta-hydride elimination allowing activities at low loadings. The fast initiation is facilitated by the electron withdrawing groups. The monothiolate however, might initiate quickly, although slower than the dichloride counterpart, but then decompose almost instantaneously in most cases.

Table x.x Values for higher loadings of nG-C1

nG-C1-S1 performed better at higher loadings, as beta hydride elimination is less of a concern. 1-10 ppm showed slightly better Z-selectivity over 40%, compared to around or under 40% for 0,1 ppm. However, the Z-selectivity diminished after loadings over 50 ppm. nG-C1 exhibited good activities at 1 ppm loadings, and favorable conversions for all loadings. The isomerization in the runs varies, for instance the thiolate exhibited less isomerization in the 10 ppm. However, when the reaction involving 100 ppm is unable to vent ethene, the choking is significant for the monothiolate, as respective isomerization is twice that of nG-C1. In summary, nG-C1-S1 performs worse overall compared to nG-C1. The results for low-level catalyst loading indicates that the thiolate-based catalyst have higher susceptibility for beta hydride elimination, essentially trading out the ability that made the Ru-CAAC-catalysts so attractive. However, the thiolate might prevent BMC at higher loadings, but higher loadings deem inefficient as there are diminishing returns for the increase of loading as 10-100 ppm is more than sufficient for the nG-C1 in this type of metathesis.

3.2 Ligand-precursor synthesis

The synthesis of 1,3,5-trimesitylpyridinium has been reported by Huang and Brown[57] . They were able to metalate it to Copper. It's applications in ruthenium-chemistry and olefin metathesis are not yet reported. Their procedure begins with 3,5-dibromopyridine, which undergoes Suzuki-Miyaura coupling, nucleophilic aromatic substitution, anion exchange, and finally a Zincke-reaction. There were several hurdles in the process with respect to reaction conditions and isolation, however these were addressed after several attempts.

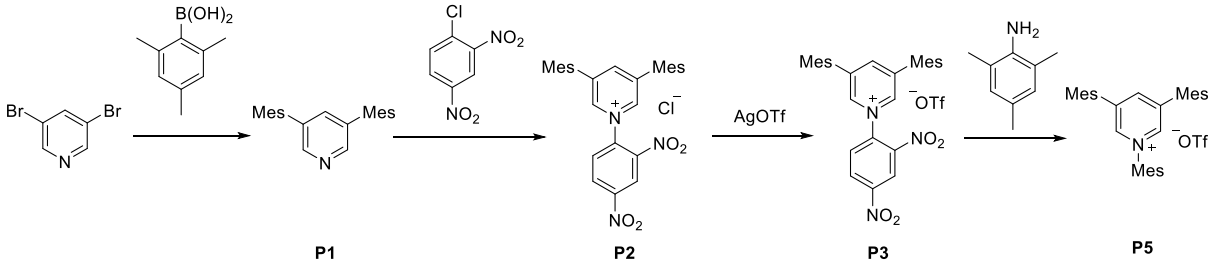

Scheme 3.5 Synthetic pathway of target molecule

3.2.1 Suzuiki- **Miyaura** coupling

The first step is a Suzuki-Miyaura coupling. This is an effective C-C bond formation reaction, involving a halogenated starting material, a boronic acid, a base, and a palladium-based catalyst. The reaction proceeds through a catalytic cycle.

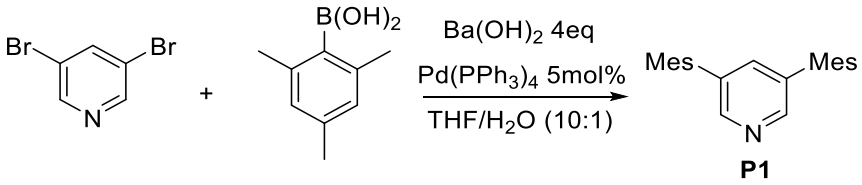

Scheme 3.6 Formation of 3,5-dimesistylpyridine (**P1**)

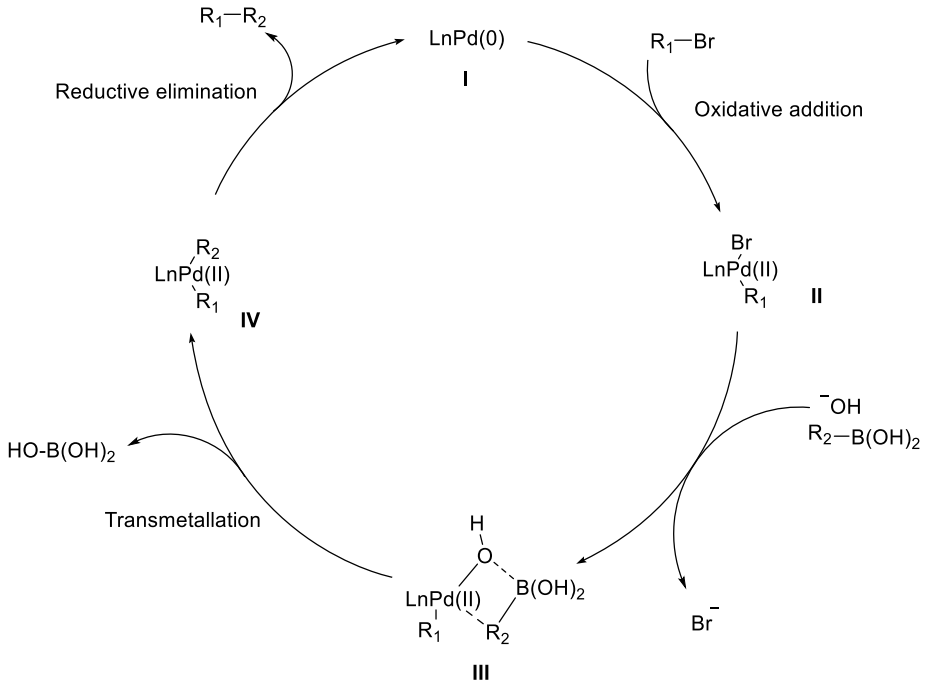

Scheme 3.7 Catalytic cycle of the Suzuki coupling

The starting material bonds with the catalyst through oxidative addition, forming **II**. The bromine gets substituted by a hydroxy-group, then the boronic acid coordinates between the metal complex, with the R-group coordinated to the metal, while the boron coordinates to the hydroxy-group, forming the cyclic intermediate **III**. The intermediate undergoes transmetallation, extruding boric acid as a leaving group and resulting in intermediate **IV**. Intermediate **IV** undergoes reductive elimination, finalizing the cycle with the product and the initial catalyst. It should be noted that this cycle occurs two times for the formation of the product, since the starting pyridine is di-bromo substituted. The reaction needs to be carried out in oxygen free conditions due to the phosphine ligands on the palladium being oxygen sensitive.

The first small scale run with 412 mg 3,5-dibromopyridine, and 829 mg boronic acid, which were refluxed for 24 hrs under argon atmosphere, resulting in a yellow slurry. The reaction mixture was quenched with water and extracted three times with ethyl acetate, with the white boric acid remaining in the water phase. The organic phase was evaporated and chromatography with EtOAc/Hexane (1:15, 1:10) was performed, yielding 536 mg of **P2** as off-white crystalline solid. The yield was a bit better than what the paper stated, 97% compared to 73%. This might be credited to the use of degassed water, and the presence of argon, which

ensured an oxygen free environment. Argon is heavier than nitrogen, which the paper used as an inert atmosphere, with the heavier gas the reaction mixture is safeguarded from convection of air in the minor gaps of the system. The presence of oxygen is detrimental to the palladium catalyst, which is vital to ensure the completions of the two cycles needed for the product. The larger scale was done with 2,00 grams of 3,5-bromopyridine the same conditions, which yielded 2,14 g of **P1** (80% yield). Additionally, 527 mg of slightly impure product was also isolated.

3.2.2 Zincke salt formation

The second step is the formation of the zincke salt. This reaction is an aryl substitution reaction (abbreviated SnAr)[37], which involves the bismesitylpyridinium substituting the chlorine on 1-chloro-2,4-dinitrophenyl (Cl-DNP). The DNP substitution is vital for the last step, due to the nitro-groups facilitating the Zincke-reaction. [58]

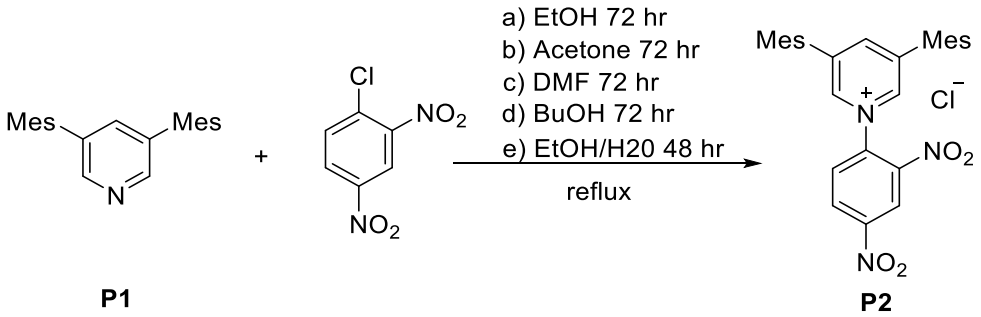

Scheme 3.8 3,5 bismesitylpyridine (**P1**) reacting with Cl-DNP in several solvent systems to yield the Zincke- salt

The reaction commences with the pyridinium attacking the *ipso*-position of the DNP, forming a Messenheimer complex, which is stabilized by resonance promoted by the electron-withdrawing nitro-groups This allows for the electron rearrangements, such as the chloride leaves, however there are instances were the pyridine leaves as well, resulting in the starting materials. If the reaction conditions are beneficial, the product is more favorable than the substrate, forming the Zincke salt. [59]

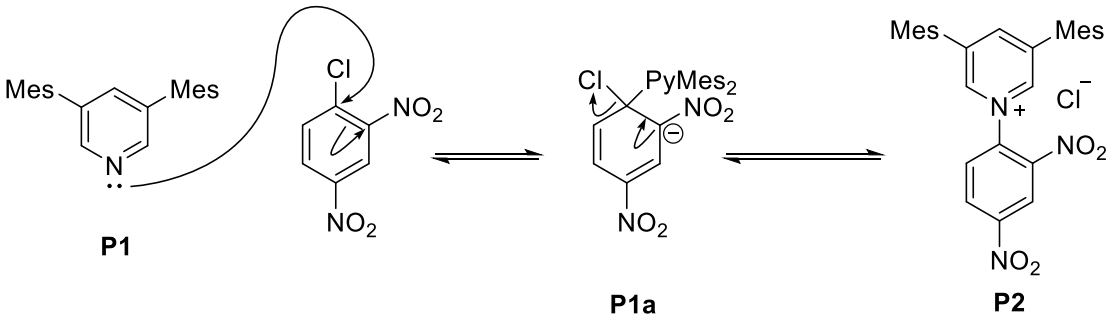

Scheme 3.9 SnAr mechanism of the formation of **P2**

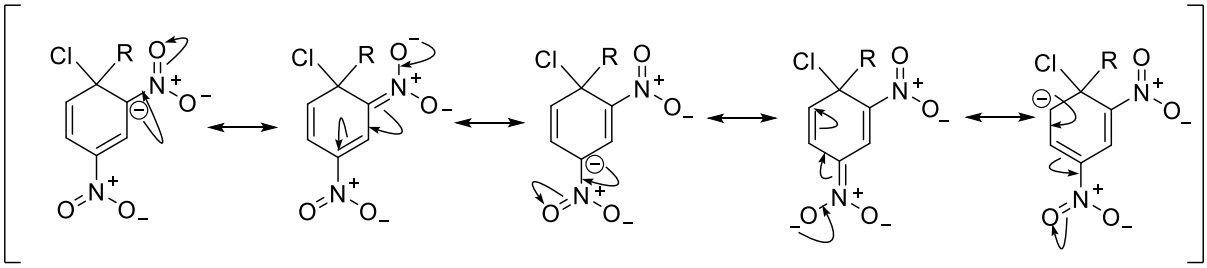

Scheme 3.10 Resonance of intermediate **P1a**

The first run was done with 250 mg 3,5-bismesityl-pyridine (**P1**) and 1.5 eq Cl-DNP, which were refluxed for 72 hours in ethanol, resulting in an orange solution. After evaporation of the ethanol, acetone was added to the crude, resulting in off-yellow precipitate in small amounts. NMR were taken, which exhibited peaks with different shifts compared to the original procedure. It was feared that the reaction was unsuccessful, so a new run with 250 mg **P1** was prepared under argon. The same situation occurred after analysis of the crude; the peaks were not similar to the target. However, the peaks were similar to the next step, where the only difference where the anion, as chloride is exchanged to triflate. This might be caused by the higher concentrations in their NMR sample, as the concentrations used in this case were low, as chloride might interact with the shift. Regardless, purification was commenced with flash chromatography using DCM/MeOH (80:20) yielding a yellow solid, which were impure. The original procedure used acetone as a precipitating agent after chromatography, but acetone were only precipitating parts of the presumed product. Diethyl ether was used instead, and worked better, precipitating in ether yielded 85,8 mg **P2** as a yellow-white solid (20% yield). This yield was quite far from the original paper, which achieved 67%. To investigate the poor

yield further, several attempts were done. The most common method of preparing the Zincke salt is using acetone as a solvent, as the product is usually insoluble in this medium.[60] The precipitation of the product during the reaction shifts the equivalence favoring the product. With this in mind, acetone was used for the first run, 1g of **P1** was used, together with 1,5 eq of Cl-DNP. After 72 hours, the solution had an orange tint to it, NMR indicated that nothing had evidently happened. This might be due to the steric substituents on the pyridinium, as more substituted pyridines need higher temperatures to undergo the SnAr required. To remedy this, DMF was used instead, since it has similar properties to acetone (polar, aprotic), but has higher boiling temperatures. 72 hours at 160°C resulted in a red solution, NMR showed nearly complete decomposition. This was highly unfortunate, and a reinforcement to that even if the conditions seem reasonable, smaller scales should always be done first. Several runs were done, with 1-butanol and ethanol, butanol seemed like a good candidate as the product might be soluble in water, while the substrates are not, so extraction in water might be possible as a workup. Two small scale reactions were done in parallel with ethanol and butanol, constituting each of 50 mg **P1**. After 72 hours in reflux, both runs resulted in a minuscule amount of precipitate when using diethyl ether, and the product was not that pure, chromatography was not performed as the amounts were small. Another reaction in butanol was carried out, using 169 mg **P1**, this resulted in an orange solid similar to previous runs, however when doing TLC in pure ethyl acetate, it was revealed that the product was stagnant, while the substrate and side-products were eluting. A silica plug was then used with 3 volumes of EtOAc, following 3 volumes of MeOH, resulting in 97 mg **P2** as slightly orange crystals (30% yield). Zeghib and colleagues[61] tested the stability of a Zincke salt in different solvents at elevated temperatures in a paper. They found that Zincke salt decomposes completely in acetonitrile, which is a polar aprotic solvent, related to acetone and DMF. They also found that alcohols facilitate decomposition as well, but with the rate decreasing with acidity (MeOH<EtOH<iPrOH) as the increased solvation of the chloride prevents it from attacking. The proposed mechanism is the reverse of **scheme 3.9;** the chloride attacks the salt at the ipso-position, extruding the pyridine. They also found that water was the best stabilizing agent for the salts. Considering this, a run was done in ethanol and water (70:30), with 153 mg **P2**, an NMR was taken 24 hours during the reaction, and it indicated few side products, and almost full conversion. Regardless, the reaction was left for 48 hours total. Workup with silicaplug yielded 170 mg **P3** as pale orange crystalline solid (69%) yield. This yield was quite better than

the previous runs and demonstrated that water did in fact stabilize the reaction. As the water solvates the chloride, the water would rather stay solvated than react with the product, shifting the equilibrium. An additional reaction was done with the same procedure, using 154 mg **P2**. Workup resulted in 217 mg **P3** (88%). This reaction was somewhat better than the previous one, due to some minor spillage under purification. Regardless, zincke-salt formation in water have not been reported before, so this might be a helpful discovery for future reactions. An additional method for this reaction could be performed using silver triflate as a secondary substrate in ethanol; the silver binds to the chloride when it leaves, precipitating out, and triflate is weak nucleophile that will not attack the pyridinium product.

3.2.3 Anion exchange

The third step is a facile anion exchange. The silver triflate solvates in the solution, where silver and chloride form a salt, which is insoluble in chloroform. The triflate salt remains in solution.

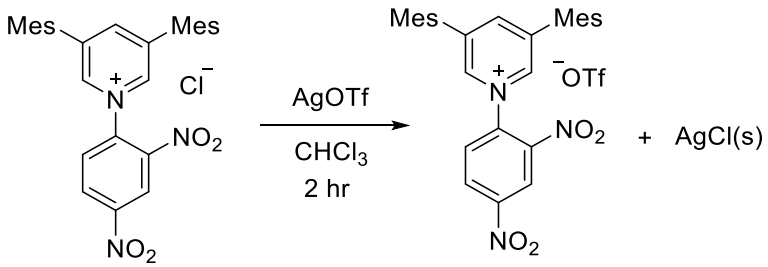

Scheme 3.11 Anion exchange with silver trifluoroethane (triflate) sulfonate

All runs developed accordingly: After solvation of the Zincke salt and addition of silver chloride, white precipitate was formed. There was an increase of precipitate over the course of two hours. Filtration and evaporation yielded a white-yellow crystalline salt. NMR was usually avoided, as the anion exchange bear few possible side-reactions. However, an NMR was taken with the product from the precursor which had been done in ethanol and water (70:30). These was unexpectantly shifted. This might be due to some hydrates being formed. There was a concern that the water in step 2 was substituting the pyridine instead of DNP, this was not the case as the final step with the aqueous-made salts proved successful. It was likely then due to the anion changing the shifts, which is possible for aromatic substances.[62]

3.2.4 Zincke reaction

The last step is called zincke reaction, where the DNP group is substituted with an aromatic group (scheme x.x). The preceding anion exchange is important before performing the zincke reaction, as chlorine can attack the reagent, and also intervene in the intermediates.[58]

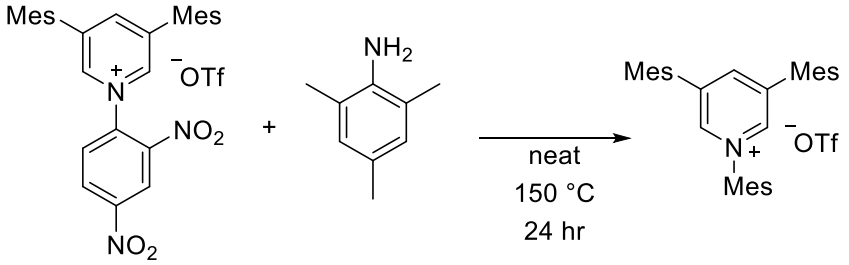

Scheme 3.12 Zincke reaction in neat mesitylamine

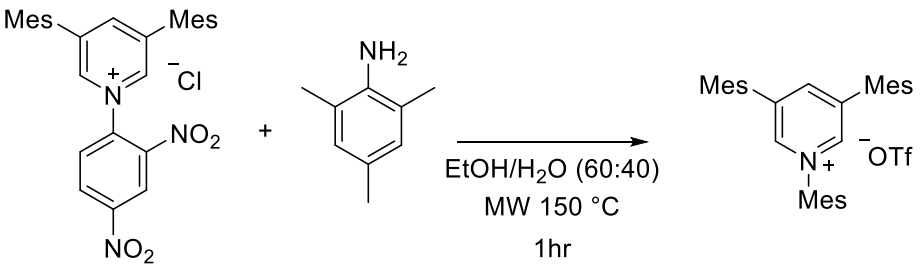

Scheme 3.13 Zincke reaction in microwave

The reaction initializes with the aniline attacking the 2-position of the pyridinium salt, the following intermediate is deprotonated by a new aniline molecule, forming an ammonium salt with the triflate. Intermediate **II** undergoes proton rearrangement, subsequently performing a ring opening and forming an imine (**III**). The imine deprotonates the ammonium salt, regenerating the aniline and forming **IV**. An aniline nitrogen attacks the nitrogen bonded carbon in the remnant of the pyridine moiety, extruding dinitroamide and forming intermediate **V**. The amide and **V** undergo a proton exchange, yielding Intermediate **VI** that gets deprotonated, forming intermediate **VII** which undergoes isomerization between cis and trans isomers. The trans-cis equilibrium is suspected to be the rate determining step. The cis isomer allows ring closure through a sigmatropic rearrangement, forming **VIII**. **VII** deprotonates an ammonium salt, forming **IX,** which allows for the elimination of aniline, resulting in the final product. [58]

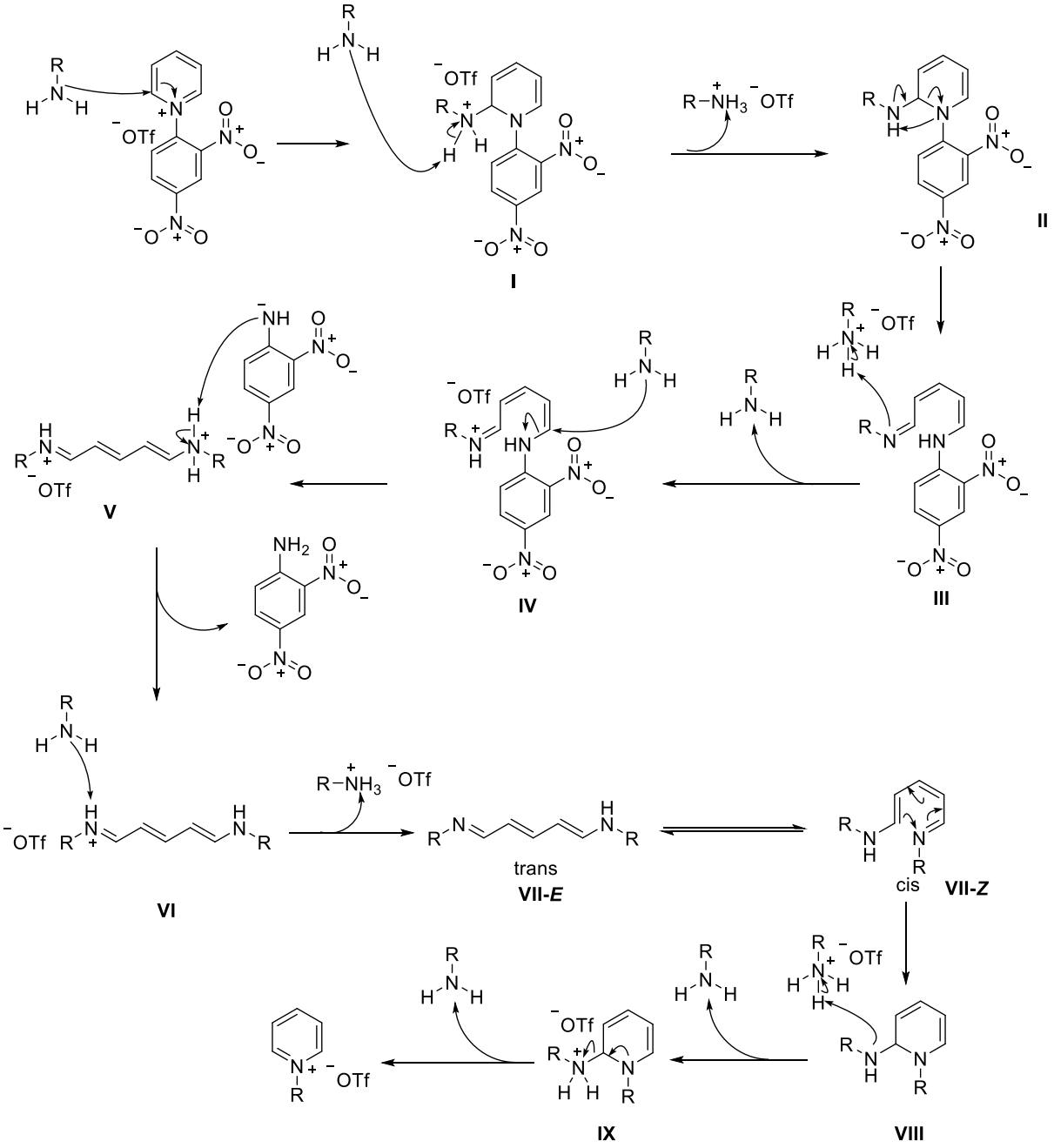

Scheme 3.14 proposed mechanism of the Zincke reaction

The first run was done with 104 mg **P4** in neat 0,7 mL mesitylamine for 24 hrs at 150°C. The amine act both as a reactant and solvent, hence the term neat. The reaction was performed in a reactor; a vial with a durable cap, suitable for higher pressures. The color of the mesitylamine changed in an instant from slightly brown to black when in contact with the salt, due to the highly reactive aniline. After 24 hours the dark-brown solution was cooled down and, flash chromatography with DCM/EtOAc, was performed. The paper used kugelhröhr distillation to remove the excess high boiling point aniline, but this was not available. The purification resulted in **P5** as a dark-brown solid, (30 mg, 42% yield). The peaks from NMR were agreeable with the reference. The neighboring fractions from the purification were solvated in DCM and hexane which after a week exhibited crystal growth. The crystals were fluorescent, emitting blue-cyan light, this indicated the pi-acidity of the ligand. An additional run was done following the procedure from Zeghib et al. As they tested the stability of Zincke salt with chloride as anion in different solvents, they concluded that a mix of water and ethanol was able to stabilize the reaction; As chloride is detrimental to the reaction, since it can both act as a nucleophile on the reagent, as well as the starting material. 97 mg of **P4** was solvated in 1mL EtOH/H_2O (60:40) and combined with 3 equivalents of mesitylamine, which were microwaved at 140 °C for 1 hour. The initial target temperature was 150°C, but as the radiation system was too efficient, a spike in pressure-rate occurred, activating the failsafe. The reaction mixture was purified according to procedure, using a flash plug with EtOAc, (and more), resulting in an orange solid. This orange solid was not pure and did not exhibit the same properties with respect to emission, compared to the previous experiment. However, when treating the orange solid with silver triflate, the solution exhibited the same fluorescent properties as the brown solid, indicating that the reaction was successful. NMR indicated some product, but this was mostly impure, as the silica plug was insufficient at removing all impurities. The first procedure was then attempted once more, except that the substrate was from the water modified second step. Using 142 mg **P4** and auto flash-chromatography as purification method, the attempt resulted in 62 mg **P5** (43% yield).

3.3Attempts at synthesizing the new Ru-carbene class

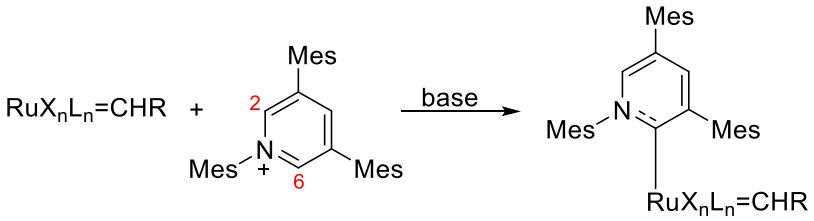

Scheme 3.15 General scheme for the metalation of the ligand, with deprotonation sites for the pyridine.

Yuan Huang and M. Kevin Brown had successfully metalated the pyridinium based carbene, using KOtBu and CuCl. However, in this case the carbene was rather challenging to metalate with ruthenium (and silver for that matter), several methods were tested:

3.3.1 HG 1.gen as precursor, KHMDS and AgCl

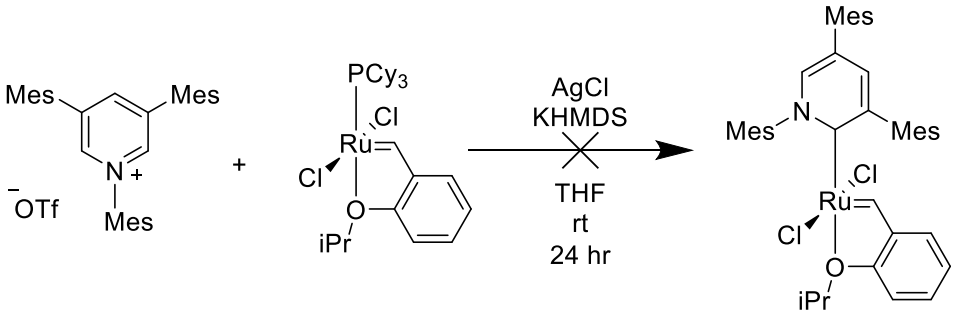

Scheme 3.16 Attempt at using **HG1** as precursor, with base and phosphine scavenger.

The first attempt was performed using 4,6 mg ligand, **HG1** (0,89eq), KHMDS (1,16 eq) as and AgCl (10 eq). It was expected that the potassium base would deprotonate the 2- and 6-carbon-bound hydrogens in the pyridinium salt, forming the free carbene which would substitute the phosphine. The substitution would be facilitated with the presence of AgCl, a common phosphine scavenger. However, NMR indicated no change in the alkylidene-region after reacting at room temperature for 24 hours. As mentioned, the alkylidene-peak for the mono-phosphine is a doublet, and if the metalation were to be a successful, this doublet would be replaced with a singlet, or several singlets if the ligand is unsymmetric.

3.3.2 **Metalation with silver(I)oxide**

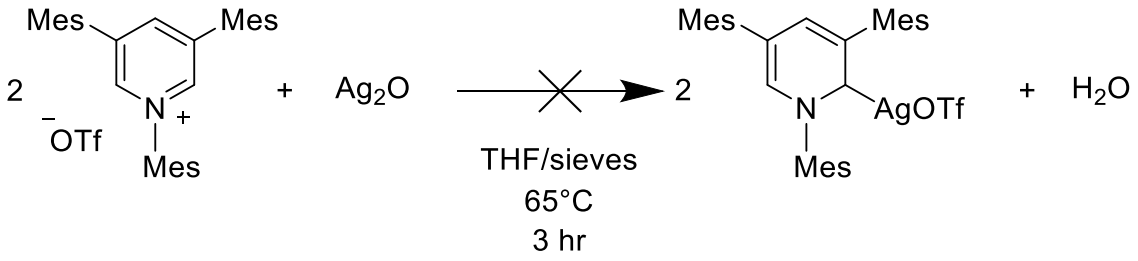

Scheme 3.17 Attempted ligand-silver metalation

This attempt was done with 3,8 mg ligand, Ag_2O (2eq) in THF containing molecular sieves. The silver oxide is quite basic, so it was suspected that it would deprotonate the pyridinium salt, binding with the anion, and form the silver (II) carbene and water (hence the sieves). This approach is successful for NHCs [63], but it did not work with the pyridinium. NMR indicated that there was no change in the starting material, as the doublet at 8,7-8,8 ppm accounting for the 2-and 6- carbon bonded proton remained unchanged, it was evident that no deprotonation had occurred.

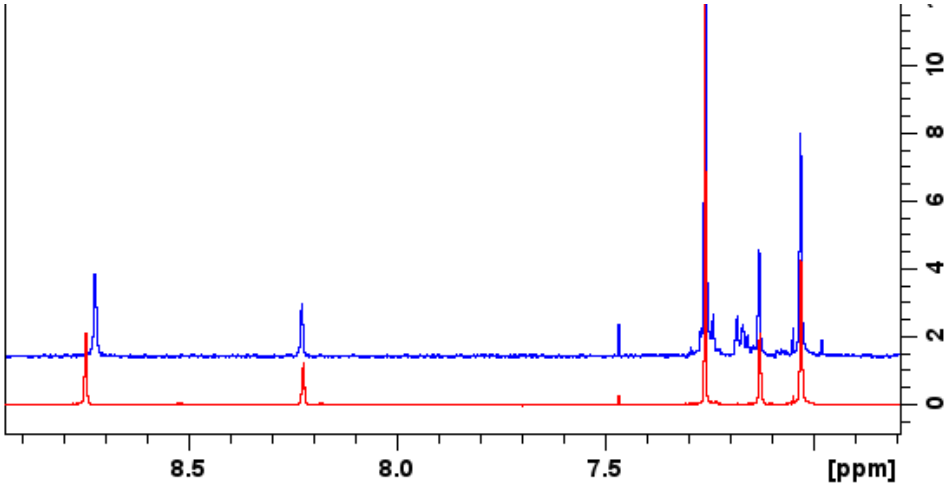

Fig 3.6

3.3.3 **Metalation with Silver(I)Chloride and LiHMDS**

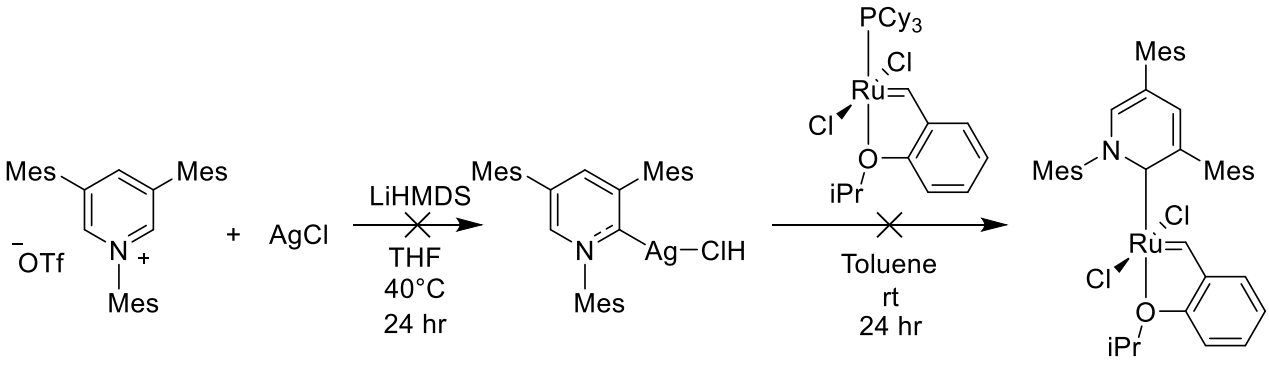

Scheme 3.7

This attempt was done with 3,8 mg ligand, LiHMDS (1,5 eq) and AgCl (1,3 eq) in THF at 40°C for 24 hrs. The ligand exhibits an initial brown color in solution, after reacting with the base the solution changed from brown to green. The green mixture was left to react for 24 hours, afterwards the evaporated reaction mixture exhibited a yellow color. The rather chaotic NMR spectra indicated that something had occurred (fig x.x), but the doublet at 8,75 ppm remained stagnant. Regardless, the 2,7 mg of the reaction residue was combined with 2,3 mg of HG 1.gen in toluene at ambient temperatures. After 24 hours, NMR indicated that the alkylidene remained unchanged.

3.3.4 Ru-p-cymeneCl2-dimer as precursor

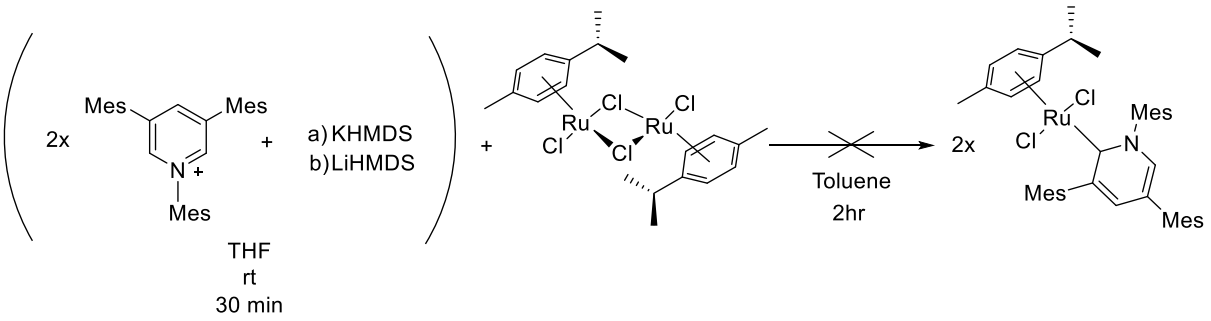

Scheme 3.8

The Ru-dimer complex is a pre-catalyst for several processes such as hydrogen-transfer reactions. Due to the lack of an alkylidene, the complex would seem rather unfit for olefin metathesis. However, in solution the dimer monomerizes, forming an 14e complex, which under the right conditions dissociates the η^6 p-cymene (an L_3-ligand) to form an methylidene in-situ. [64]Two runs were done as two-pot reactions, meaning the ligand and base was stirred separately in THF for 30 min in ambient temperatures, before being treated with the p-cymene complex in toluene solution. Two separate bases were used: KHMDS and LiHMDS, respectively. Reacting the 2 mg pyridinium salt with KHMDS (1 eq) resulted in a color change from brown to red. After treatment with an orange solution of the pre-catalyst (0,5 eq) the color shifted to a more reddish orange. Conversely, 4,2 mg with pyridinium salt and LiHMDS shifted the color from brown to green, after adding the p-cymene-solution the mixture became greenish orange. NMR indicated that doublet for the N-bonded pyridinium carbons were slightly shifted up field in the KHMDS reaction. Conversely the shift was even higher for the reaction mixture with LiHMDS, and evidence that the doublet might have been converted to a singlet, indicating metalation. The metalation with LiHMDS seems incongruent with the other attempts with this base, however it might be the case that the carbene metalates to Lithium. This is possible due to the small ionic radius of Li^+, which with the presumed strong sigma donation for the ligand, might form a strong C-Li bond, disenabling transmetallation.

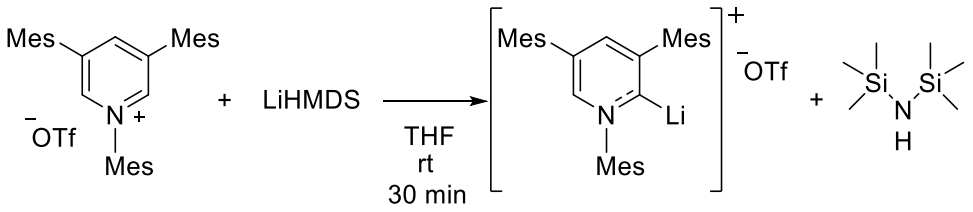

Scheme 3.9 The ligand metalating to lithium.

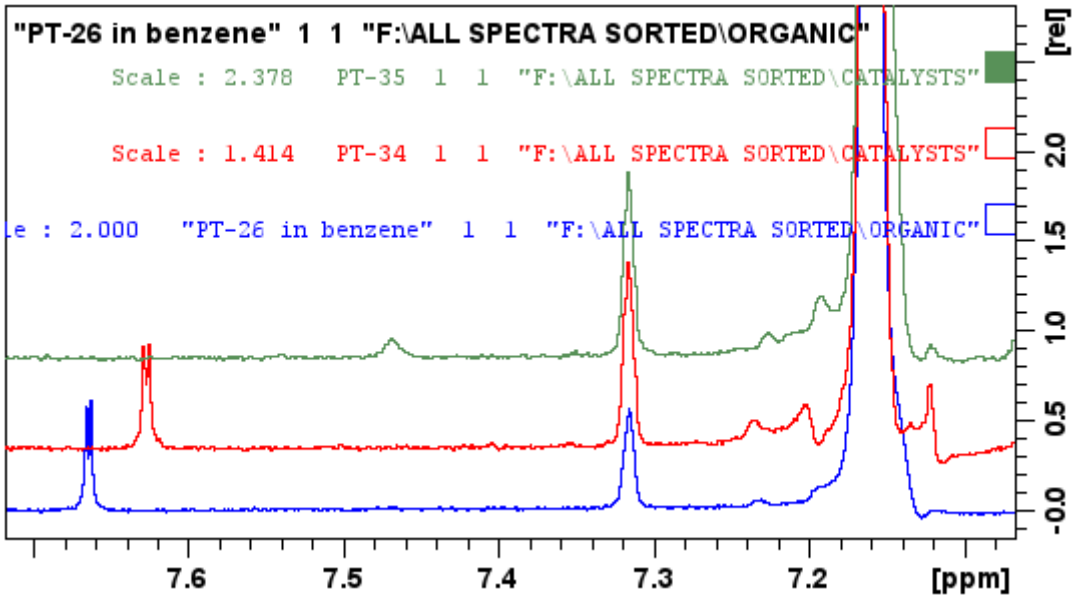

Fig 3.7 LiHMDS in green, KHMDS in red, Ligand in blue

3.3.5 Grubbs 1. gen bis-pyridine as precursor

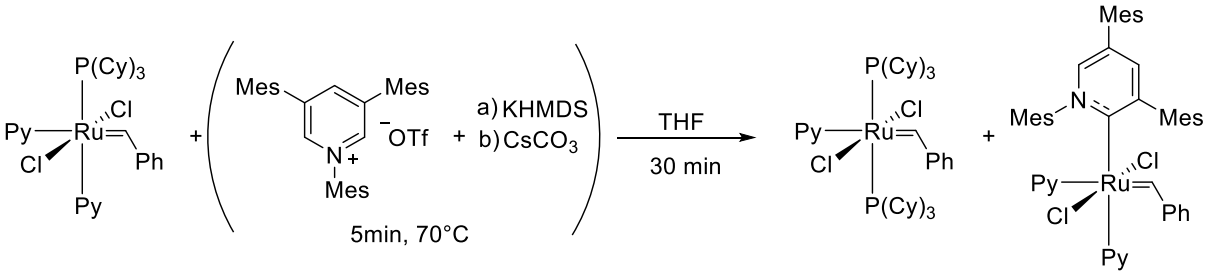

Scheme 3.10

With the suspicion of LiHMDS binding too strongly to the carbene, KHMDS and Cs_2CO_3 was used as base instead. As the cations are larger, and less likely to coordinate to the ligand in the same suspected manner as Li. In this run bispyridine Grubbs 1.gen (**G1py2)** was used as a precursor, which would seem appropriate with respect to its higher reactivity. The first run was attempted using 1,3 mg ligand, **G1py2** (1 eq) and KHMDS (1,1 eq) in a two-pot reaction. The ligand reacted with the base for 5 minutes at 70°C, forming a red solution. Afterwards the solution was treated with **G1py2** solvated in toluene, which were set to react for 30 minutes in room temperature. The second run was done with 0,7 mg ligand with the same conditions except Cs_2CO_3 as a base. NMR of the first run with KHMDS exhibited three new peaks in addition to the 1. generation alkylidene. Indicating the formation of a novel complex.

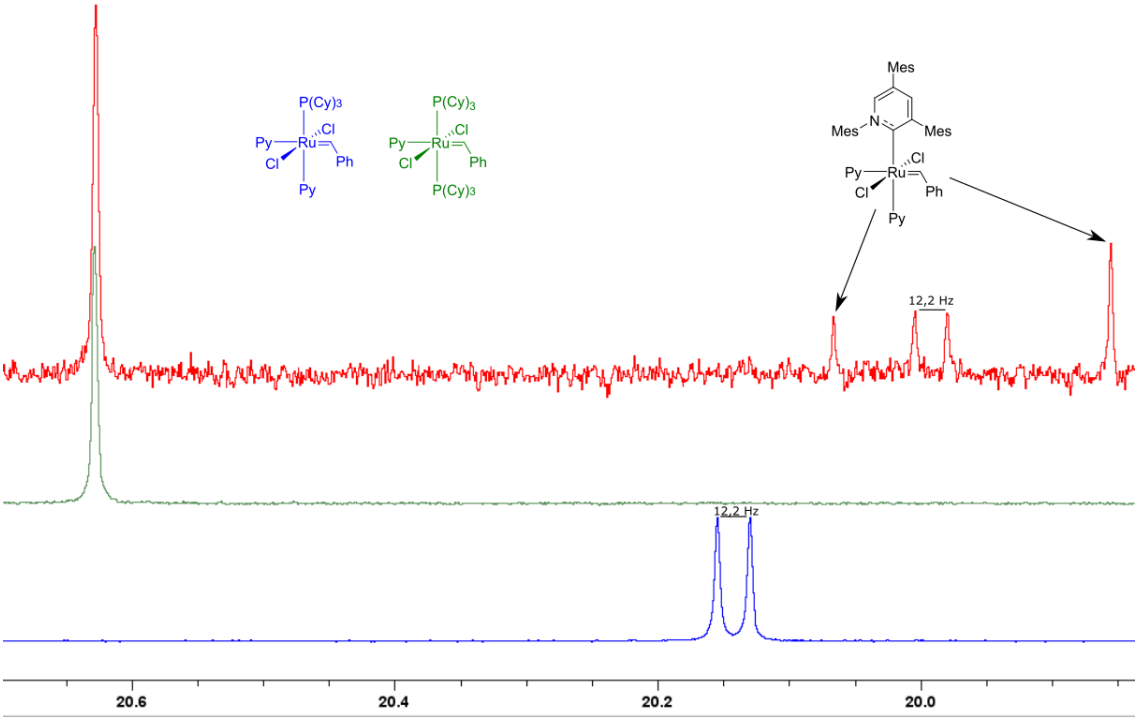

Fig 3.8. Alkylidene comparisons between the catalysts in

The alkylidene region now contain four peaks; the doublet from the starting material is shifted up-field, exhibits the same coupling constants (12,2 Hz), indicating incomplete conversion. The two new peaks adjacent to the **G1py2** doublet are new, and this might be the desired catalyst. The molecule is unsymmetric with respect to the nitrogen, as it can constitute two rotamers, which interacts with the alkylidene proton differently. The additional new peak at 20.62 is in fact the alkylidene for Grubbs 1. generation (**G1)**; as mentioned one phosphine interacts with the alkylidene proton, forming a doublet, however due to **G1** bearing two phosphines, the interactions cancel each other out, forming a singlet. The presence of **G1** in the reaction mixture is peculiar, however this might be addressed. When one phosphine is dissociated following ligand substitution, one unreacted precursor molecule may substitute its pyridine for the phosphine ligand, as pyridines are substitutionally labile[65]. The precursor is essentially acting as its own phosphine scavenger. $CsCO_3$ however, did not perform as KHMDS, as NMR indicated few to none new peaks, indicating low reactivity. This is likely to be due to Cs_2CO_3 being a weaker base than KHMDS, and a strong base is indeed required to deprotonate the aromatic pyridinium salt. With this in mind, several optimization attempts were performed. A run was done with a larger equivalence of the ligand; 15 mg ligand (2,4 eq), base (2,9 eq) and **G1py2** (1eq) was performed with the same reaction procedures as previously used. The crude was then filtered through celite, solvated in miniscule amounts of toluene, then stirred with hexane. This was to separate side product from the crude, as **G1** is assumed to be more soluble in hexane than the product. After 24 hours in the freezer (-37 °C) the vial exhibited precipitate with a solution of purple color, which is the distinct color **G1**. The solution was decanted, and the green precipitate was washed with hexane. The NMR exhibited almost exclusively the alkylidene peaks of the presumed product, however there was a probability of slight contaminations of **G1**. Unfortunately, the product decomposed in the NMR tube, as it was stored in a fridge over the weekend, which might be an opportunity for air to decompose the catalyst if the cap was not situated correctly. A new NMR with an 850Hz NMR-instrument showed the presence of **G1** as the sole alkylidene, which is concurrent with the stability of **G1**, and also it most likely being the decomposition product of catalyst bearing the carbene. Regardless, additional optimization runs were performed, and with the previous results indicating that the excess of ligand was beneficial, this should be pursued. However, the amounts of available ligand were small, so the focus was also shifted to the base, as this is the key to generating the free carbene.

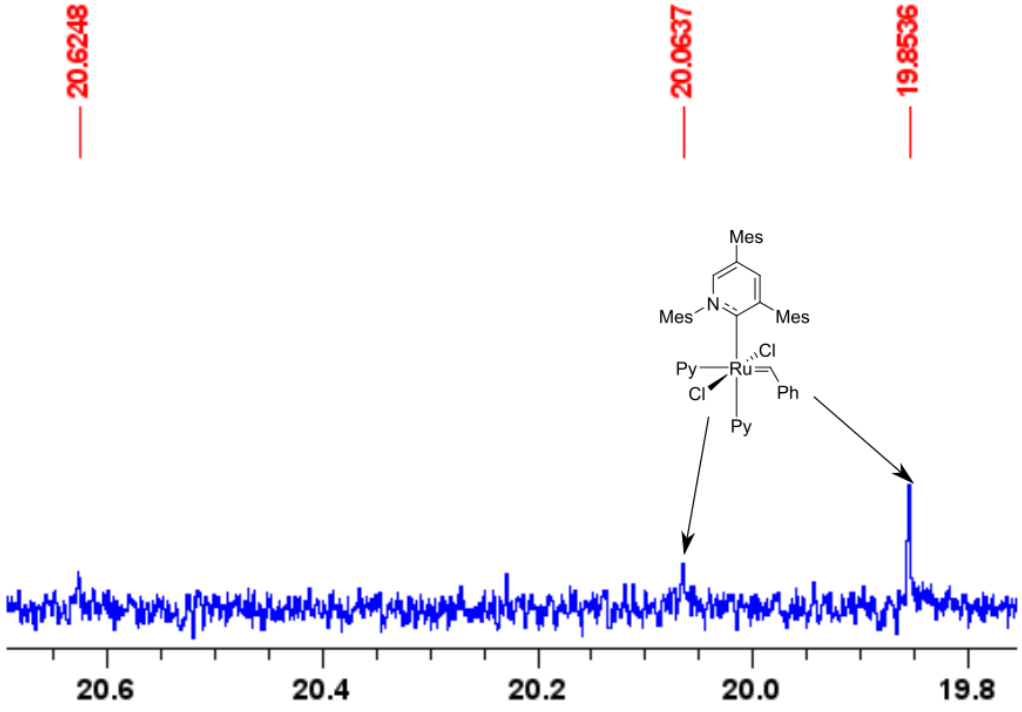

Fig x.x NMR-shifts for the presumed alkylidenes for the complex in the precipitate

As KHMDS tends to be contaminated with other solids it should be sublimated to ensure optimal purity. A sublimation was not performed, it was a possibility that not enough base was present to deprotonate the ligand fully. This is could be fitting with previous results, as more ligand equivalents subsequently leads to larger amounts of base. To investigate this, a run was done with 2,2 eq base, 3,8 mg ligand (1eq) in toluene before adding it to **G1py2** (0,95 eq). Additionally, a run with 3,1 eq base and 5,8 mg ligand in THF was performed. Both reactions were two pots, with the ligand and base reacting at 70°C for 5 minutes. The reaction with 2,2 eq base had only the alkylidenes of **G1py2** and **G1**, this might indicate that the base was unable to deprotonate the pyridinium, this might be due to toluene hampering the reaction, as excess base would be able to attack **G1py2** when added, decomposing it to **G1,** which were not the case. The reaction with 3,1 eq base had only the alkylidene peak of **G1**, indicating complete decomposition of the starting material. **G1** might be the more resilient against the base, as the phosphine ligands prevent the bulky base from attacking the alkylidene.

After considering previous results, the choice of base might be the issue. The bulky Hexamethylsilane-bases might not be able to deprotonate the pyridinium properly, as the N-bound carbons are situated between two bulky mesityl-substituted carbons. Both Li-and K have a pka of around 26, which should be sufficient as the original KOtBu base have a pKa of 17. As evident in the 5th attempt, the unreacted base decomposes the precursor catalyst. A candidate for a base could be KH, as the hydride is not bulky at all, having easy access to the N-bound carbons in the pyridinium. The experiment should then be done with 1,1 eq KH, and 1 eq ligand in THF with the same conditions, except for that the precursor is also solvated in THF.

4. Conclusion

Three novel bearing thiolates were successfully synthesized and characterized. Thiolates did not seem to increase Z-selectivity as much as speculated. Thiolates also a exhibited a decrease in activity compared to their precursors, as initiation and activity gets weakened with thiolate-bearing Hoveyda catalysts as seen in the catalytic tests. Low loadings and less venting resulting in a build-up of ethene, also hints to that the thiolates might be more susceptible to beta-hydride elimination, as the thiolates did exhibit more isomerization.

The new carbene was successfully synthesized, although rather challenging. A novel optimization of the solvent-system in step 2 proved successful. The metalation however was challenging, as several attempts failed. Using **G1py2** turned out to be the most successful, exhibiting new alkylidenes, agreeable to the presence of a rotamer. The new carbene complex was unfortunately not isolated, as the reaction is not yet optimized. However KH, or a base more suitable to deprotonate would serve as a good outlook.

5. **Experimental**

NMR spectra were recorded on Bruker BioSpin AV500, with calibrated solvent signals C_6D_6 (δ =7.16) and $CDCl_3$ (δ =7.26)

All organometallic reactions were carried out in a glove box (MBraun unilab), unless stated otherwise. All organic reactions were done in air, or in a Schlenk line if air sensitive. Most chemicals were bought from sigma Aldrich, although some where from strem, TCI, and the **nG-C1** was from Aiperon.

The substrate 1-octene were degassed with the use of the Schlenk-technique. After importation to glovebox, the 1-octene was filtrated three times through basic alumina, before being stored in molecular sieves (4 Å).

Catalytic stocks were made by solvating various amounts of catalyst (2-5mg) in toluene (5-10g) as by the means to 0,1-0.4µM solution pr mg of toluene. A few mg was used each run, with appropriate amount of 1-octene. The stocks were diluted if necessary, such as the 0.1 ppm tests.

Organometallic experimental

Determining proton shifts and integrals for the organometallic complexes are challenging, as the complexes can constitute various isomers and with protons ranging from 39 to 70, which all have different shifts that can overlap, which makes interpreting somewhat incorrect. The spray reagent in MS was acetonitrile, which will sometimes replace a chloride (yielding 5.6 m/z greater than actual), and sometimes remove it completely (35,45 m/z lower).

HG-C1

In a glovebox, a 25 mL vial, equipped with a magnetic stirring bar, was charged with 100 mg **HG-1** (dichloro(o-isopropoxyphenylmethylene) (tricyclohexylphosphine) ruthenium(II)) (0.17mmol, 1eq), 157 mg 1-(2,6-diethylphenyl)-2,4-dimethyl-4-phenyl-3,4-dihydro-2H-pyrrol-1-ium tetrafluoroborate (0.4 mmol, 2.4 eq), 92 mg KHMDS (0.47 mmol 2.8 eq) and THF (5mL). The vial was capped and let to stir in room temperature. After 24 hours the mixture was filtered through celite, eluted with DCM, and concentrated. The concentrate was purified outside of glovebox by flash chromatography using Hexane/EtOAc (8:2), affording **HG-C1** as a green solid (32 mg, 26% yield). 1H NMR (500 MHz, C6D6, 283 K): δ = 17.89 (s, 0.28 H), 16.5 (s, 0.80), 8.36 (s 1.48H), 7.85 (s 0.46H), 7,77 (d, 0.1 H), 7.70 (d, 0.29 H), 1.69 (s, 1.57H), 7.3 (t 2.66H), 6.39 (d 1.2H), 4.53 (t, 1.18 H), 2.9 (m, 2.88H), 2.48 (m, 4.69H), 1.5084 (s,2.43H), 1.3597 (s, 6.21H), 1.07 (s, 5.73 H), 0.97 (s, 4.1H), 0.85 (m, 2.97H). ESI+=645.21-5.6=641.69 m/z Expected=640.17 m/z

HG-C1-S1

In a glovebox, a 25 mL vial, equipped with a magnetic stirring bar, was charged with 28.9 mg **HG-C1** (0.040 mmol, 1eq), 16,5 mg 2,4,6-triphenylbenzenethiolate (0.044 mmol, 1.1 eq) and THF (3mL). The vial was capped and let to stir in room temperature. After three hours the mixture was filtered through celite, concentrated, and washed with pentane several times (total 10mL). The residue was concentrated, then solvated in a minimal amount of toluene, pentane was then added slowly until solution became cloudy. The vial was placed in a freezer (-37°C) for two days. The brown microcrystals were washed three times in pentane and dried to afford **HG-C1-S1** as nodule-shaped clusters (14 mg, 37%yield). 1H NMR (500 MHz, C6D6, 283 K): δ =15.66 (s, 0.47H), 13.84(s, 0.91H), 7.88 (s, 3.34H), 7.60 (s, 7.60H), 6.75 (s, 1.90H), 6.66 (2.01H), 6.42 (0.92H), 6.40 (s, 1.03H), 4,42 (s, 0.9H), 2.69(m, 4.06H), 2.26 (m, 3.95H), 2.09 (s, 3.33H), 1.63-

1.57.(ss, 1.63H), 1.32-1.12 (m, 9.61), 0.98-0.85 (6.45H), 0.80-0.68 (m, 12.29H). ESI+= 906.32+35.45= 941.77 m/z Expected=941.30

HG-C1-S2

In a glovebox, a 25 mL vial, equipped with a magnetic stirring bar, was charged with 28.9 mg **HG-C1** (0.040 mmol, 1eq), 16,5 mg 2,4,6-tris (3,5- dimethylphenyl)benzenethiolate (0.044 mmol, 1.1 eq) and THF (3mL)**.** After three hours the mixture was filtrated through celite, concentrated, solvated in pentane, and stirred with basic alumina for 30 minutes, the alumina was extracted with toluene, and filtered through celite again. The filtrate was concentrated and solvated in minimal amounts of toluene, pentane was added slowly until solution became cloudy. The vial was placed in a freezer for two days. The brown microcrystals were washed three times in pentane and dried to give **HG-C1-S2** as prism-like crystals (5 mg, 13% yield). 1H NMR (500 MHz, C6D6, 283 K): δ =15.64 (s, 0.48H), 13.93 (s, 0.17H), 7.73 (t, 1.95H), 7.75 (s, 1.79 H), 7.44(s, 1.91H), 7.30 (d, 4.39H), 6.91 (s, 1.19H), 6.81 (s, 1.2H), 6.75 (s, 0.8H), 6.67 (d, 3.29H), 2.08 (s, 4.50H), 1.89 (d (6.60H), 1.69 (m, 12H), 1.33 (m, 6.99H), 1.18 (m, 22,42H), 3.06 (s, 0.76H), 2.63 (s, 1.66H), 2.06 (m, 2.07H), 1.43 (m, 4.61H), 0.7 (s, 4.15H), 0.55 (s, 4.79H). ESI+=990.42+35.45= 1025.87 Expected=1025.39 m/z

nG-C1-S1

30 mg nG-**C1** (0.043 mmol, 1eq) and 18 mg 2,4,6-triphenylbenzenethiolate (0.047 mmol, 1.1 eq) was reacted following the same procedure as **HG-C1-S1**, affording **nG-C1-S1** as brown crystals (14 mg, 38% yield). 1H NMR (500 MHz, C6D6, 283 K): δ =15.31(s, 0.21H), 13.48 (s, (1.02H), 7.94 (s, 1.245H), 7.52 (s, 6.41H), 7.33 (s, 8.21H), 7.06 (m, 7.71H), 6.89 (t, 1.58H), 6.59(s, 1.97H), 5.97 (s, 1.22H), 4.20 (1.11H), 3.05 (s, 1.12H), 2.63 (s, 2.43H), 2.06-2.00 (m, 3.04H), 1.44 (s, 2.67H), 1.38-1.33 (m, 3.92H), 0.70 (s, 6.10H), 0.54 (s, 7.02H). ESI+=951.31+35.45 =986.76. Expected=986.30 m/z

nG-C1-NCO

In a glovebox, a 25 mL vial, equipped with a magnetic stirring bar, was charged with 25.0 mg **nG-C1** (0.037 mmol, 1eq), 18 mg Ag (NCO) (0.12 mmol, 3.2 eq) and toluene (3mL). The vial was capped and let to stir in room temperature. After 2 hours the mixture was filtered through celite, concentrated, and washed with pentane several times (total 10mL). The residue was concentrated, then solvated in a minimal amount of toluene, pentane was then added slowly until solution became cloudy. The vial was placed in a freezer for two days. The bright green microcrystals were washed three times in pentane and dried to afford **nG-C1-NCO** as a bright green solid (17mg, 67%yield). 1H NMR (500 MHz, C6D6, 283 K): δ =17.37 (s, 0.12H), 16.36 (s, 0.72H), 8.28 (s, 0.58H), 8.03 (s, 0.57H), 7.88-7.77 (m, 1.95H), 7.72 (d, 0.72H), 7.64 (d, 0.39), 7.50-7.44 (ss, 2.04H), 5.96-5.82 (m, 1.30H), 4.34-4.081 (ttt, 1.39H), 2.79 (s, 1.95H), 2.47 (ss, 3.90H), 1.95 (s, 1.06H), 1.88 (t, 1.20H), 1.27-1.21 (m, 4.78H), 1.05-0.85 (m, 16.37). ESI+=697.23 Expected=698.20 m/z

Experimental data for organic reactions

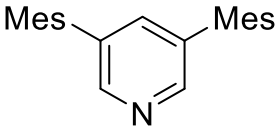

P1

Synthesis of 3,5-dimesitylpyridine (P1)

A 100mL dry vacuum flask equipped with a stir bar and filled with argon, was charged with 3,5-dibromopyridine (2.00g, 8.5 mmol, 1eq), 2,4,6-trismethylphenylboronic acid (4.02 g, 24.5 mmol, 2.9 eq), $Ba(OH)_2$ (5.84 g, 34.1 mmol, 4eq), $PD(PPh_3)_4$ (0.49 g, 0,04 mmol, 0,05 eq), and a mixture of dry THF (42mL) and H_2O (4.2 mL). The reaction was flushed thoroughly with argon, sealed, and set to stir at reflux. After 24 hours, the reaction was quenched with 9mL H_2O, and extracted with 3x15 mL EtOAc. The organic phase was dried over Na_2SO_4, then concentrated. The crude was purified using flash chromatography using gradient chromatography with EtOAc/hexanes (1:10-1:4), affording 2,14 g of **P1** as a white crystalline solid (80% yield). 1H NMR (500 MHz, $CDCl_3$, 283 K): δ =8.42 (d, 2.05 Hz,2H), 7.41 (s, 1H), 6.98 (s,4H), 2.33 (s, 6H), 2,05 (s,12H).

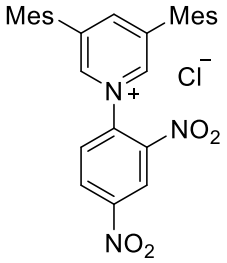

P2

Synthesis of 1-(2,4-dinitrophenyl)-3,5-dimesitylpyridin-1-ium chloride (P2)

A 25mL round bottom flask equipped with was charged with 3,5-dimesitylpyridine **P1** (154 mg, 0,49 mmol, 1eq), 1-chloro, 2,4-dinitrophenyl (147 mg, 0.73 mmol, 1.5 eq) and a mixture of ethanol (2.1mL) and H_2O (0.9mL). The reaction was set to stir at reflux. After 48 hours the mixture was cooled down, dry loaded to a silicaplug, washed with 300mL EtOAc, eluted with MeOH and concentrated. Yielding 217 mg of **P2** as a white-orange crystalline solid (85% yield). 1H NMR (500 MHz, $CDCl_3$, 283 K): δ =9,95 (d, 8.7Hz, 1H), 9.14 (d, 2.5Hz 1H), 8,87 (d, 1.6Hz 2H), 8.4-8.2 (dd, 8.7Hz, 2.5Hz, 1H), 8.31 (t, 1.6Hz 1H), 7.03 (s, 2H), 6.98 (s, 2H), 2.38 (s, 6H), 2.33 (s, 6H), 2.10 (s, 6H).

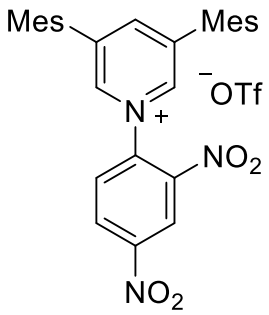

P3

Synthesis of 1-(2,4-dinitrophenyl)-3,5-dimesitylpyridin-1-ium trifluoromethyl sulfonate(P3)

To a 25 mL vial, 1-(2,4-dinitrophenyl)-3,5-dimesitylpyridin-1-ium chloride **(**140 mg, 0.27 mmol, 1eq), silver trifluromethyl sulfonate (69 mg, 0.27 mmol, 1 eq), and $CDCl_3$(3mL) was added together with a stir bar. The reaction was capped and covered with metal foil and stirred. After 2 hours the mixture was filtered through filter paper twice, the collected solvent was evaporated to afford 167 mg of **P3** as an off-white solid (98% yield). 1H NMR (500 MHz, $CDCl_3$, 283 K): δ =9.17 (d, 2,5 Hz, 1H), 9.00-8.98 (d, 8.7 Hz, 1H), 8.90-8.6 (dd, 8.7Hz, 1H) 8.62 (d, 1.6Hz, 2H), 8.35 (t, 1.6Hz), 7.05 (s, 2H), 7.00 (s, 2H), 2.34(s, 6H), 2.26 (s, 6H), 2.09 (s, 6H)

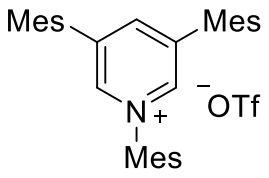

P3

Synthesis of 1,3,5-trimesitylpyridin-1-ium salt.

A 50mL glass reactor with a stir-bar was charged with 1-(2,4-dinitrophenyl)-3,5-dimesitylpyridin-1-ium trifluoromethyl sulfonate **P3** (142 mg, 0.22 mmol 1eq) and 2,4,6-trimethylaniline 0.6mL. The reactor was sealed and let to stir at 150°C. After 24 hours the reaction mixture was directly purified by gradient auto-flash chromatography with EtOAc/DCM (1:10-1:1), affording 62 mg **P4** as a brown solid (43% yield). 1H NMR (500 MHz, $CDCl_3$, 283 K): δ =8.72 (d, 1.7Hz, 2H), 8.23 (t, 1.7Hz, 1H), 7.13 (s, 2H), 7.03 (s, 4H), 2.39 (s, 2H) 2,34 (s, 6H), 2.14 (s, 6H), 2.14 (s, 12 H)

(1) Steinborn, D. *Fundamentals of Organometallic Catalysis*; Master; Wiley-VCH: Weinheim, 2012.
(2) Atkins, P. W. *Elements of Physical Chemistry*, Seventh edition / Peter Atkins, Julio De Paula.; De Paula, J., Series Ed.; Oxford University Press: Oxford, 2017.
(3) Housecroft, C. E. *Inorganic Chemistry*, 4th ed.; Sharpe, A. G., Series Ed.; Pearson: Harlow, 2012.
(4) Kozuch, S.; Martin, J. M. L. "Turning Over" Definitions in Catalytic Cycles. *ACS Catal.* **2012**, *2* (12), 2787–2794. https://doi.org/10.1021/cs3005264.
(5) Catlow, C. R.; Davidson, M.; Hardacre, C.; Hutchings, G. J. Catalysis Making the World a Better Place. *Philos Trans A Math Phys Eng Sci* **2016**, *374* (2061), 20150089. https://doi.org/10.1098/rsta.2015.0089.
(6) Lichtarowicz, M. Catalysis in industry https://www.essentialchemicalindustry.org/processes/catalysis-in-industry.html (accessed 2021 -11 -22).
(7) Blakemore, D. Chapter 1 Suzuki–Miyaura Coupling. **2015**, 1–69. https://doi.org/10.1039/9781782622086-00001.
(8) Namazi, H. Polymers in Our Daily Life. *Bioimpacts* **2017**, *7* (2), 73–74. https://doi.org/10.15171/bi.2017.09.
(9) Handbook of Metathesis | Wiley Online Books https://onlinelibrary.wiley.com/doi/book/10.1002/9783527619481 (accessed 2021 -11 -13).
(10) Ivin, K. J.; Mol, J. C. 1 - Introduction. In *Olefin Metathesis and Metathesis Polymerization (Second Edition)*; Ivin, K. J., Mol, J. C., Eds.; Academic Press: London, 1997; pp 1–11. https://doi.org/10.1016/B978-012377045-5/50002-1.
(11) Calderon, N. Olefin Metathesis Reaction. *Acc. Chem. Res.* **1972**, *5* (4), 127–132. https://doi.org/10.1021/ar50052a002.
(12) Jean-Louis Hérisson, P.; Chauvin, Y. Catalyse de transformation des oléfines par les complexes du tungstène. II. Télomérisation des oléfines cycliques en présence d'oléfines acycliques. *Die Makromolekulare Chemie* **1971**, *141* (1), 161–176. https://doi.org/10.1002/macp.1971.021410112.
(13) Trnka, T. M.; Grubbs, R. H. The Development of L2X2RuCHR Olefin Metathesis Catalysts: An Organometallic Success Story. *Acc. Chem. Res.* **2001**, *34* (1), 18–29. https://doi.org/10.1021/ar000114f.
(14) The Ring Opening Metathesis Polymerisation Toolbox - Slugovc - 2004 - Macromolecular Rapid Communications - Wiley Online Library https://onlinelibrary.wiley.com/doi/full/10.1002/marc.200400150 (accessed 2021 -11 -13).
(15) Dias, E. L.; Nguyen, S. T.; Grubbs, R. H. Well-Defined Ruthenium Olefin Metathesis Catalysts: Mechanism and Activity. *J. Am. Chem. Soc.* **1997**, *119* (17), 3887–3897. https://doi.org/10.1021/ja963136z.
(16) Maughon, B. R.; Grubbs, R. H. Ruthenium Alkylidene Initiated Living Ring-Opening Metathesis Polymerization (ROMP) of 3-Substituted Cyclobutenes. *Macromolecules* **1997**, *30* (12), 3459–3469. https://doi.org/10.1021/ma961780s.
(17) Weskamp, T.; Schattenmann, W. C.; Spiegler, M.; Herrmann, W. A. A Novel Class of Ruthenium Catalyst for Olefin Metathesis: Correction. *Angew. Chem., Int. Ed* **1999**, *38*, 262–262.
(18) Gimferrer, M.; Salvador, P.; Poater, A. Computational Monitoring of Oxidation States in Olefin Metathesis. *Organometallics* **2019**, *38* (24), 4585–4592. https://doi.org/10.1021/acs.organomet.9b00591.
(19) Nelson, D. J.; Queval, P.; Rouen, M.; Magrez, M.; Caijo, F.; Borré, E.; Laurent, I.; Crévisy, C.; Baslé, O.; Mauduit, M.; Percy, J. M. Synergic Effects Between N-Heterocyclic Carbene and Chelating Benzylidene–Ether Ligands Toward the Initiation Step of Hoveyda–Grubbs Type Ru Complexes. *ACS Catal.* **2013**, *3* (2), 259–264. https://doi.org/10.1021/cs400013z.
(20) Michrowska, A.; Bujok, R.; Harutyunyan, S.; Sashuk, V.; Dolgonos, G.; Grela, K. Nitro-Substituted Hoveyda−Grubbs Ruthenium Carbenes: Enhancement of Catalyst Activity through

Electronic Activation. *J. Am. Chem. Soc.* **2004**, *126* (30), 9318–9325. https://doi.org/10.1021/ja048794v.
(21) Gawin, R.; Kozakiewicz, A.; Guńka, P. A.; Dąbrowski, P.; Skowerski, K. Bis(Cyclic Alkyl Amino Carbene) Ruthenium Complexes: A Versatile, Highly Efficient Tool for Olefin Metathesis. *Angewandte Chemie International Edition* **2017**, *56* (4), 981–986. https://doi.org/10.1002/anie.201609009.
(22) Morvan, J.; Mauduit, M.; Bertrand, G.; Jazzar, R. Cyclic (Alkyl)(Amino)Carbenes (CAACs) in Ruthenium Olefin Metathesis. *ACS Catal.* **2021**, *11* (3), 1714–1748. https://doi.org/10.1021/acscatal.0c05508.
(23) Pinter, B.; Speybroeck, V. V.; Waroquier, M.; Geerlings, P.; Proft, F. D. Trans Effect and Trans Influence: Importance of Metal Mediated Ligand–Ligand Repulsion. *Phys. Chem. Chem. Phys.* **2013**, *15* (40), 17354–17365. https://doi.org/10.1039/C3CP52383G.
(24) J. Nelson, D.; Manzini, S.; A. Urbina-Blanco, C.; P. Nolan, S. Key Processes in Ruthenium-Catalysed Olefin Metathesis. *Chemical Communications* **2014**, *50* (72), 10355–10375. https://doi.org/10.1039/C4CC02515F.
(25) Ashworth, I. W.; Hillier, I. H.; Nelson, D. J.; Percy, J. M.; Vincent, M. A. Olefin Metathesis by Grubbs–Hoveyda Complexes: Computational and Experimental Studies of the Mechanism and Substrate-Dependent Kinetics. *ACS Catal.* **2013**, *3* (9), 1929–1939. https://doi.org/10.1021/cs400164w.
(26) Thiel, V.; Hendann, M.; Wannowius, K.-J.; Plenio, H. On the Mechanism of the Initiation Reaction in Grubbs–Hoveyda Complexes. *J. Am. Chem. Soc.* **2012**, *134* (2), 1104–1114. https://doi.org/10.1021/ja208967h.
(27) Stewart, I. C.; Keitz, B. K.; Kuhn, K. M.; Thomas, R. M.; Grubbs, R. H. Nonproductive Events in Ring-Closing Metathesis Using Ruthenium Catalysts. *J. Am. Chem. Soc.* **2010**, *132* (25), 8534–8535. https://doi.org/10.1021/ja1029045.
(28) Chapter4_Keitz.Pdf.
(29) Nascimento, D. L.; Fogg, D. E. Origin of the Breakthrough Productivity of Ruthenium–Cyclic Alkyl Amino Carbene Catalysts in Olefin Metathesis. *J. Am. Chem. Soc.* **2019**, *141* (49), 19236–19240. https://doi.org/10.1021/jacs.9b10750.
(30) Bailey, G. A.; Foscato, M.; Higman, C. S.; Day, C. S.; Jensen, V. R.; Fogg, D. E. Bimolecular Coupling as a Vector for Decomposition of Fast-Initiating Olefin Metathesis Catalysts. *J. Am. Chem. Soc.* **2018**, *140* (22), 6931–6944. https://doi.org/10.1021/jacs.8b02709.
(31) Romero, P. E.; Piers, W. E. Mechanistic Studies on 14-Electron Ruthenacyclobutanes: Degenerate Exchange with Free Ethylene. *J. Am. Chem. Soc.* **2007**, *129* (6), 1698–1704. https://doi.org/10.1021/ja0675245.
(32) Keitz, B. K.; Grubbs, R. H. Probing the Origin of Degenerate Metathesis Selectivity via Characterization and Dynamics of Ruthenacyclobutanes Containing Variable NHCs. *J. Am. Chem. Soc.* **2011**, *133* (40), 16277–16284. https://doi.org/10.1021/ja207252r.
(33) Higman, C. S.; Plais, L.; Fogg, D. E. Isomerization During Olefin Metathesis: An Assessment of Potential Catalyst Culprits. *ChemCatChem* **2013**, *5* (12), 3548–3551. https://doi.org/10.1002/cctc.201300886.
(34) Marx, V. M.; Sullivan, A. H.; Melaimi, M.; Virgil, S. C.; Keitz, B. K.; Weinberger, D. S.; Bertrand, G.; Grubbs, R. H. Cyclic Alkyl Amino Carbene (CAAC) Ruthenium Complexes as Remarkably Active Catalysts for Ethenolysis. *Angewandte Chemie International Edition* **2015**, *54* (6), 1919–1923. https://doi.org/10.1002/anie.201410797.
(35) McClennan, W. L.; Rufh, S. A.; Lummiss, J. A. M.; Fogg, D. E. A General Decomposition Pathway for Phosphine-Stabilized Metathesis Catalysts: Lewis Donors Accelerate Methylidene Abstraction. *J. Am. Chem. Soc.* **2016**, *138* (44), 14668–14677. https://doi.org/10.1021/jacs.6b08372.
(36) Hong, S. H.; Wenzel, A. G.; Salguero, T. T.; Day, M. W.; Grubbs, R. H. Decomposition of Ruthenium Olefin Metathesis Catalysts. *J. Am. Chem. Soc.* **2007**, *129* (25), 7961–7968. https://doi.org/10.1021/ja0713577.

(37) McMurry, J. *Organic Chemistry*, Ninth edition.; Cengage Learning: Australia, 2016.
(38) Khan, R. K. M.; Torker, S.; Hoveyda, A. H. Readily Accessible and Easily Modifiable Ru-Based Catalysts for Efficient and Z-Selective Ring-Opening Metathesis Polymerization and Ring-Opening/Cross-Metathesis. *J. Am. Chem. Soc.* **2013**, *135* (28), 10258–10261. https://doi.org/10.1021/ja404208a.
(39) Dang, Y.; Wang, Z.-X.; Wang, X. A Thorough DFT Study of the Mechanism of Homodimerization of Terminal Olefins through Metathesis with a Chelated Ruthenium Catalyst: From Initiation to Z Selectivity to Regeneration. *Organometallics* **2012**, *31* (20), 7222–7234. https://doi.org/10.1021/om300784k.
(40) Nelson, J. W.; Grundy, L. M.; Dang, Y.; Wang, Z.-X.; Wang, X. Mechanism of Z-Selective Olefin Metathesis Catalyzed by a Ruthenium Monothiolate Carbene Complex: A DFT Study. *Organometallics* **2014**, *33* (16), 4290–4294. https://doi.org/10.1021/om500612r.
(41) Occhipinti, G.; Törnroos, K. W.; Jensen, V. R. Pyridine-Stabilized Fast-Initiating Ruthenium Monothiolate Catalysts for Z-Selective Olefin Metathesis. *Organometallics* **2017**, *36* (17), 3284–3292. https://doi.org/10.1021/acs.organomet.7b00441.
(42) Smit, W.; Koudriavtsev, V.; Occhipinti, G.; Törnroos, K. W.; Jensen, V. R. Phosphine-Based Z-Selective Ruthenium Olefin Metathesis Catalysts. *Organometallics* **2016**, *35* (11), 1825–1837. https://doi.org/10.1021/acs.organomet.6b00214.
(43) Friebolin, H.; Becconsall, J. K. *Basic One- and Two-Dimensional NMR Spectroscopy*; Wiley, 1998.
(44) Smith, R. M.; Busch, K. L. *Understanding Mass Spectra: A Basic Approach*; Hoboken: John Wiley & Sons, Incorporated: Hoboken, 2004.
(45) Bunaciu, A. A.; Udriştioiu, E. gabriela; Aboul-Enein, H. Y. X-Ray Diffraction: Instrumentation and Applications. *Critical Reviews in Analytical Chemistry* **2015**, *45* (4), 289–299. https://doi.org/10.1080/10408347.2014.949616.
(46) Thomas, E. Crystal Growth and the Search for Highly Correlated Ternary Intermetallic Antimonides and Stannides. **2006**.
(47) Chalk, S.; McEwen, L. The IUPAC Gold Book: An Exemplar for IUPAC Asset Digitization. *Chemistry international* **2017**, *39* (3), 25–30. https://doi.org/10.1515/ci-2017-0307.
(48) Astruc, D. *Organometallic Chemistry and Catalysis*; Grenoble Sciences, Series Ed.; Springer: Berlin, 2007.
(49) Atkins, P. W.; Shriver, D. F. *Shriver & Atkins' Inorganic Chemistry*, 5th ed.; Oxford University Press: Oxford, 2010.
(50) Rahman, M. Matiur.; Liu, H. Ye.; Prock, Alfred.; Giering, W. P. Quantitative Analysis of Ligand Effects. 2. Steric and Electronic Factors Influencing Transition-Metal-Phosphorus(III) Bonding. *Organometallics* **1987**, *6* (3), 650–658. https://doi.org/10.1021/om00146a037.
(51) Golovin, M. N.; Rahman, M. M.; Belmonte, J. E.; Giering, W. P. Quantitative Separation of .Sigma.- and .Pi.-Components of Transition Metal-Phosphorus Bonding and the Application of Ligand Effects in Organometallic Chemistry. *Organometallics* **1985**, *4* (11), 1981–1991. https://doi.org/10.1021/om00130a011.
(52) Zhu, D.; Budzelaar, P. H. M. A Measure for σ-Donor and π-Acceptor Properties of Diiminepyridine-Type Ligands. *Organometallics* **2008**, *27* (12), 2699–2705. https://doi.org/10.1021/om701160b.
(53) Occhipinti, G.; Jensen, V. R. Nature of the Transition Metal–Carbene Bond in Grubbs Olefin Metathesis Catalysts. *Organometallics* **2011**, *30* (13), 3522–3529. https://doi.org/10.1021/om200181y.
(54) Marx, V. M.; Sullivan, A. H.; Melaimi, M.; Virgil, S. C.; Keitz, B. K.; Weinberger, D. S.; Bertrand, G.; Grubbs, R. H. Cyclic Alkyl Amino Carbene (CAAC) Ruthenium Complexes as Remarkably Active Catalysts for Ethenolysis. *Angewandte Chemie International Edition* **2015**, *54* (6), 1919–1923. https://doi.org/10.1002/anie.201410797.

(55) Occhipinti, G.; Törnroos, K. W.; Jensen, V. R. Pyridine-Stabilized Fast-Initiating Ruthenium Monothiolate Catalysts for Z-Selective Olefin Metathesis. *Organometallics* **2017**, *36* (17), 3284–3292. https://doi.org/10.1021/acs.organomet.7b00441.
(56) Comparison of GC/MS and NMR for quantification of methyleugenol in food | SpringerLink https://link.springer.com/article/10.1007%2Fs00217-012-1879-4 (accessed 2021 -11 -22).
(57) Huang, Y.; Brown, M. K. Synthesis of Bisheteroarylalkanes by Heteroarylboration: Development and Application of a Pyridylidene–Copper Complex. *Angewandte Chemie International Edition* **2019**, *58* (18), 6048–6052. https://doi.org/10.1002/anie.201902238.
(58) Cheng, W.-C.; Kurth, M. J. THE ZINCKE REACTION. A REVIEW. *Organic Preparations and Procedures International* **2002**, *34* (6), 585–608. https://doi.org/10.1080/00304940209355784.
(59) Rohrbach, S.; Smith, A. J.; Pang, J. H.; Poole, D. L.; Tuttle, T.; Chiba, S.; Murphy, J. A. Concerted Nucleophilic Aromatic Substitution Reactions. *Angewandte Chemie International Edition* **2019**, *58* (46), 16368–16388. https://doi.org/10.1002/anie.201902216.
(60) Li, J. J. Zincke Reaction. In *Name Reactions: A Collection of Detailed Mechanisms and Synthetic Applications*; Li, J. J., Ed.; Springer: Berlin, Heidelberg, 2009; pp 596–598. https://doi.org/10.1007/978-3-642-01053-8_277.
(61) Microwaves and Aqueous Solvents Promote the Reaction of Poorly Nucleophilic Anilines with a Zincke Salt | The Journal of Organic Chemistry https://pubs.acs.org/doi/full/10.1021/acs.joc.6b00208 (accessed 2021 -11 -21).
(62) Vinh Huynh, H.; Tien Lam, T.; T. Luong, H. T. Anion Influences on Reactivity and NMR Spectroscopic Features of NHC Precursors. *RSC Advances* **2018**, *8* (61), 34960–34966. https://doi.org/10.1039/C8RA05839C.
(63) Hayes, J. M.; Viciano, M.; Peris, E.; Ujaque, G.; Lledós, A. Mechanism of Formation of Silver N-Heterocyclic Carbenes Using Silver Oxide: A Theoretical Study. *Organometallics* **2007**, *26* (25), 6170–6183. https://doi.org/10.1021/om700898d.
(64) Smit, W.; Foscato, M.; Occhipinti, G.; Jensen, V. R. Ethylene-Triggered Formation of Ruthenium Alkylidene from Decomposed Catalyst. *ACS Catal.* **2020**, *10* (12), 6788–6797. https://doi.org/10.1021/acscatal.0c02206.
(65) Sanford, M. S.; Love, J. A.; Grubbs, R. H. A Versatile Precursor for the Synthesis of New Ruthenium Olefin Metathesis Catalysts. *Organometallics* **2001**, *20* (25), 5314–5318. https://doi.org/10.1021/om010599r.

Appendix

Catalytic section

Appendix 1. Catalytic results for HG-C1-S1

Loadings	hr	Conversion (%)	Yield (%)	Iso (%)	Z% of yield	TON 10^3
1 ppm						
	0,25	10,9	10,5	0,3	44	52,6
	0,5	15,8	15,4	0,4	44	77,2
	1	26,8	26,4	0,4	44	132,2
	26	82,4	80,3	2,0	28	401,4
1 ppm						
	0,25	5,7	5,4	0,3	40	27,2
	0,5	4,5	5,3	0,2	41	26,6
	1	7,2	6,9	0,3	42	34,6
	2	23,0	22,5	0,5	43	112,7
	24	40,4	38,4	2,0	39	192,2
	48	45,4	42,9	2,6	38	214,4
	72	46,2	43,6	2,6	39	218,0
10 ppm						
	1	20,5	19,0	1,5	41	9,5
	24	65,0	49,3	15,6	31	24,7
	48	95,7	61,5	34,2	23	30,7
	72	95,9	61,1	34,9	21	30,5
10 ppm						
	72	66,6	44,0	22,4	34	22,0
	96	70,6	41,9	28,1	30	21,0
	120	75,3	48,6	26,5	32	24,3
10 ppm						
	1	7,4	6,8	0,6	34	3,4
	24	29,9	18,6	11,3	30	9,3
100 ppm						
	72	76,5	70,1	6,3	26	3,5
	96	77,5	70,7	6,7	25	3,5
	120	90,6	86,1	4,7	25	4,3

Appendix 2. Catalytic results for HG-C1-S2

HG-C1-S2	hr	Conversion (%)	Yield (%)	Isomer pk	%Z	TON (estim)
1 ppm						
	0,5	14,1	13,7	0,4	44	68,6
	1	18,2	17,6	0,6	43	88,0
	24	38,1	35,5	2,6	41	177,3
10 ppm						
	120	70,5	61,0	9,5	29	30,5
	144	79,6	72,1	7,5	29	36,0
	168	86,1	80,1	6,0	29	40,0
10 ppm						
	24	54,3	42,7	11,5	34	21,4
	168	65,8	47,5	18,1	29	23,8
	192	72,5	57,0	15,6	30	28,5

Appendix 3. Catalytic results for nG-C1

nG-C1	hr	Conversion (%)	Yield (%)	%iso	%Z	TON (estim)
1 ppm						
	0,5	70,5	69,4	1,1	27	346,8
	1	71,2	70,3	0,9	26	351,6
	2	73,4	72,4	1,0	26	362,1
10 ppm						
	0,5	80,4	79,4	1,1	21	39,7
	2	83,7	82,4	1,3	21	41,2
	24	89,3	87,8	1,5	21	43,9
	48	89,6	87,1	2,5	19	43,5
50 ppm						
	1	88,7	87,4	1,3	20	8,7
	24	93,5	90,7	2,7	20	9,1
100 ppm						
	0,5	82,9	81,8	1,1	21	4,1
	2	90,7	89,3	1,5	21	4,5
	48	97,3	94,3	3,0	20	4,7
	72	99,4	94,3	5,1	20	4,7
100 ppm						
	48	87,4	82,6	4,8	21	4,1
	72	96,2	88,4	7,8	20	4,4

Appendix 4. Catalytic results for nG-C1-S1

nG-C1-S1	hr	Conversion (%)	Yield (%)	%iso	%Z	TON (K)
0,1 ppm						
	0,5	0,7	N/A	N/A	N/A	N/A
0,1 ppm						
	0,5	0,8	N/A	N/A	N/A	N/A
	26	12,9	12,6	0,6	40,5	629,2
0,1 ppm						
	0,5	3,0	2,5	0,9	36,6	125,4
	2	3,4	2,9	0,9	36,6	145,4
	24	3,5	2,8	1,4	35,4	139,0
0,1 ppm						
	0,5	1,0	N/A	N/A	N/A	N/A
	1	1,2	0,6	0,4	37,4	32,4

Appendix 5. Catalytic results for nG-C1

nG-C1	hr	Conversion (%)	Yield (%)	%iso	%Z	TON (K)
0,1 ppm						
	0,5	8,2	7,9	0,5	41,0	395,3
	1	8,9	8,6	0,7	41,1	430,3
	2	8,4	8,1	0,5	41,3	404,4
0,1 ppm						
	0,5	12,3	12,0	0,6	40,0	599,4
	1	12,2	12,0	0,6	40,6	597,9
	26	11,9	11,7	0,4	39,8	586,7
0,1 ppm						
	0,5	19,1	18,9	0,3	40,3	947,2
	1	20,2	19,9	0,7	40,7	994,6
	2	19,7	19,4	0,7	40,8	967,8
0,1 ppm						
	0,5	12,4	12,4	0,2	40,6	622,1
	1	14,6	14,3	0,5	40,6	714,2
	2	14,3	14,0	0,6	40,9	699,4

Appendix 6

nG-C1	hr	Conversion (%)	Yield (%)	%iso	%Z	TON (K)
1 ppm						
	0,5	70,5	69,4	1,1	27	346,8
	1	71,2	70,3	0,9	26	351,6
	2	73,4	72,4	1,0	26	362,1
10 ppm						
	0,5	80,4	79,4	1,1	21	39,7
	2	83,7	82,4	1,3	21	41,2
	24	89,3	87,8	1,5	21	43,9
	48	89,6	87,1	2,5	19	43,5
50 ppm						
	1	88,7	87,4	1,3	20	8,7
	24	93,5	90,7	2,7	20	9,1
100 ppm						
	0,5	82,9	81,8	1,1	21	4,1
	2	90,7	89,3	1,5	21	4,5
	48	97,3	94,3	3,0	20	4,7
	72	99,4	94,3	5,1	20	4,7
100 ppm						
	48	87,4	82,6	4,8	21	4,1
	72	96,2	88,4	7,8	20	4,4

Appendix 7 Catalytic results for nG-C1-S1

ng-C1-S1	hr	Conversion (%)	Yield (%)	%iso	%Z	TON (K)
1ppm						
	0,25	5,1	4,8	0,6	39	24,1
	1	16,8	16,2	1,1	44	80,9
	24	21,0	20,5	1,0	44	102,7
	48	23,3	22,4	1,8	43	111,8
1 ppm						
	0,5	1,5	1,3	0,2	41	6,6
	1	1,8	1,6	0,2	42	8,0
1 ppm						
	24	17,1	16,6	0,5	44	83,0
10 ppm						
	0,5	20,4	20,0	0,4	44	10,0
	2	37,4	36,8	0,6	43	18,4
	24	56,7	55,6	1,1	41	27,8
	48	74,1	72,9	1,2	41	36,4
50 ppm						
	0,5	56,0	55,1	0,7	24	5,5
	2	73,5	72,3	1,3	26	7,2
	24	90,9	87,8	3,0	22	8,8
	48	91,2	86,3	4,9	22	8,6
100 ppm						
	0,5	56,6	55,7	0,9	20	2,8
	2	75,9	74,5	1,4	20	3,7
	48	94,4	91,0	3,4	20	4,5
	72	93,7	89,1	4,8	20	4,5
100 ppm						
	48	83,9	68,7	15,2	26	3,4
	72	93,2	77,7	15,5	24	3,9

Appendix 8. Catalytic results for nG-C1-NCO

nG-C1-NCO	hr	Conversion (%)	Yield (%)	%iso	%Z	TON (estim)
1 ppm						
	0,5	32,0	31,4	0,6	23	157,0
	1	31,6	31,0	0,6	23	155,2
	24	32,9	31,7	1,2	23	158,3
	48+	33,8	30,9	2,7	22	154,7
10 ppm						
	48	80,8	74,4	6,3	20	37,2
	72	90,8	81,5	9,3	20	40,7

Organometallic section

Appendix 9. HG-C1.gen, C_6D_6

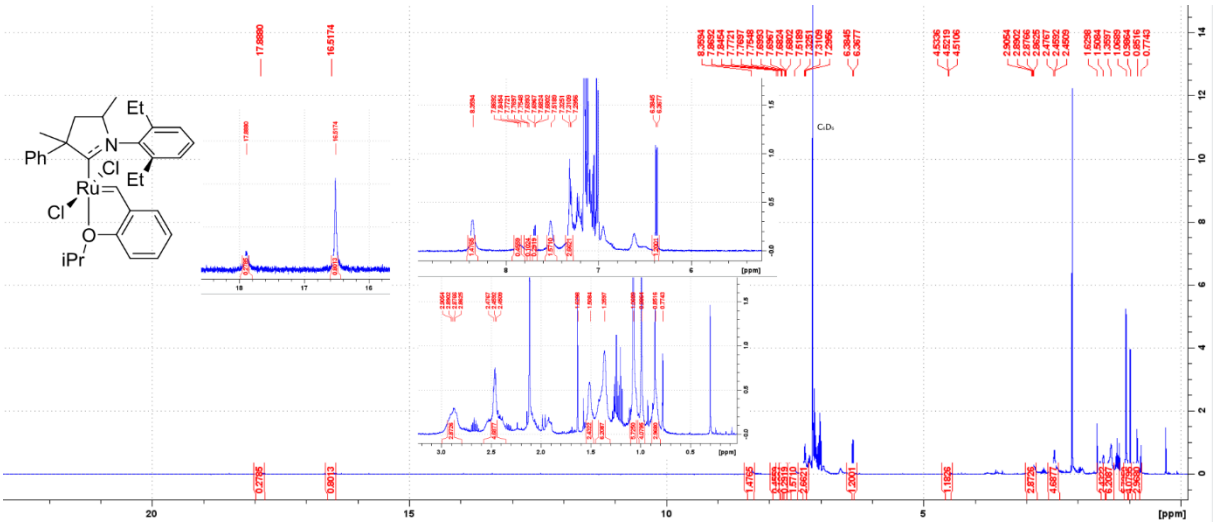

Appendix 10. HG-C1-S1, C_6D_6

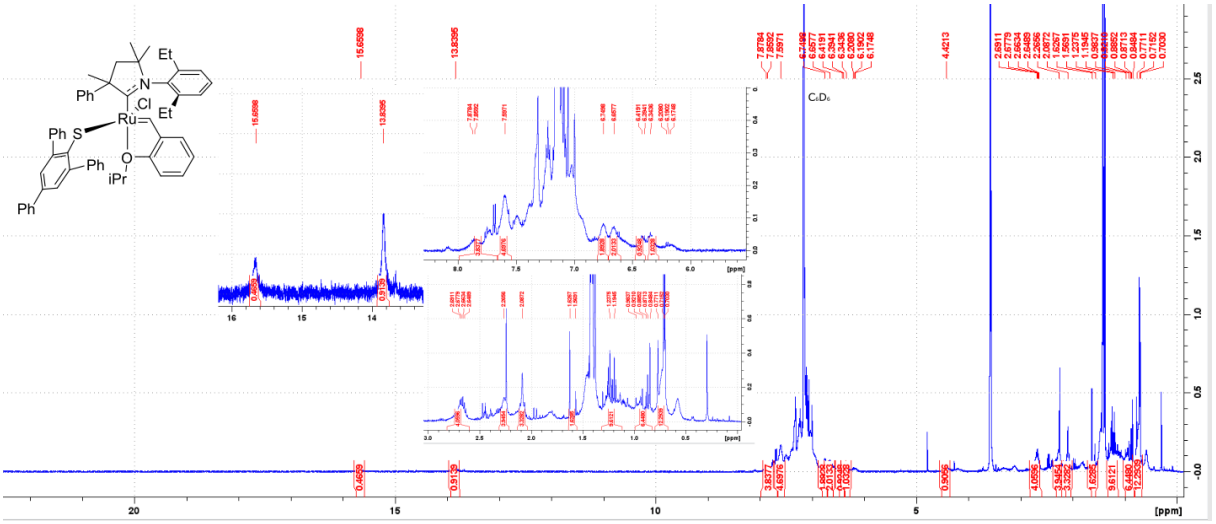

Appendix 11. HG-C1-S2, C_6D_6

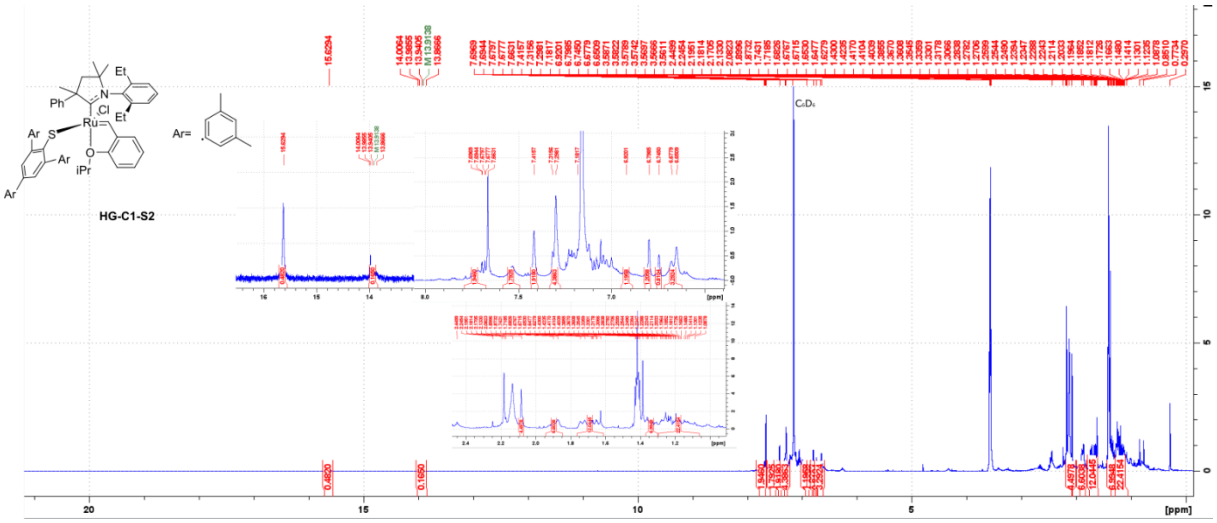

Appendix 12. nG-C1-S2, C_6D_6

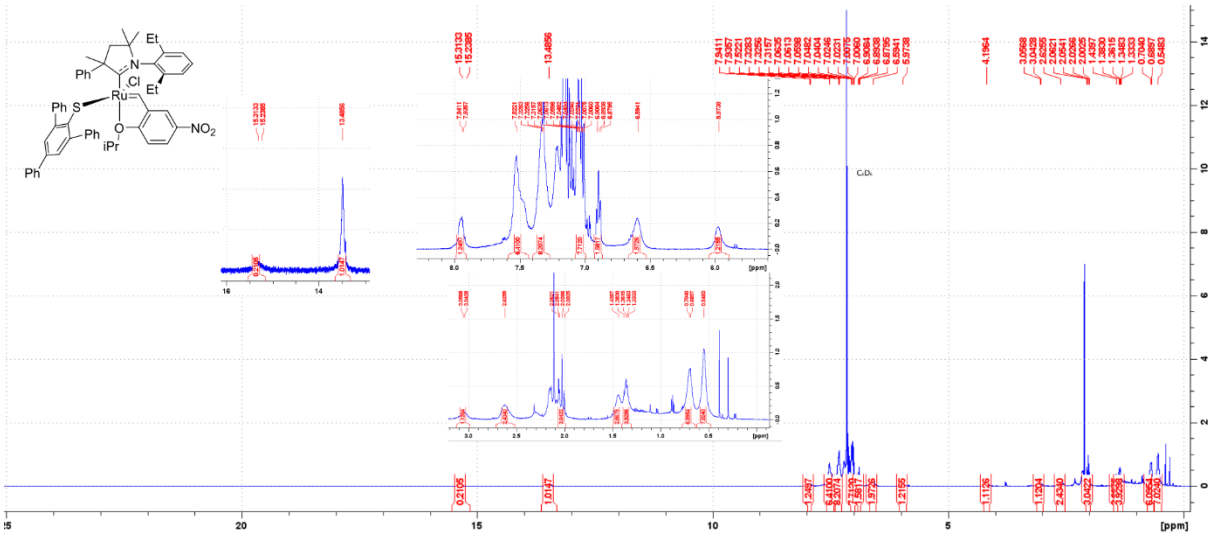

Appendix 13. nG-C1-NCO, C_6D_6

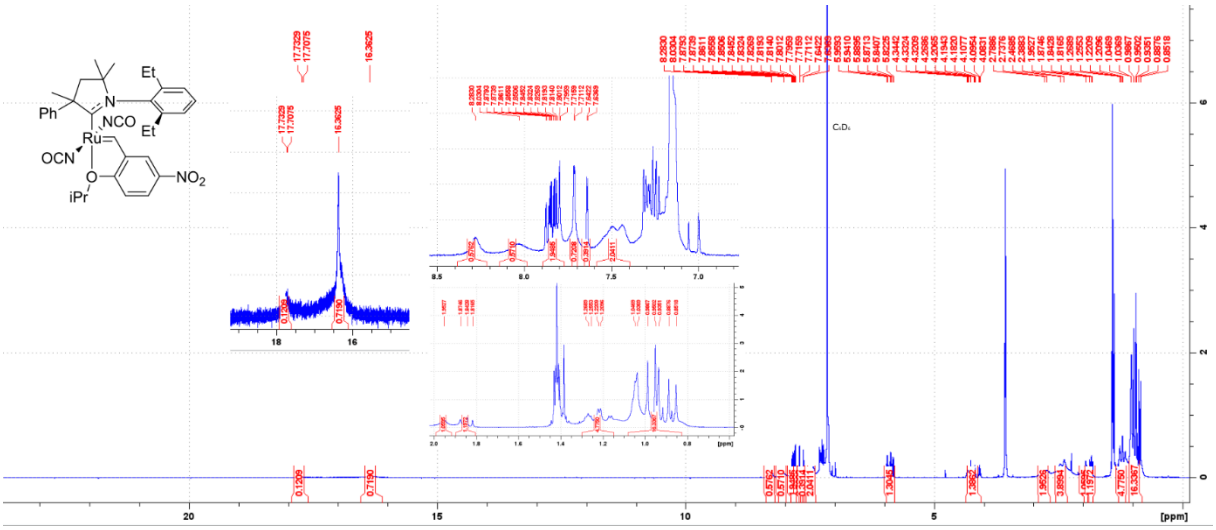

Appendix 14. Novel alkylidene peaks in C_6D_6 (peaks not integrated due to low concentrations, and possible contamination with **G1.**

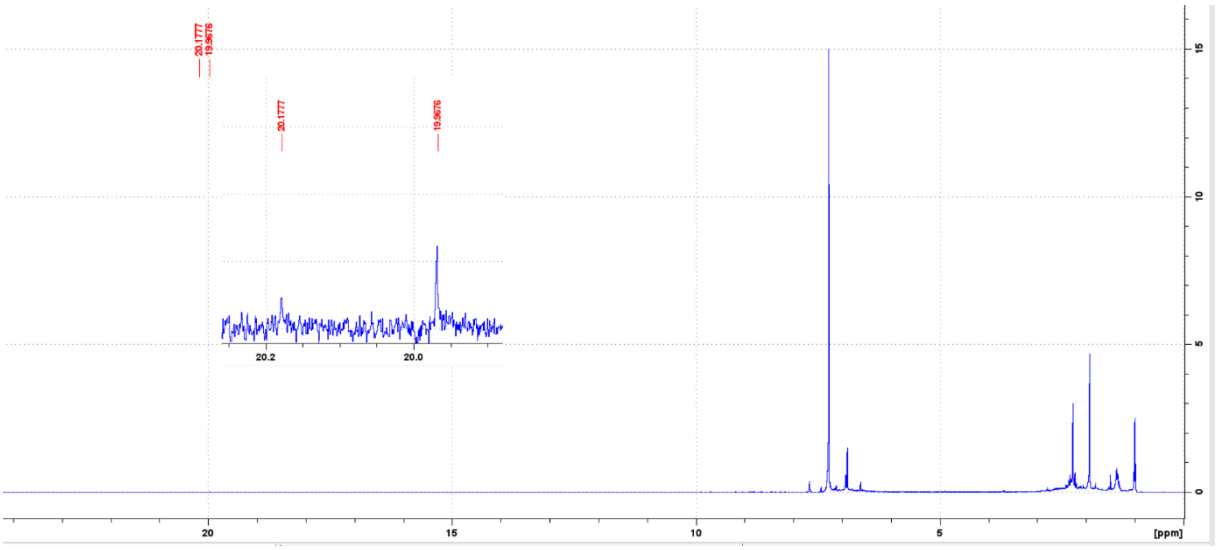

Catalytic examples

Appendix 15. HG-C1 1-octene metathesis, 1 ppm 24 hr.

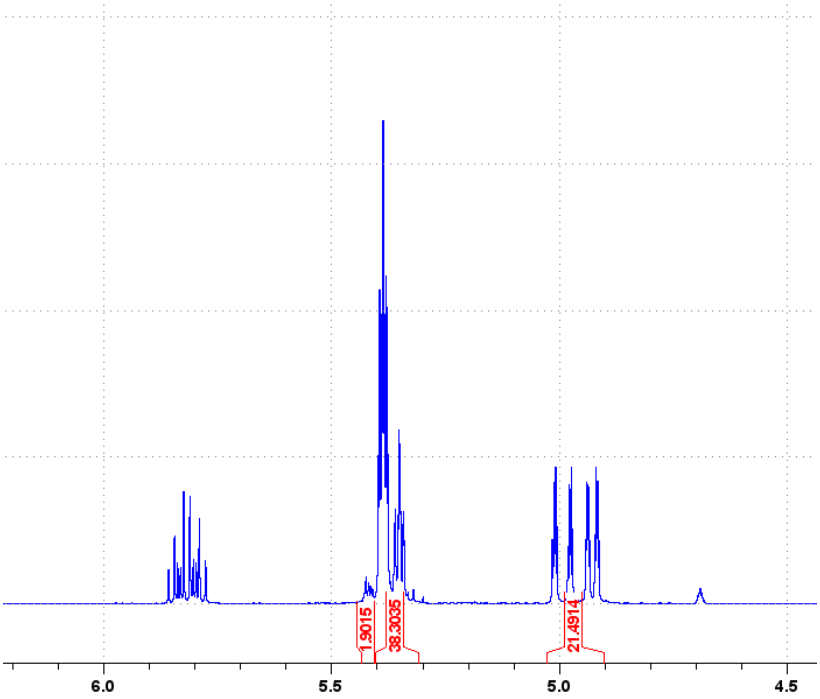

Appendix 16. HG-C1-S11-octene metathesis, 1 ppm 24 hr.

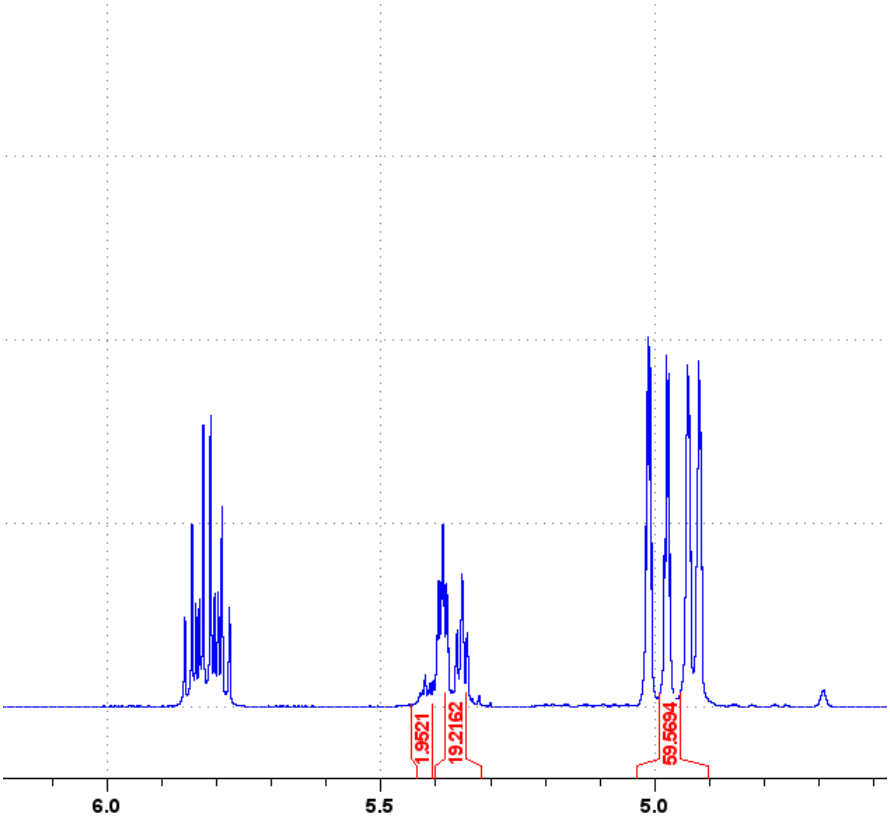

Organic section

Appendix 17. **P1** in $CDCl_3$

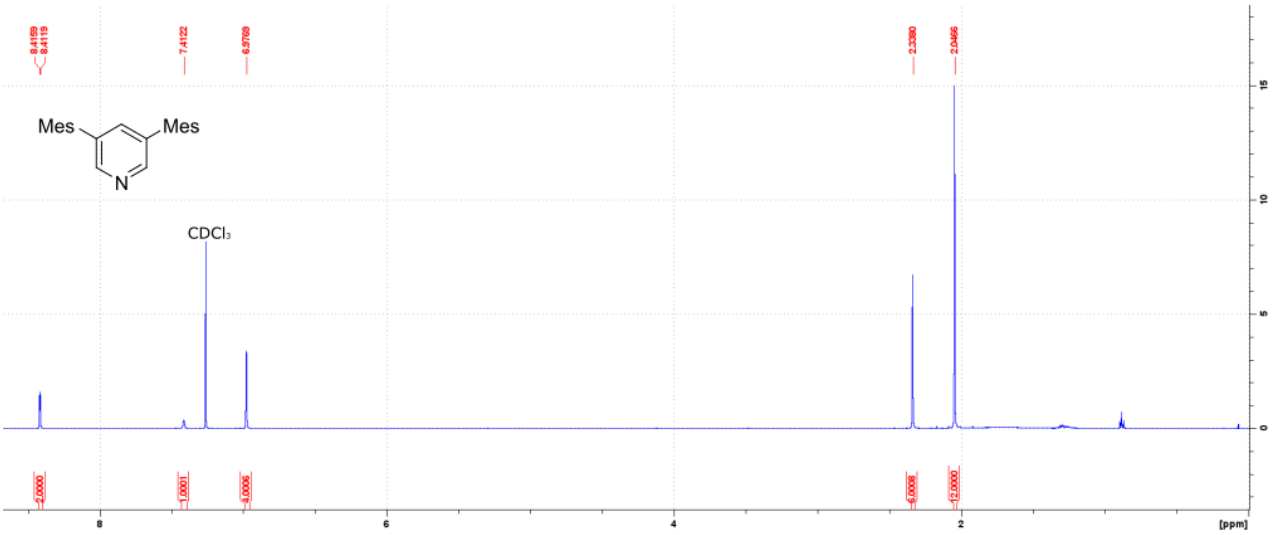

Appendix 18

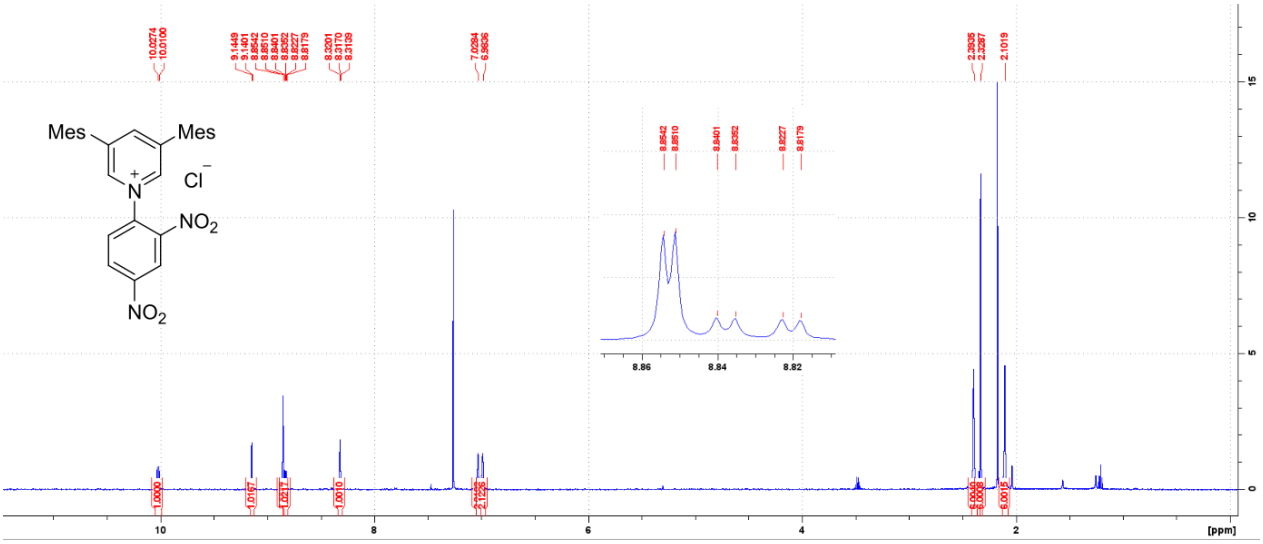

Appendix 19

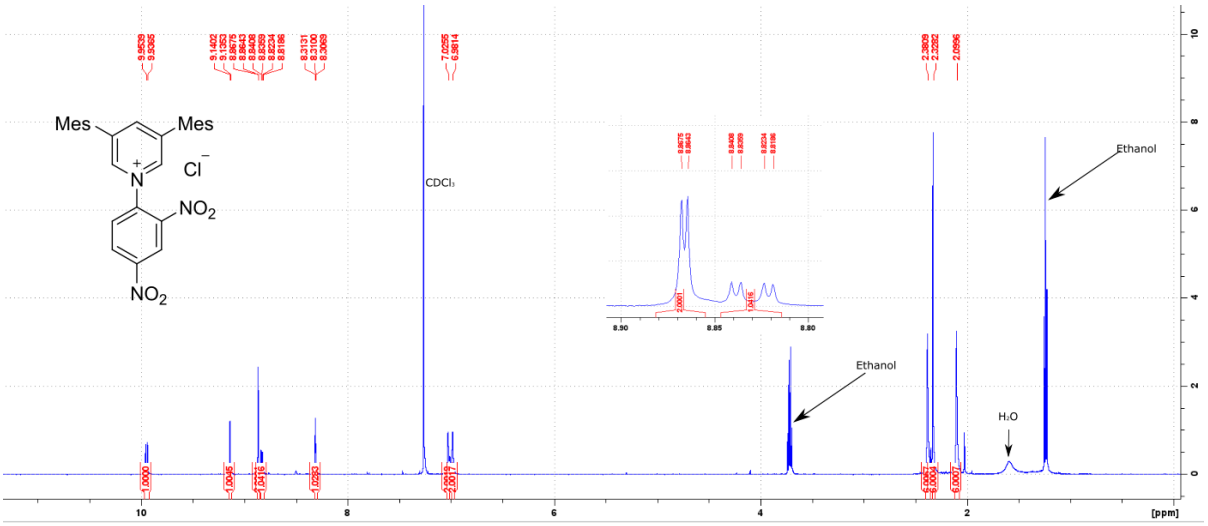

Appendix 20

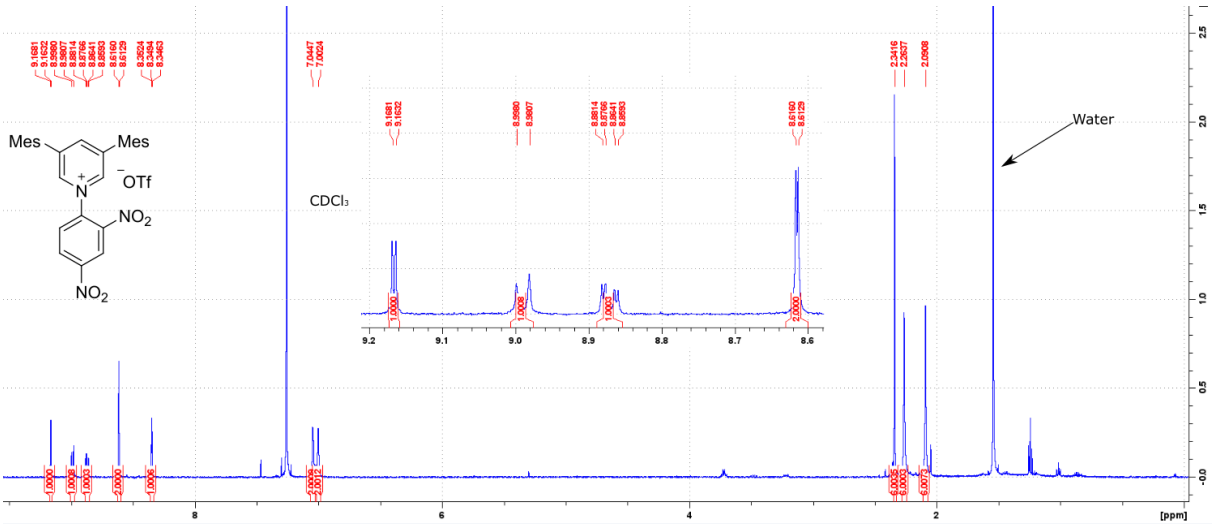

Appendix 21

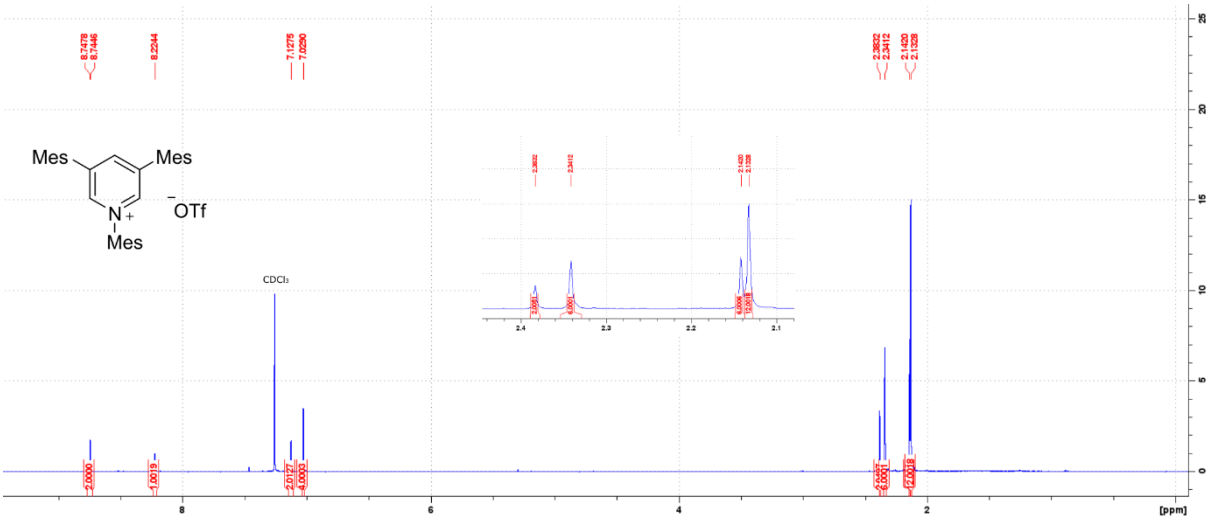

Appendix 22

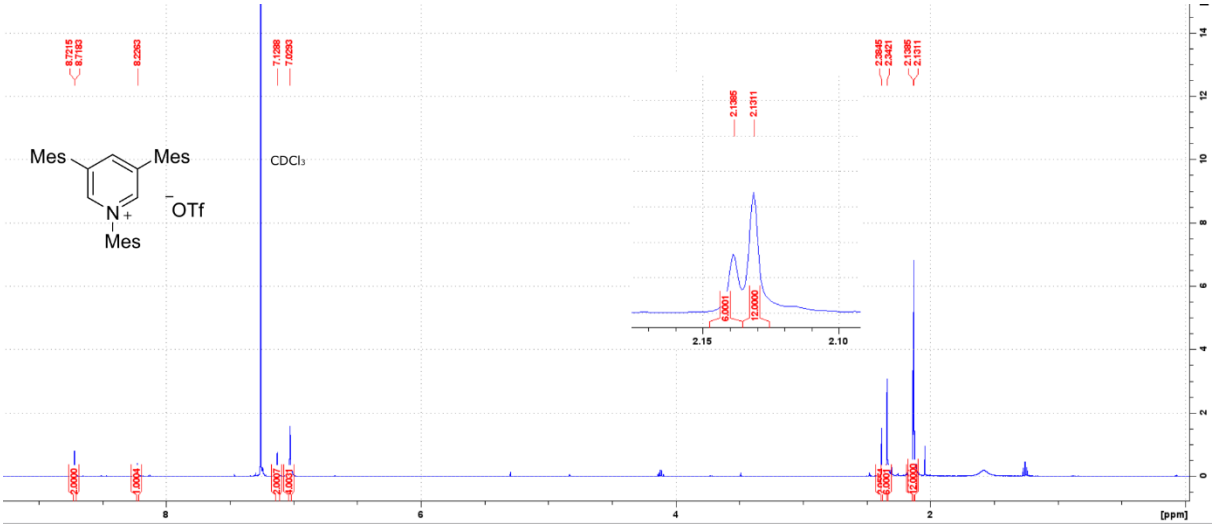

Appendix 23